A Standalone Proton Exchange Membrane Fuel Cell Generation System with Different Tracking Techniques

By

© Venkataraghavan Karunamurthy Kumaraswamy, B.E

A Thesis submitted to the
School of Graduate Studies in
partial fulfillment of the
requirements for the degree of
Master of Engineering

Faculty of Engineering and Applied Science
Memorial University of Newfoundland

May 2017
St. John's, Newfoundland, Canada

Abstract

The proton exchange membrane fuel cell (PEMFC) may be operated at the maximum power point (MPP) or maximum efficiency point (MEP). In this thesis, a complete user-friendly Simulink model of the PEMFC is developed to implement the maximum power point tracking (MPPT) technique and maximum efficiency point tracking (MEPT) technique. A new tracking technique referred to as the midpoint tracking (MDT) technique, is proposed to overcome the limitations of the MPPT and MEPT techniques. A detailed analysis of the tracking techniques based on simulation results using the Ballard MK5-E PEMFC as reference is presented. Simulation results indicate that the midpoint tracking technique provides a trade-off operation with acceptable efficiency derating of 15%, high output power, and small size of the fuel cell when compared with the maximum efficiency point tracking technique. In order to analyse the effects of the tracking techniques on the PEMFC system economics, a detailed economic analysis for ten different cases of standalone PEMFC system is carried out. From the point of view of the economics of a standalone fuel cell generation system, it is found that the MPPT technique is suitable for low power applications (<50kW) and MDT technique is suitable for medium to high power applications. Finally, based on the particular requirements of stationary PEMFC application, suitable tracking techniques are suggested.

Dedicated to my loving family

Acknowledgments

First and foremost, I would like to express my sincere gratitude and appreciation to my supervisor Dr. John Quaicoe for his guidance, encouragement, advice, and support over the past two years.

I would like to gratefully acknowledge the Natural Sciences and Engineering Research Council of Canada (NSERC) and School of Graduate Studies for the financial support towards the research.

I would also like to thank Ms. Moya Crocker, Secretary of the Associate Dean of Graduate Studies and Research, and Dr. Leonard Lye, Associate Dean of Graduate Studies and Research, for ensuring smooth operation of the administrative aspects of my graduate program.

I would like to thank my parents Mr. Karunamurthy and Ms. Maheswari and my sister Dr. Bhuvaneswari Sasikumar for their unconditional love and affection. I am thankful to my uncle Dr. Munaswamy Katna and my aunt Ms. Saraswathy Katna for their continued support for the past two years, and also to my cousin Dr. Dhamodhar Kosanam for being a constant source of inspirations and encouragement.

I would also like to extend my thanks to my friends and colleagues for their continuous support during my graduate program.

Table of Contents

List of Tables

List of Figures

Nomenclature

Abbreviations

AC	:	Alternating Current
AFC	:	Alkaline Fuel Cell
ANOVA	:	Analysis of Variance
BBD	:	Box-Behnken Design
BPR	:	Back Pressure Regulator
CCD	:	Central Composite Design
CHP	:	Combined Heat and Power
COE	:	Cost of Electricity
DC	:	Direct Current
DMFC	:	Direct Methanol Fuel Cell
DOE	:	Design of Experiment
ESC	:	Extremum Seeking Control
FC	:	Fuel Cell
FFF	:	Fast Flexible Filling
FLC	:	Fuzzy Logic Control
GDL	:	Gas Diffusion Layer
HOMER	:	Hybrid Optimization Model for Electrical Renewables
IC	:	Internal Combustion
IncCond	:	Incremental Conductance
LCOE	:	Levelized Cost of Electricity
MCFC	:	Molten Carbonate Fuel Cell
MD	:	Midpoint
MDT	:	Midpoint Tracking

MEA	:	Membrane Electrode Assembly
MEP	:	Maximum Efficiency Point
MEPT	:	Maximum Efficiency Point Tracking
MPP	:	Maximum Power Point
MPPT	:	Maximum Power Point Tracking
NPC	:	Net Present Cost
NSS	:	Natural Switching Surface
O&M	:	Operation and Maintenance
P&O	:	Perturb and Observe
PAFC	:	Phosphoric Acid Fuel Cell
PEM	:	Polymer Electrolyte Membrane
PEMFC	:	Proton Exchange Membrane Fuel Cell
PR	:	Pressure Regulator
PV	:	Photovoltaic
PWM	:	Pulse Width Modulation
RSM	:	Response Surface Methodology
slpm	:	Standard Liter Per Minute
SMC	:	Sliding Mode Control
SOFC	:	Solid Oxide Fuel Cell

List of Symbols

Proton Exchange Membrane Fuel Cell System

Symbol	*Parameter*	*Unit*
A	Effective Cell Area	cm^2
$a_1 \ldots a_{13}$	Constants for P_{net} FFF Design	-
C	Double Layer Capacitance	F
c'_{H_2}	Anode Reactant Concentration	mol cm^{-3}
c'_{O_2}	Cathode Reactant Concentration	mol cm^{-3}
F	Faraday Constant	C mol^{-1}
f_a	Anode Flow Constant	mol s^{-1} atm^{-1}
f_c	Cathode Flow Constant	mol s^{-1} atm^{-1}
$f_{H_2,in}$	Hydrogen Inlet Flow Rate	mol s^{-1}
$f_{H_2,out}$	Hydrogen Outlet Flow Rate	mol s^{-1}
$f_{H_2,used}$	Rate of Hydrogen Consumption	mol s^{-1}
$f_{O_2,in}$	Oxygen Inlet Flow Rate	mol s^{-1}
$f_{O_2,out}$	Oxygen Outlet Flow Rate	mol s^{-1}
$f_{O_2,used}$	Rate of Oxygen Consumption	mol s^{-1}
H	Hydrogen	-
h	Scaling Factor for P_{net} FFF design	-
H_2O	Water	-
i_{fc}	Stack Current	A
i_{limit}	Fuel Cell Current Limit	A
I_n	Normalized Stack Current	A
K_v	Motor Constant	rpm
L	Normalized Membrane Water Content	-
n	Number of Cells	-
O	Oxygen	-
p_{BP}	Regulated Back Pressure	atm
P_{comp}	Compressor Power	W
$P_{fuel,c}$	Chemical Power Obtained from Fuel	W

p'_{H_2}	Partial Pressure of Hydrogen	atm
P_{net}	Net Power	W
p'_{O_2}	Partial Pressure of Oxygen	atm
P_{others}	Other Auxiliary Power	W
P_{out}	Net Output Power	W
P_s	Stack Power	W
P_{sn}	Normalized Stack Power	W
p_{tank}	Regulated Tank Pressure	atm
R	Gas Constant	J mol^{-1} K^{-1}
R_{act}	Activation Resistance	Ω
R_{cm}	Motor Constant	Ω
R_{conc}	Concentration Resistance	Ω
r_m	Membrane Resistivity	Ω
R_{ohm}	Ohmic Resistance	Ω
S_b	Bulk Concentration in the Gas Channels	mol cm^{-3}
S_s	Surface Concentration of Reaction Sites	mol cm^{-3}
T	Stack Temperature	K
t_m	Membrane Thickness	cm
T_n	Normalized Stack Temperature	K
$V_{o,cell}$	Reference Potential	V
$V'_{o,cell}$	Reference Potential at Standard Test Condition	V
V_a	Anode Volume	m^3
V_{act}	Activation Voltage Drop	V
V_c	Double Layer Capacitor Voltage	V
V_{cc}	Cathode Volume	m^3
V_{cm}	Motor Voltage	V
V_{conc}	Concentration Voltage Drop	V
V_{load}	Load Voltage	V
V_{nernst}	Reversible Potential	V
V_{ohm}	Ohmic Voltage Drop	V
V_{out}	Effective Output Voltage	V
α	Number of Participating Electrons	-
ΔH	Low Heating Value of Hydrogen	kJ mol^{-1}
η	Electrical Efficiency	%
η_s	Stack Efficiency	%
λ	Membrane Water Content	-
$\sigma_1 \ldots \sigma_4$	Activation voltage drop parametric coefficients	V or V K^{-1}
ϕ	Temperature Constant	V K^{-1}

ω_{cp}	Rotational Speed of the Motor	rad s^{-1}

DC-DC Boost Converter

Symbol	*Parameter*	*Unit*
d	Duty Ratio	-
i_C	Capacitor Current	A
i_D	Diode Current	A
i_L	Inductor Current	A
i_o	Load Current	A
R_{equiv}	Equivalent Resistance	Ω
R_{load}	Load Resistance	Ω
V_o	Load Voltage	V

Hysteresis Current Controller

Symbol	*Parameter*	*Unit*
Δhys	Hysteresis Bandwidth	A
Δi_-	Lower limit	A
Δi_+	Upper limit	A

Tracking Techniques

Symbol	*Parameter*	*Unit*
a_{mep}	Perturbation Amplitude for MEP	-
a_{mpp}	Perturbation Amplitude for MPP	-
$b_1 \ldots b_{11}$	Constants for MDT FFF Design	-
dI	Perturbation Step Size	A
I_0	Initial Current	A
i_{mdt}	Midpoint Reference Current	A
i_{mep}	Maximum Efficiency Point Current	A
i_{mpp}	Maximum Power Point Current	A
I_{old}	Previous PEMFC Current	A
$I_{old_{dd}}$	Stack Current at the Start of Perturbation	A
i_{ref}	Reference Current	A
k_{mep}	Adaptation Gain for MEP	-

k_{mpp}	Adaptation Gain for MPP	-
N	Normalized Number of Cells	-
P_{old}	Previous PEMFC Power	W
P_{on}	Normalized Net Output Power	W
u	Scaling Factor for MDT FFF Design	-
V_b	Battery Voltage	V
V_{bmax}	Battery Voltage Limit	V
V_{old}	Previous PEMFC Voltage	V
ξ	ESC Demodulated Output Signal	-
ψ	Sliding Surface	-
ω	Perturbation Signal Frequency	rad s^{-1}
ω_e	Perturbation Signal Frequency for MEPT	rad s^{-1}
ω_h	High-pass Filter Cut-off Frequency	rad s^{-1}
ω_{he}	High-pass Filter Cut-off Frequency for MEPT	rad s^{-1}
ω_l	Low-pass Filter Cut-off Frequency	rad s^{-1}
ω_{le}	Low-pass Filter Cut-off Frequency for MEPT	rad s^{-1}

Economic Analysis

Symbol	*Parameter*	*Unit*
C_c	Capital Cost	$
$C_{MDT/MEPT}$	Cost Including Additional Stacks	$
$C_{an,tot}$	Total Annualized Cost	$ yr^{-1}
C_b	Cost of Boiler	$
C_{diesel}	Cost of Thermal Energy Supplied by the Boiler	$ kWh^{-1}
C_{NPC}	Total Net Present Cost	$
COE	Cost of Electricity	$ kWh^{-1}
$C_{t,PEM}$	Cost of Thermal Energy Supplied by the PEMFC	$ kWh^{-1}
E_{AC}	AC Load	kWh yr^{-1}
E_{DC}	DC Load	kWh yr^{-1}
E_t	Thermal Load	kWh yr^{-1}
H_p	Quantity of Hydrogen Produced by Electrolyzer	kg yr^{-1}
H_r	Quantity of Hydrogen Fuel	kg
H_t	Quantity of Remaining Hydrogen	kg
i	Annual Real Interest Rate	%
$LCOE$	Levelized Cost of Electricity	$ kWh^{-1}
N_{yr}	Lifetime of the Project	yr

P_{elec}	Electrolyzer Rated Power	W
$P_{inverter}$	Inverter Rated Power	W
P_{load}	Maximum Power Required by the Load	W
P_{MPPT}	Power at maximum power point	W
P_{MEPT}	Power at maximum efficiency point	W
P_{MDT}	Power at midpoint	W
P_{rating}	PEMFC rated power	W
η_p	Efficiency of Power Converter	%
η_t	Mean Total Efficiency	%
η_{ther}	Thermal Efficiency	%

Chapter 1

Introduction

Fuel cells (FCs) transform the chemical energy liberated during the electrochemical reaction to electrical energy. Fuel cells have the potential to operate as a primary energy source with high efficiency, quiet operation, high energy density, and low cost of electricity [1]. The fuel cell market is rapidly expanding and the megawatts of fuel cells shipped worldwide per year has increased from 65 MW in 2009 to 181 MW in 2014, which is a 174% increase, as shown in Fig. 1.1 [2].

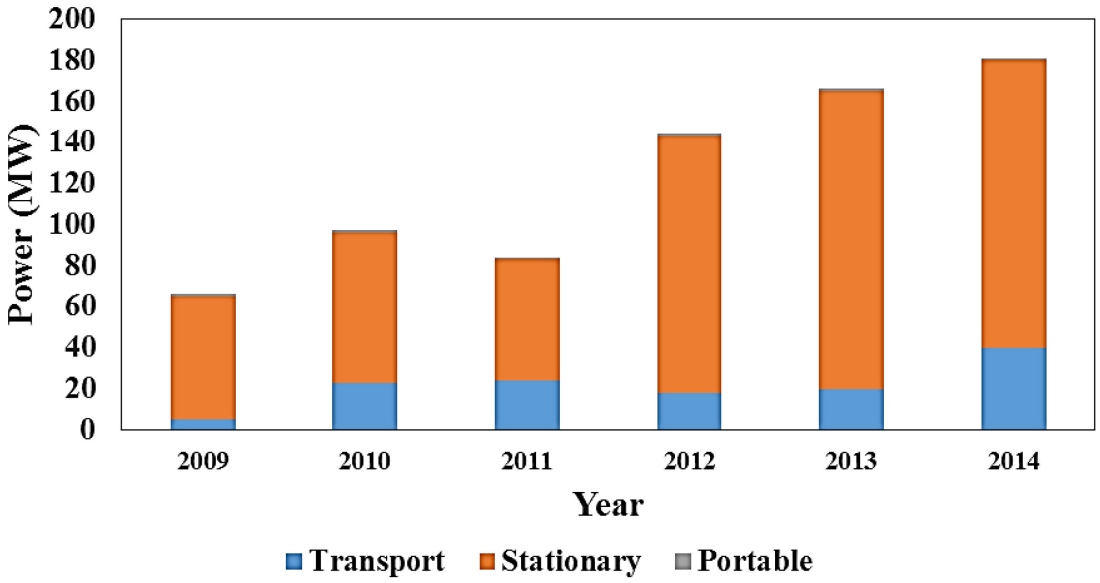

Fig. 1.1. Megawatts of fuel cells shipped worldwide based on the application [2]

In the case of transportation applications, the Toyota automobile company has predicted a massive increase in the amount of fuel cells that will be produced for

transportation applications with the introduction of the Toyota Mirai PEMFC car in 2015, as shown in Fig. 1.2 [3]. On the other hand, the stationary power applications are also gaining momentum as the Dutch fuel cell company Nedstack is installing a first-of-its-kind 2 MW PEMFC in China [4].

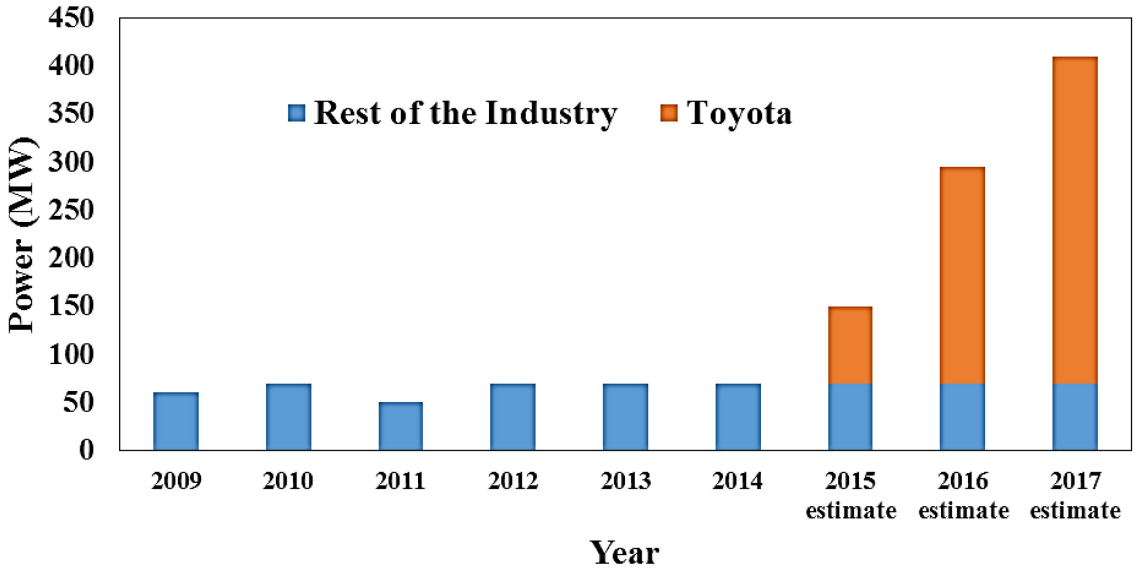

Fig. 1.2. Megawatts of PEMFCs produced worldwide for transportation applications [3]

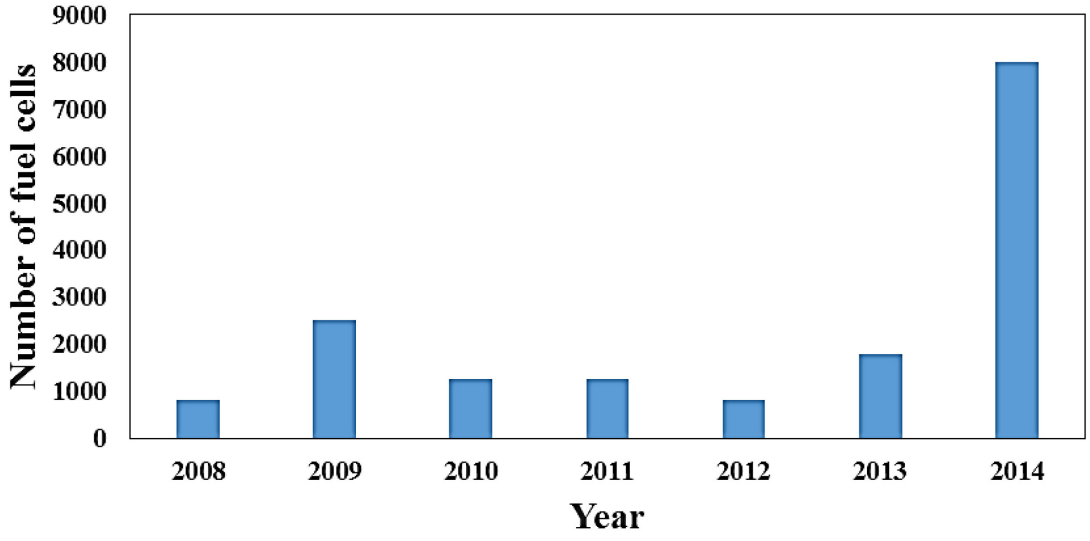

Fig. 1.3. Number of portable fuel cells shipped worldwide [2]

As shown in Fig. 1.3, the number of portable fuel cells shipped worldwide is also increasing drastically [2]. The financial report of the Ballard power systems for the last quarter of 2015 indicates that 26% of its revenue is from portable fuel cell products, which shows that FCs in portable applications are also increasing in demand [5].

The basic components required for FCs are similar to those required for batteries, such as the anode, cathode, and electrolytes. The output voltage obtained from the fuel cell is typically around 1.2 V (theoretically). The actual output voltage is less than 1.2 V due to several losses in the fuel cell. Therefore, single fuel cells are stacked in series or parallel to obtain the required voltage and current, respectively. FCs can be classified into two groups based on the type of fuel. The proton exchange membrane fuel cell (PEMFC), alkaline fuel cell (AFC), and phosphoric acid fuel cell (PAFC) are supplied with hydrogen (H_2) as fuel to produce electricity and water (by-product). The solid oxide fuel cell (SOFC), direct methanol fuel cell (DMFC), and molten carbonate fuel cell (MCFC) are supplied with hydrocarbon fuels to produce electricity and carbon dioxide (by-product) [6].

In order to generate green energy, hydrogen-based FCs are preferred over carbon-fuel-based FCs. The specific energy of hydrogen is also high when compared to other types of fuels as shown in Fig. 1.4 [7]. Hence, fuel cells with hydrogen fuel are commonly used for stationary, transportation, and portable applications. AFCs have superior efficiency when compared with PEMFCs and PAFCs; however, they are highly sensitive to CO_2, which reduces the durability of the AFCs. In the case of the PAFCs, the tolerance to impurities in the fuel and the operating temperature are high when compared with PEMFCs and AFCs. The efficiency of the PAFC can be increased to 80% with combined heat and power (CHP) configuration, but the electrical efficiency is very low (typically 37% - 42%).

On the other hand, PEMFCs are highly efficient and durable when compared with PAFCs and AFCs. PEMFCs also exhibit quick start up and moderate operating temperature. All of these above-mentioned advantages indicate that the PEMFC is a suitable FC for transportation, portable, and stationary power applications. Hence, the PEMFC is considered in this work to analyse the performance of the tracking techniques.

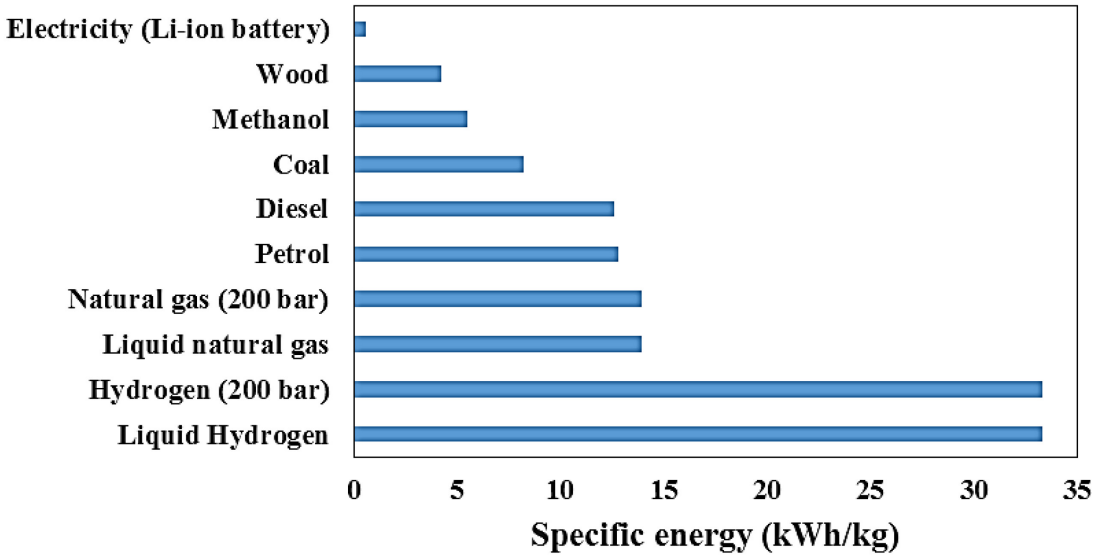

Fig. 1.4. Specific energy of different fuels [7]

PEMFCs exhibit non-linear output characteristics, as shown in Fig. 1.5. There exist unique operating points, namely the maximum power point (MPP) at which the PEMFC produces maximum power; and the maximum efficiency point (MEP) at which the PEMFC operates at maximum efficiency. The lifetime of the PEMFC can be increased by operating at a constant load [8]. Hence, it is ideal to select the maximum power point (MPP) or the maximum efficiency point (MEP) as the constant operating point. The MPP and MEP are influenced by changes in the PEMFC operating and loading conditions. Therefore, a power management system is required to operate at the required operating point (MPP or MEP)

throughout the operation of the PEMFC. The power management system consists of a power converter with tracking controller to track the changes in the required operating point. It is connected in-between the load and the PEMFC. In order to analyse the performance and the economic impacts of the tracking techniques, several experimental runs are required, which are expensive due to high fuel cell cost. Hence, the development of an accurate simulation model of the PEMFC, power converter, tracking controller, and real-time load are required to effectively analyse the performance and economic impacts of the tracking techniques.

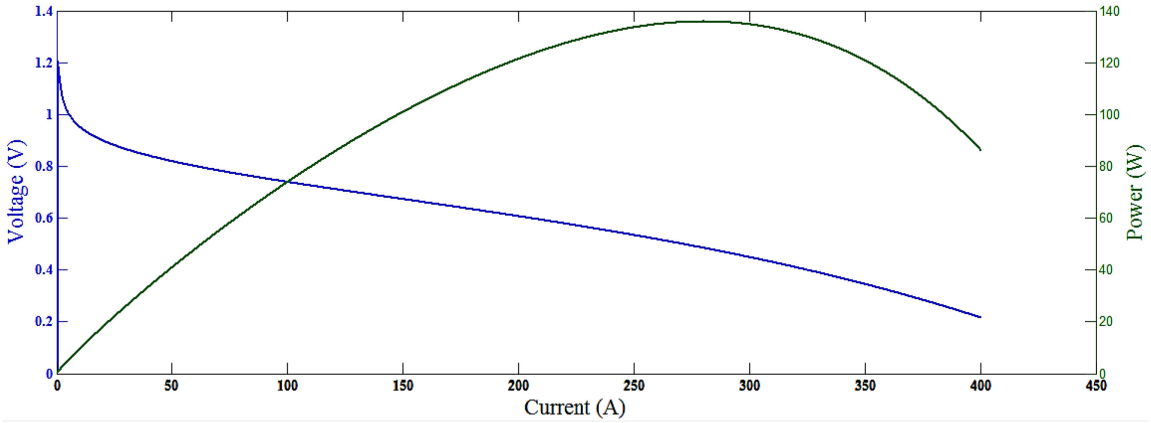

Fig. 1.5. PEMFC characteristics

1.1 Literature review

The rapid advancement in fuel cell technology and power electronics have become an added advantage to the growth of FC-based power systems. In [9], [10], the PEMFC Simulink model available in the MATLAB-Simulink® platform is used to represent the fuel cell model. However, the double-layer charge effect is neglected, parasitic power consumed by the auxiliary equipment is not taken into account, and ohmic (internal) resistance is set to a constant value, though in reality, it depends on membrane water content. Hence, a

complete versatile Simulink model of the PEMFC based on its electrical, electrochemical, and thermodynamic equations is required. The tracking control can be directly implemented in the PEMFC by controlling the inlet fuel flow, which in turn controls the stack current (i_{fc}) to operate at the required operating point [9]. However, the direct control is sensitive to load variations. On the other hand, the tracking control can be implemented using a DC-DC converter that follows a reference signal generated by the tracking algorithm to avoid the problems associated with load variations [11]–[13].

Several economic analyses of the PEMFC system have been presented in the literature [14]–[18]. However, the effects of the tracking techniques on the economics of the PEMFC have not been analyzed. A detailed literature review of the required components for the analysis of tracking techniques and their impacts on the cost of electricity (COE) is presented in the following subsections.

1.1.1 PEMFC Models

A detailed analysis of tracking techniques with a high degree of accuracy using simulation studies requires a complete and versatile model of the PEMFC. Literature on the PEMFC models can be found in [19]–[30]. In [22], the authors developed steady state and dynamic PEMFC models using the curve fitting method based on the experimental results obtained from a 5 kW PEMFC system. However, the developed model is not generic and therefore is not suitable for the analysis of the performance of the tracking techniques for a wide range of PEMFC systems with different ratings and configurations. To overcome this problem, several generic PEMFC models have been proposed using state space and partial differential equations based on the electrochemical, thermodynamic, and electrical

properties of the PEMFC [23]–[26]. However, the cathode and anode reactant flow models, which help in realising hydrogen and oxygen consumption rate and partial pressure for various operating conditions, are not taken into consideration. This problem has been addressed by developing reactant flow models to obtain more detailed information regarding hydrogen and oxygen utilization, which influences the performance of the PEMFC [27], [28]. Nevertheless, the concentration voltage drop was not taken into account, which makes the model incomplete. All the above-mentioned limitations are eliminated by developing a complete PEMFC model in [29], [30]. The stack efficiency of the PEMFC can be obtained using these models; however, calculating the PEMFC system efficiency, which requires the power consumed by the auxiliaries, is not possible.

Finally, the authors in [31] developed a complete model involving electrochemical and mechanical equations to accurately represent all the components of PEMFC with auxiliary equipment, such as air compressor, water management system, and heat exchanger system. The resulting model is very complex, although it provides an in-depth and accurate analysis of the behaviour of PEMFC for various operating and loading conditions.

In this thesis, a net output power model using fast flexible space filling design [32] is proposed to obtain an accurate, model-independent, and less complex air compressor model. A PEMFC Simulink model is developed, which combines the relevant features of published models [25], [27]–[31], [33] that are associated with the stack design and reactant flow models to obtain a complete and versatile PEMFC model.

1.1.2 Power Converter

In the case of indirect implementation of the tracking control, both the topology and the configuration of the power converter connected between the PEMFC and the load play a significant role. The output of the PEMFC is DC; hence, the DC-DC converter and DC-AC converter are the possible converter configurations that can be implemented. The tracking technique can only be implemented using a Z-source inverter in the case of the DC-AC converter to achieve the voltage boost, as well as the tracking requirements [34]. However, the control becomes complex, and the speed of the tracking technique deteriorates.

In the case of the DC-DC power conversion system, the coupled inductor Cuk converter is used to implement the MPPT technique based on nonlinear curve fitting and recursive least-squares estimation [35]. The major disadvantage of the DC-DC Cuk converter is the high number of reactive components and high current stress on the switch, diode, and capacitor. In general, DC-DC converters such as buck, boost, and buck-boost converters are commonly used to implement the tracking technique [36]. The buck-boost converter is used to implement the tracking control in [37]; however, it has limitations, such as negative output voltage for positive input voltage, no common ground, and requirement of p-channel metal-oxide-semiconductor field-effect transistor (PMOSFET). In the case of the MPPT implementation using the buck converter [38], there is a possibility of the battery (load) discharging into the PEMFC due to the absence of a blocking diode. The DC-DC buck converter also reduces the output voltage, which is not suitable for FCs that require voltage boost to meet the application requirements. In general, the DC-DC boost converter

is preferred over the buck and buck-boost converter due to the presence of the blocking diode at the load end and its ability to provide the required voltage boost [36].

1.1.3 Tracking Techniques

The main objective of the tracking technique is to find and operate at the maximum point, which may be the maximum power point (MPP) in the case of the maximum power point tracking (MPPT) technique or the maximum efficiency point (MEP) in the case of the maximum efficiency point tracking (MEPT) technique. The maximum point is affected by the changes in the operating conditions. Hence, the tracking technique should operate in such a way as to track all the changes to maintain the operation of PEMFC at the maximum point. The net output power (P_{out}) or efficiency (η) is given as input to the tracking technique to track MPP or MEP, respectively. The same tracking algorithm can be used to track MPP and MEP. Several tracking algorithms designed specifically for photovoltaic (PV) applications have been presented in the literature [39]–[45]. In this section, the tracking algorithms that are suitable for FCs are discussed.

The tracking algorithms were mainly developed to track the MPP of PV arrays. Later some of these algorithms were implemented to track the MPP of wind turbines and FCs. A brief description of the algorithms follows:

- The incremental conductance (IncCond) algorithm compares the instantaneous conductance (I/V) to the incremental conductance (ΔI/ΔV) of the fuel cell to determine the peak point [40]. It has the ability to track the maximum point under rapidly varying operating conditions. However, the incremental conductance

algorithm is complex. The accuracy and tracking speed of the IncCond algorithm depends on the step size of the stack current [46].

- The perturb and observe (P&O) algorithm is similar to hill climbing. The stack current increases step by step until the maximum point is reached. However, the P&O algorithm never operates at the maximum point; it always oscillates around it [39]. A large step size will result in rapid response; however, it decreases the accuracy of the P&O algorithm. On the other hand, a smaller step size results in low tracking speed, and the system may not reach a steady state [46].
- The fuzzy logic control (FLC) algorithm eliminates the oscillation around the maximum point [41]. However, the fuzzy logic algorithm is model dependent, complex, and its accuracy is based on the knowledge of the user or control engineer in choosing the right error computation [39], [41], [42].
- The voltage and current based maximum point tracking algorithms are developed to reduce the complexity [43]. Nevertheless, they depend on the regression equation based on the current and voltage corresponding to the maximum point, which leads to a model-dependent algorithm.
- The sliding mode control (SMC) algorithm is developed to overcome the problem of model-dependence [44]. This algorithm operates based on the principle that the value of the slope at the maximum point is zero. However, the implementation complexity of the algorithm is high.
- In order to overcome all the above-mentioned limitations of the tracking algorithms, the extremum seeking control (ESC) algorithm is introduced [11]. The ESC

algorithm is model independent, fast, accurate, and less complex when compared with other tracking algorithms.

In this thesis, the ESC, P&O, and SMC tracking algorithms are implemented to investigate the performance of the maximum power point tracking and maximum efficiency point tracking techniques.

1.1.4 Economic Analysis

The efficiency and economics of the PEMFC are interrelated [14]. The cost of electricity (COE) plays a significant role in selecting the energy source. Hence, a detailed economic analysis of the PEMFC is required. Economic analysis of a hybrid system with PEMFC and PV arrays used to power a telecommunication tower is considered in [16]. The economic analysis was carried out using an optimization tool to find the low value of COE. However, most of the power required by the load in this system is supplied by the PV, which resulted in an incomplete economic analysis of the PEMFC. A similar hybrid system with wind turbines replacing the PV arrays is used to power a building in [17]. In this case, several locations and configurations of the wind turbine and PEMFC are considered. However, the wind turbine provides most of the power to the building and the economics of the PEMFC are not investigated in detail. In order to obtain a detailed economic analysis of the PEMFC, a standalone PEMFC system should be considered to overcome the above-mentioned limitations.

A detailed economic analysis of a standalone PEMFC is presented in [14], [15]. The impacts of the power density and efficiency of the PEMFC on the COE are discussed. However, real-time loads are not considered; instead, a load with step variation at specific

intervals is considered in the investigation. The efficiency calculation is also based on an expression that ignores the power consumed by the auxiliaries. Finally, to overcome the above-mentioned limitations, a real-time load profile of a residential building is considered in the investigation [18]. The PEMFC is supplied with hydrogen from the reformer and the cost of all the components involved in the system is taken into account to obtain an accurate value of the COE. Yet an accurate economic analysis of PEMFC generation system with different tracking techniques is lacking in the literature.

1.1.5 Limitations of Previous PEMFC Systems with Tracking Control

The number of PEMFCs with tracking techniques reported in the literature to date is very limited. The first attempt to track the MPP in a PEMFC was based on a curve fitting approach [45], which is model-dependent and undesirable. The ESC algorithm was directly implemented to track the MPP by controlling the fuel flow of the PEMFC [9], [47]. The inbuilt model available in the Simulink was used to represent the PEMFC. This reduced the number of accessible parameters required to evaluate the performance of the PEMFC for different operating conditions. This problem is resolved by using the PEMFC model based on electrochemical and electrical equations in [48]. Nevertheless, the direct implementation of the tracking technique is sensitive to load variations, which is a major disadvantage. The load sensitivity problem is resolved by introducing a DC-DC power converter with a tracking controller between the PEMFC and the load [49]–[51].

The efficiency of the PEMFC at the MPP is low due to its non-linear characteristics. The low efficiency operation leads to increased fuel consumption, which in turn increases the cost of fuel consumed [14].

In order to solve the low efficiency problem, the MEPT technique is introduced to track the MEP of the PEMFC [52]. A complete model involving electrochemical and mechanical equations to accurately represent all of the components of the PEMFC is used to track the MEP based on the ESC algorithm [13]. The compressor model is based on a static motor equation that is not suitable for dynamic analysis. Finally, a dynamic compressor model based on the stack current (i_{fc}) is developed to accurately calculate the efficiency in [31]. However, the developed model is highly complex. The low efficiency problem at the MPP is resolved, but the output power of the PEMFC at the MEP is very low (~28% of MPP). Hence, a bigger and more expensive PEMFC would be required to deliver high output power at high efficiency. This is a major disadvantage.

An optimum operating point was proposed to achieve moderate efficiency and power [53]. Nevertheless, the selection of the optimum point is random and the variations in operating conditions are not taken into account. For the above-mentioned reasons, it is necessary to develop an alternative tracking technique that can track all the variations in the desired operating point (trade-off point).

1.2 Thesis Objectives

The goal of the thesis is to develop a detailed economic analysis of the PEMFC, taking into account the impact of the tracking techniques on the COE. In order to achieve the proposed goal, a new technique, namely the midpoint tracking (MDT) technique, is

introduced. All the limitations associated with PEMFC models are also resolved by developing a versatile PEMFC Simulink model based on the electrical, electrochemical, double layer charge effect, reactant flow, and thermodynamic equations.

The tracking technique used in the thesis employs a DC-DC converter to avoid the load sensitive problems discussed in the previous sections. The configuration of the entire system used to investigate the performance of the tracking technique is shown in Fig. 1.6. The components required for the PEMFC system with tracking controller will be discussed throughout the thesis.

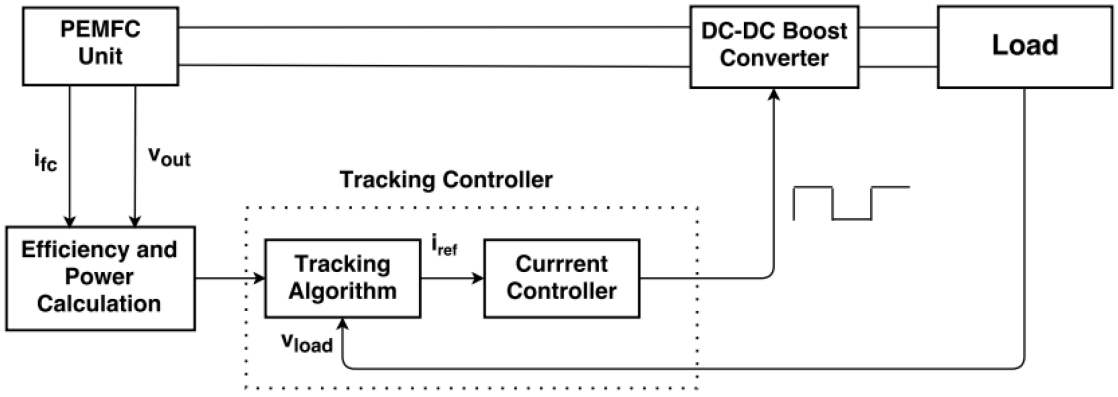

Fig. 1.6. System block diagram

The complexity and model dependency of the compressor model is eliminated by developing a simple and generic net output power model. The limitations, such as incomplete PEMFC model, absence of real-time load, impacts of hydrogen infrastructure on the COE, and impacts of tracking techniques on the COE associated with the economic analysis of the PEMFC are addressed. A detailed economic analysis is carried out by considering real-time loads, the cost of hydrogen infrastructure, cost of operation, cost of maintenance, and cost of PEMFC for ten different cases.

Based on the simulation results obtained from the tracking techniques and the economic analysis, a detailed comparison of the tracking technique is presented. Finally, based on the conclusions from the comparison of the tracking techniques, a procedure is developed to select a suitable technique for standalone PEMFC generation system.

1.3 Thesis Organization

The development of the economic analysis of the PEMFC system with tracking techniques are organized into six chapters. The introduction, literature review, limitations of previous work, and thesis objectives are discussed in Chapter 1.

In Chapter 2, the development of the PEMFC model based on the electrochemical, electrical, and thermodynamic equations is presented. The reactant flow models to represent the hydrogen and oxygen operating pressures are discussed. The development of the generic net output power model to obtain the net output power of the PEMFC and the power consumed by the auxiliaries is discussed. The results obtained from the developed Simulink model are compared with experimental results to validate the developed model.

The selection of the tracking algorithms is discussed in Chapter 3. The DC-DC boost converter model required for the tracking technique is developed in this chapter. A detailed comparison of the tracking algorithms used to track the MPPT and MEPT is discussed. The selected tracking algorithm is used to track the MPP and MEP of the PEMFC. Finally, the results of the simulation-based investigation of the MPPT and MEPT techniques are discussed.

The development of the MDT technique to overcome the limitations of the MPPT and MEPT techniques is presented in Chapter 4. The selection of a suitable operating point

for trade-off operation from several possible operating points is discussed. The development and validation of the midpoint tracking technique (MDT) based on the selected trade-off point are presented. The developed MDT technique is used to control the DC-DC converter and the results of the simulations are discussed.

In Chapter 5, the economic analyses of the PEMFC with MPPT, MEPT, and MDT are discussed. The configuration of the system and the components used for the economic analysis are presented and discussed. In order to investigate the performance of the PEMFC system over a wide range of operating conditions, a detailed analysis of ten different cases; and their configurations are discussed. The simulation results obtained from the energy system analysis tool (HOMER) are presented and discussed. An algorithmic procedure, based on the outcomes of the comparison of the tracking techniques, is presented to select a suitable tracking technique for a particular requirement of the PEMFC application.

In Chapter 6, the conclusions of the work are summarized and the contributions and scope for future work are discussed.

Chapter 2

Model of the Proton Exchange Membrane Fuel Cell

A PEMFC transforms the chemical energy liberated during the electrochemical reaction of hydrogen and oxygen to electrical energy. PEMFCs operate at moderate temperatures (60˚C - 100˚C) with quick start up, zero carbon emission, and high energy density when compared to other types of FCs such as SOFC, DMFC, and MCFC [54]. The water produced as a by-product from the PEMFC can be supplied to an electrolyzer to produce hydrogen.

A complete and versatile PEMFC model is required in order to evaluate the performance of the PEMFC under varying operating conditions. The model should be highly accurate to facilitate the investigation of the performance of tracking techniques. The advantages and limitations of previous PEMFC models discussed in the literature [11], [13], [23]–[27] are taken into consideration to develop a complete and versatile PEMFC model.

In this chapter, the modelling of PEMFC in Simulink is developed using electrochemical, electrical, and thermodynamic equations. Initially, the working principle

of the PEMFC is analyzed to obtain the behaviour of the PEMFC. Then, the expressions required to develop the stack model of the PEMFC with various associated losses are discussed. In order to obtain the hydrogen flow rate, oxygen flow rate, hydrogen partial pressure, and oxygen partial pressure, anode and cathode reactant flow models are developed. The validation of the developed model with published experimental results is presented to demonstrate the accuracy of the developed model.

Efficiency calculation of the PEMFC requires knowledge of the power consumed by the auxiliaries. Numerous parameters are required to develop a model to determine the parasitic power consumed, which increase the complexity of the system. In order to overcome this limitation, a generic model of an air compressor using fast flexible filling statistical design is developed and validated. Finally, the behaviour of the PEMFC under varying operating conditions is investigated using the developed model.

2.1 Principle of Operation

PEMFCs consist of three major components, the polymer electrolyte membrane (PEM), the cathode, and the anode, as shown in Fig. 2.1. The combination of these three components is referred to as the membrane electrode assembly (MEA). The PEM acts as the electrolyte in-between the anode and cathode, which is similar to a battery assembly. The anode and cathode electrodes are constructed with porous carbon fibre with flow channels embedded in the surface of electrodes. The PEM consists of a Nafion membrane with platinum catalyst. The selection of Nafion membrane thickness play a significant role in determining the energy density of the PEMFC [55]. The practical stack of the PEMFC

includes several other components other than the electrodes and electrolytes, as shown in Fig. 2.2.

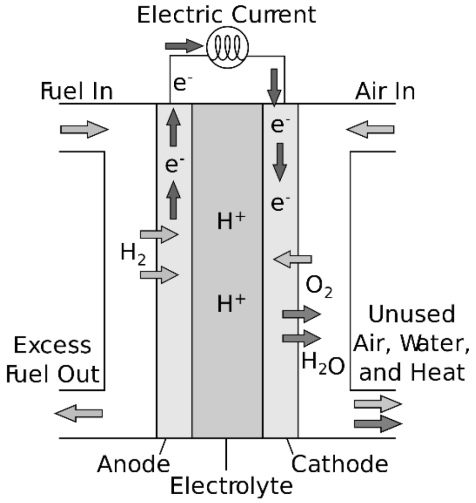

Fig. 2.1. Cross section of PEMFC

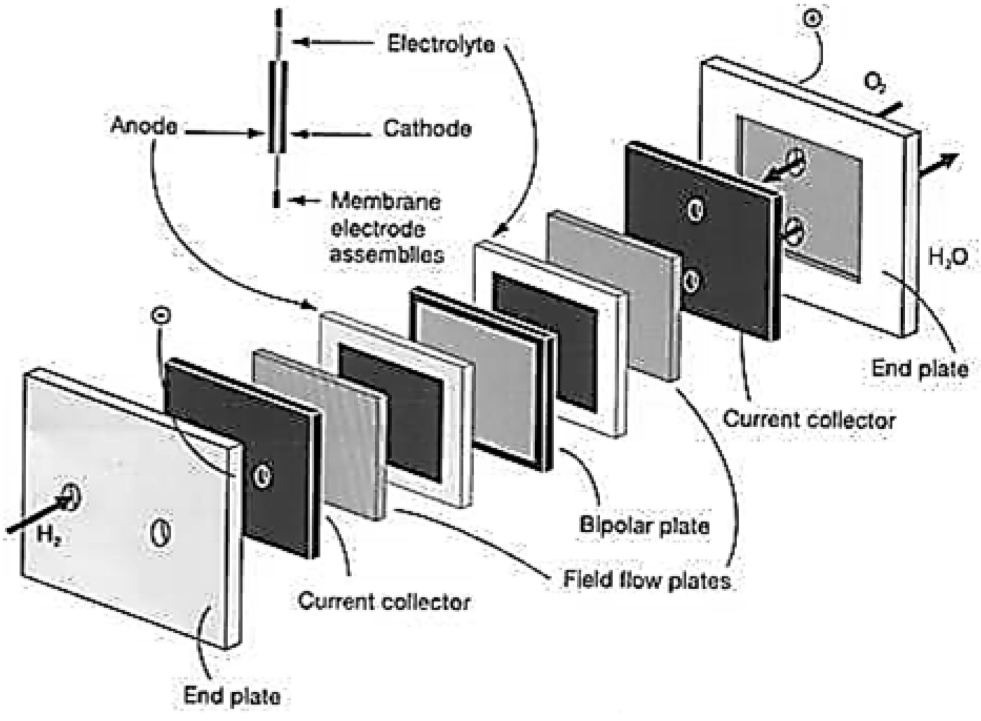

Fig. 2.2. Typical stack assembly of PEMFC

A gas diffusion layer (GDL) is placed between the MEA to reduce the friction between the flow plates and MEA. The effective utilization of flow plates increases the performance of the PEMFC. Current collector plates are used to collect electrons produced from the electrochemical reaction to produce electricity.

The hydrogen (fuel) is supplied to the anode side of the PEMFC and air is supplied at the cathode side of the PEMFC, as shown in Figs. 2.1 and 2.2. The PEM between the anode and cathode separates the protons and electrons of the supplied hydrogen by allowing the protons to pass through it and blocking the electrons. The blocked electrons pass through the external connection to produce electricity and enter the cathode side. The electrons entering the cathode side react with oxygen in the supplied air to form water. The energy from the chemical reaction which produces water is liberated as heat. The water produced is drained through the cathode outlet, as shown in Fig. 2.1. The unreacted or excess hydrogen in the anode side is circulated back to the hydrogen tank through the anode outlet. The process continues, and electricity is produced as long as the hydrogen is supplied. The equations of the electrochemical reaction are described as follows:

$$\text{Anode: } H_2 \rightarrow 2H^+ + 2e^- \tag{2.1}$$

$$\text{Cathode: } \tfrac{1}{2} O_2 + 2H^+ + 2e^- \rightarrow H_2O_{(l)} \tag{2.2}$$

where (*l*) indicates liquid state. The overall reaction is described as

$$\text{Overall: } H_2 + \tfrac{1}{2} O_2 \rightarrow H_2O_{(l)} + Heat \tag{2.3}$$

The PEMFC requires pressure regulator (PR) to maintain the pressure of hydrogen and oxygen at a certain level defined by the PEMFC control unit. The hydrogen storage tank supplies hydrogen to the PEMFC and is also used for storing hydrogen produced from the reformer or electrolyzer. The air compressor helps to supply the required amount of air with adequate pressure to the cathode. The pressure regulator is used to maintain a constant pressure inside the PEMFC stack. A heat exchanger is installed to take away the generated heat and maintain the required temperature levels described by the control unit. A general schematic of the PEMFC system is shown in Fig. 2.3.

In this thesis, the Ballard MK5-E PEMFC is considered for modelling the PEMFC in Simulink [11], [19], [56]. The Ballard MK5-E is a 5 kW PEMFC with 35 cells connected in series configuration. The unit is well researched and all the parameters required to develop an accurate PEMFC model in Simulink are available in the literature.

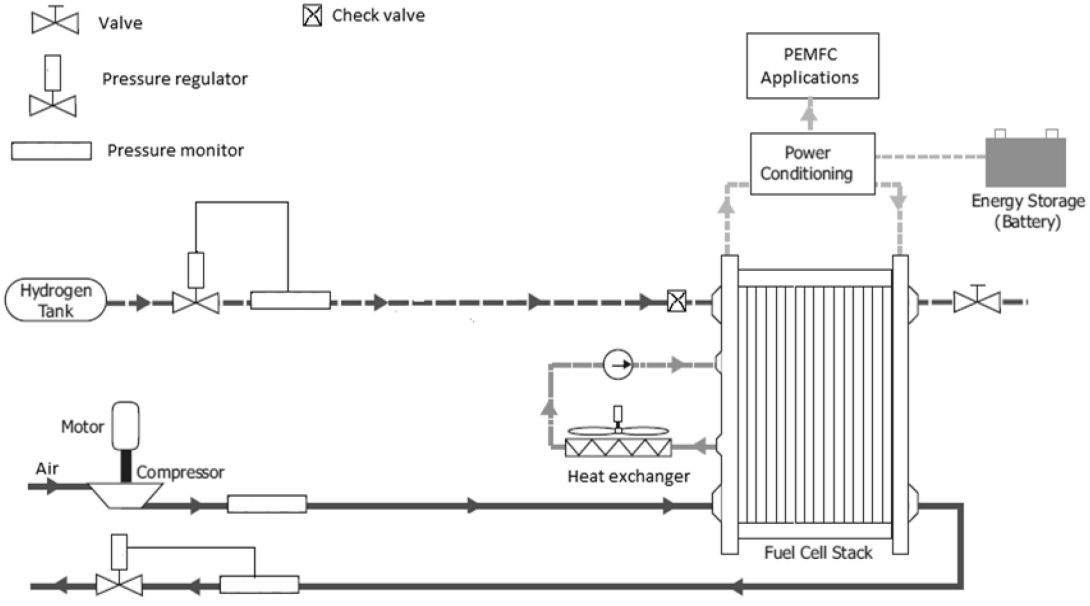

Fig. 2.3. Schematic of a PEMFC system

2.2 PEMFC Stack Model

The theoretical output voltage obtained from a PEMFC is around 1.2 V as mentioned in the introduction. However, the practical output voltage is less than the theoretical output voltage due to several losses associated with the PEMFC, as shown in Fig. 2.4. The stack model and expressions for calculating the ohmic, activation, and concentration losses of the PEMFC are discussed in the following subsections.

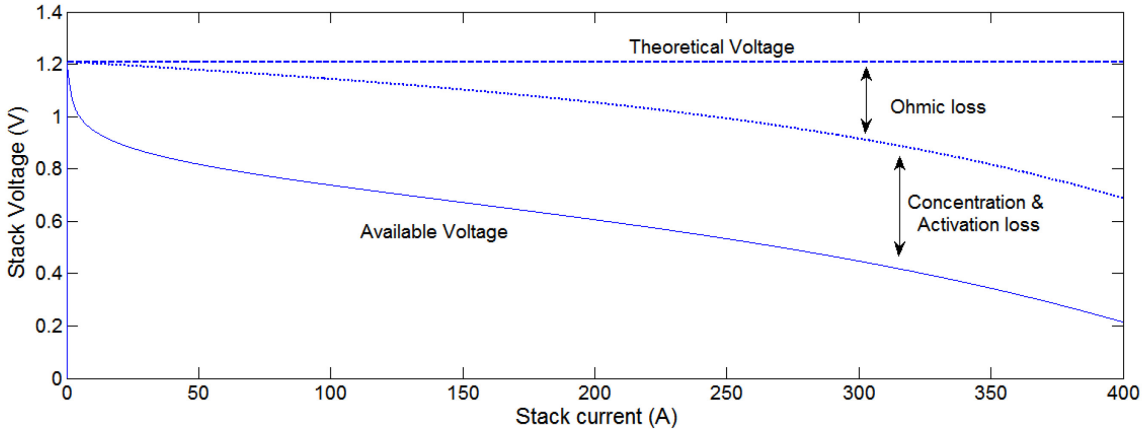

Fig. 2.4. I-V Polarization curve of PEMFC

2.2.1 PEMFC Output Voltage

The modified Nernst equation used to calculate the reversible potential of the chemical reaction explained in (2.3) is given as [57]

$$V_{Nernst} = V_{o,cell} + \frac{RT}{2F}\ln\left[p'_{H_2}\left(p'_{O_2}\right)^{0.5}\right] \tag{2.4}$$

where, R is the gas constant (J mol^{-1} K^{-1}); F is the Faraday constant (C mol^{-1}); p'_{H2} is the partial pressure of hydrogen (atm); p'_{O2} is the partial pressure of oxygen (atm); T is the

stack temperature (K). The reference potential ($V_{o,cell}$) of each cell considering the variation of stack temperature can be expressed as [57]

$$V_{o,cell} = V'_{o,cell} - \varphi(T - 298) \tag{2.5}$$

where, φ is the temperature constant; $V'_{o,cell}$ is the reference potential at standard test conditions (T = 298 K and pressure = 1atm). The generated current flows through the MEA assembly, which leads to ohmic and activation losses.

2.2.2 Ohmic Voltage Drop

The ohmic voltage drop is mainly due to the resistance offered to the flow of current by the electrodes and the PEM. However, accurate measurement of the ohmic resistance is generally difficult and an empirical approach is preferred, as discussed in [58]. The ohmic voltage drop in the PEMFC is represented by an internal resistance expressed in terms of the fuel cell stack current (i_{fc}), stack temperature (T), effective cell area (A), membrane thickness (t_m), and the membrane water content (λ) as [58]

$$V_{ohm} = i_{fc} \frac{r_m t_m}{A} \tag{2.6}$$

$$r_M = \frac{181.6\left[1 + 0.03\left(\frac{i_{fc}}{A}\right) + 0.062\left(\frac{T}{303}\right)^2\left(\frac{i_{fc}}{A}\right)^{2.5}\right]}{\left[\lambda - 0.634 - 3\left(\frac{i_{fc}}{A}\right)\right]\exp\left[4.18\left(\frac{T-303}{A}\right)\right]} \tag{2.7}$$

The value of λ indicates the membrane water content of the PEMFC and it can vary between 0 and 23, which is equivalent to 0% and 182% saturation. The value of λ ranging

from 15 and 23 is referred to as the super saturated region and the range of λ between 0 and 13 is called the sub saturated region. The stack is 100% humidified when the value of λ is 14.

The PEMFC can be operated in the super saturated region to improve its performance; however, the large quantity of water produced in this region floods the PEM, which leads to degradation of the membrane. In the case of the sub saturated region, the water production is low and hence, the flooding of the membrane is controlled, but the performance of the PEMFC is reduced. The mean value of λ is selected in many cases to simplify the analysis [11], [28]. In this thesis, the value of λ is varied between 10.5 and 17.5, which represents 75% and 125% of saturation. This range of λ is adequate for the analysis of the performance of the tracking technique around 100% humidity conditions. The ohmic voltage drop of the Ballard MK5-E model developed in Simulink is shown in Fig. 2.5.

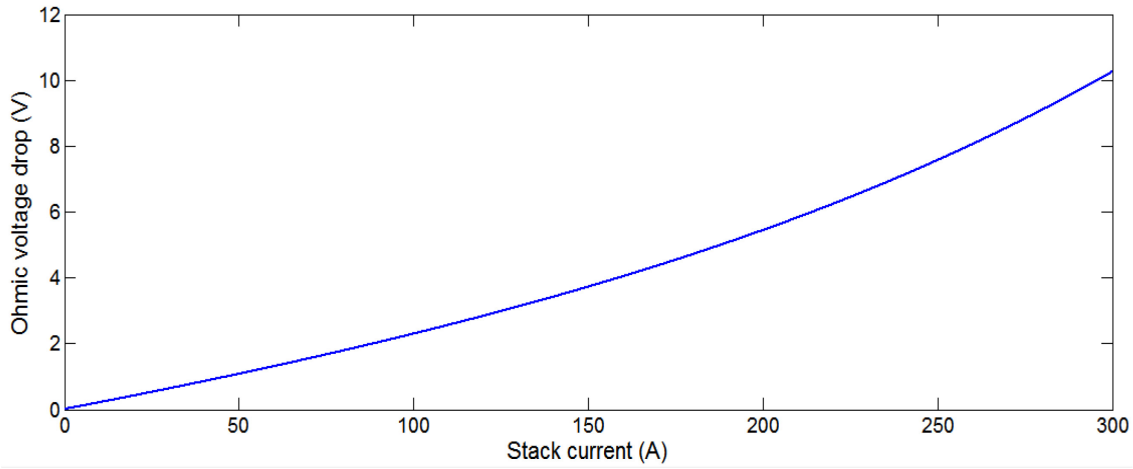

Fig. 2.5. Ohmic voltage drop

The parameters associated with the output voltage and ohmic voltage drop are tabulated in Table 2.1. The equivalent resistance of the ohmic voltage drop (R_{ohm}) is given as

$$R_{ohm} = \frac{V_{ohm}}{i_{fc}} \tag{2.8}$$

Table 2.1: PEMFC parameters for output voltage and ohmic voltage drop

Symbol	Parameter	Value	Unit
R	Gas constant	8.314	J mol^{-1} K^{-1}
F	Faraday constant	96487	C mol^{-1}
$V'_{o,cell}$	Standard reference potential	1.229	V
φ	Temperature constant	0.0085	-
t_m	Membrane thickness of Nafion 117	0.0178	cm
A	Effective cell area	232	cm^2
n	Number of cells	35	-

2.2.3 Activation Voltage Drop

The activation voltage is mainly dependent on the stack temperature (T) and stack current (i_{fc}). The process of oxygen reduction at the cathode is slow when compared with the process of hydrogen oxidation at the anode, which results in activation voltage loss. The activation voltage drop is mostly from the cathode reaction at the lower region of stack current. An empirical approach is used to calculate the activation voltage drop, which can be expressed as [58], [59]

$$V_{act} = \sigma_1 + \sigma_2 T + \sigma_3 T\left[\ln\left(c'_{O_2}\right)\right] + \sigma_4 T\left[\ln\left(i_{fc}\right)\right] \tag{2.9}$$

where,

σ_1 = -0.948

σ_2 = 0.00286 + 0.0002ln(A) + 4.3e^{-5}ln(c'_{H_2})

σ_3 = 0.000076

σ_4 = -0.000193

The anode reactant concentration (c'_{H_2}) and cathode reactant concentration (c'_{O_2}) at the membrane can be determined by using Henry's law, given by [28]

$$c'_{O_2} = 1.97e^{-1}\exp\left(\frac{498}{T}\right)p'_{O_2} \tag{2.10}$$

$$c'_{H_2} = 9.17e^{-1}\exp\left(\frac{-77}{T}\right)p'_{H_2} \tag{2.11}$$

The equivalent resistance of the activation voltage drop (R_{act}) is given by

$$R_{act} = \frac{V_{act}}{i_{fc}} \tag{2.12}$$

2.2.4 Concentration Voltage Drop

The concentration voltage drop is due to the mass diffusion from the gas channels. It is mostly attributed to the slow transportation of the reactants to the reaction site. The concentration voltage drop is predominant at high current densities [57]. The formation of water film at the anode and cathode also contributes to the concentration voltage drop. The concentration voltage drop is given as [57]

$$V_{conc} = \frac{RT}{\alpha F}\ln\left(\frac{S_s}{S_b}\right) \tag{2.13}$$

where, α is the number of electrons participating in the reaction; S_s is the surface concentration of reaction sites; S_b is the bulk concentration in gas channels. The calculation of these concentrations are difficult. Hence, an alternative expression based on Fick's and Faraday's law is used, as given below [57]

$$V_{conc} = \frac{RT}{\alpha F} \ln\left(1 - \frac{i_{fc}}{i_{limit}}\right) \tag{2.14}$$

where, i_{limit} is the maximum current that the PEMFC can operate (A).

The equivalent resistance of the concentration voltage drop (R_{conc}) can be expressed as

$$R_{conc} = \frac{V_{conc}}{i_{fc}} \tag{2.15}$$

A dynamic PEMFC model based on the electrical equivalent circuit is presented in [57]. There exists a capacitor across the equivalent resistance of the activation and concentration voltage drop as shown in Fig. 2.6.

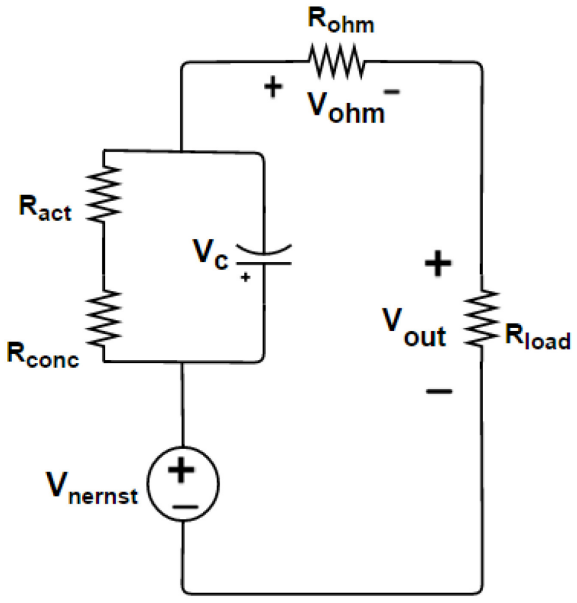

Fig. 2.6. Equivalent electrical circuit of PEMFC

The main cause of the capacitor across the R_{act} and R_{conc} and the expression to determine the voltage across the capacitor are discussed in the following subsection.

2.2.5 Double Layer-Charge Effect

The PEM between the anode and cathode acts like a dielectric material and thus, two charged layers of opposite polarity are formed across the boundary between the cathode and anode. This acts like a super-capacitor (C), which can store energy [57]. The accurate model of this capacitance is required to analyze the dynamic behavior of the PEMFC. The voltage across the capacitance (V_c) is given as [57]

$$V_c = \left(i_{fc} - C\frac{dV_c}{dt} \right)\left(R_{act} + R_{conc} \right) \tag{2.16}$$

where, C is the value of the capacitor which varies from 13 mF cm^{-2} to 42 mF cm^{-2} [56], [58]–[62]. Hence, an intermediate value is chosen, as shown in Table 2.2. The RC time constant determines the response time of the PEMFC for a sudden change in the operating conditions. The voltage drop across the capacitance of the Ballard MK5-E is shown in Fig. 2.7.

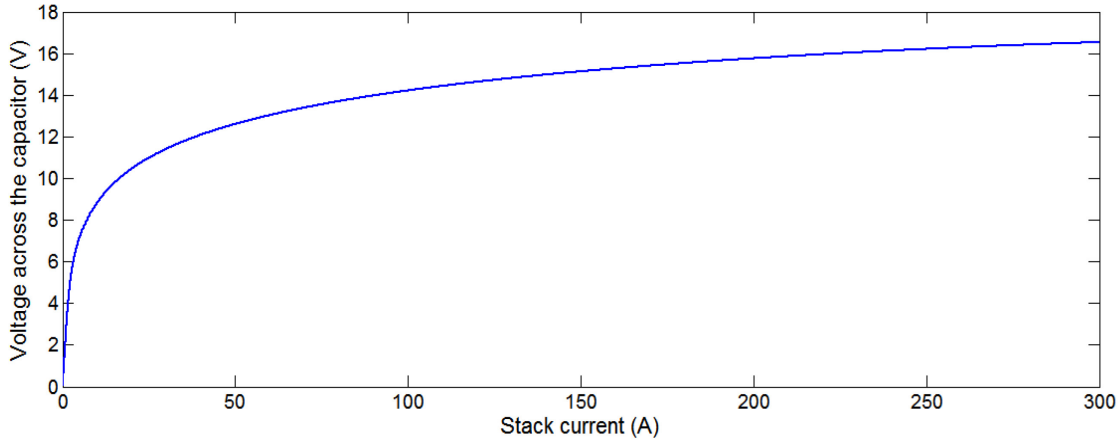

Fig. 2.7. Voltage drop across the capacitor

Table 2.2: PEMFC parameters for V_c

Symbol	Parameter	Value	Unit
α	Number of participating electrons	2	-
i_{limit}	Current limit	300	A
C	Capacitor value	35	mF cm^{-2}

Parameters associated with calculating the voltage across the capacitor are tabulated in Table 2.2. From Fig. 2.6, the effective output voltage (V_{out}) for n cells connected in series to obtain a stack can be obtained by using (2.17). In the case of parallel connected stacks, the effective voltage remains the same, but the output current will be multiplied with the number of fuel cells.

$$V_{out} = n\left(V_{nernst} - V_c - V_{ohm}\right) \tag{2.17}$$

The effective output voltage (V_{out}) obtained from this dynamic model is generic. Hence, the effective output voltage of different PEMFCs can be obtained by simply changing values of the parameters, such as the area of the cross section, membrane thickness, hydrogen pressure, oxygen pressure, and the number of stacks according to the requirement of the specified PEMFC.

2.3 Reactant Flow Model

The reactant flow model helps in calculating the flow and relative humidity of the reactants inside the PEMFC. The effective partial pressure of hydrogen and oxygen is obtained from the reactant flow models of the anode and cathode, respectively. The value of the partial pressure decreases as the stack current increases [28].

2.3.1 Cathode Flow Model

The airflow and the amount of air inside the PEMFC stack are represented using the cathode flow model. It is developed based on ideal gas law and molar conservation principles. The reactant pressure at any instance is expressed as [28]

$$\frac{V_{cc}}{RT}\frac{dp'_{O_2}}{dt} = f_{O_2,in} - f_{O_2,out} - f_{O_2,used} \tag{2.18}$$

where, V_{cc} is the cathode volume (m^3); $f_{O_2,in}$ is the oxygen inlet flow rate (mol s^{-1}); $f_{O_2,out}$ is the oxygen outlet flow rate (mol s^{-1}). The above equation can be modified based on the stack current and number of cells as follows [28]:

$$\frac{V_{cc}}{RT}\frac{dp'_{O_2}}{dt} = f_{O_2,in} - f_{O_2,out} - \frac{ni_{fc}}{4F} \tag{2.19}$$

The oxygen outlet flow can be obtained using the partial pressure of the oxygen inside the stack and the pressure of oxygen at the cathode outlet as [28]

$$f_{O_2,out} = f_c\left(p'_{O_2} - p_{BP}\right) \tag{2.20}$$

where, f_c is the cathode flow constant (mol $s^{-1}atm^{-1}$); p_{BP} is the regulated back pressure at the cathode outlet (atm). The partial pressure of oxygen can be obtained by substituting (2.20) in (2.19). As shown in Fig. 2.3, the cathode flow is controlled by a backpressure regulator (BPR) connected to the cathode outlet. This backpressure regulator helps in maintaining a constant pre-defined pressure from the FC control unit.

2.3.2 Anode Flow Model

The anode flow model helps to determine the flow rate and amount of hydrogen present inside the stack at any given instance. The anode reactant pressure can be found by using the same principle implemented for the cathode. The anode of the PEMFC is supplied with pure hydrogen (99.99%) from a storage tank. The reactant pressure at any instance can be expressed in terms of the volume of the anode (V_a), hydrogen inlet flow rate ($f_{H_2,in}$), hydrogen outlet flow rate ($f_{H_2,out}$), and amount of hydrogen used ($f_{H_2,used}$) as [28]

$$\frac{V_a}{RT}\frac{dp'_{H_2}}{dt} = f_{H_2,in} - f_{H_2,out} - f_{H_2,used} \tag{2.21}$$

The amount of hydrogen used inside the stack can be obtained using the number of cells and the stack current as [28]

$$f_{H_2,used} = \frac{ni_{fc}}{2F} \tag{2.22}$$

A pressure regulator regulates the hydrogen pressure at the input of the anode, as shown in Fig. 2.3, and circulates the excess hydrogen back to the anode. The hydrogen outlet rate can be obtained using the difference in hydrogen partial pressure and tank pressure as follows [28]:

$$f_{H_2,out} = f_a(p'_{H_2}, -p_{\text{tank}}) \tag{2.23}$$

where, V_a is the anode volume (m^3); f_a is the anode flow constant ($mols^{-1}atm^{-1}$); p_{tank} is the regulated tank pressure (atm). The partial pressure of hydrogen at any instance can be obtained using (2.21). The output voltage based on (2.17) is shown in Fig. 2.8.

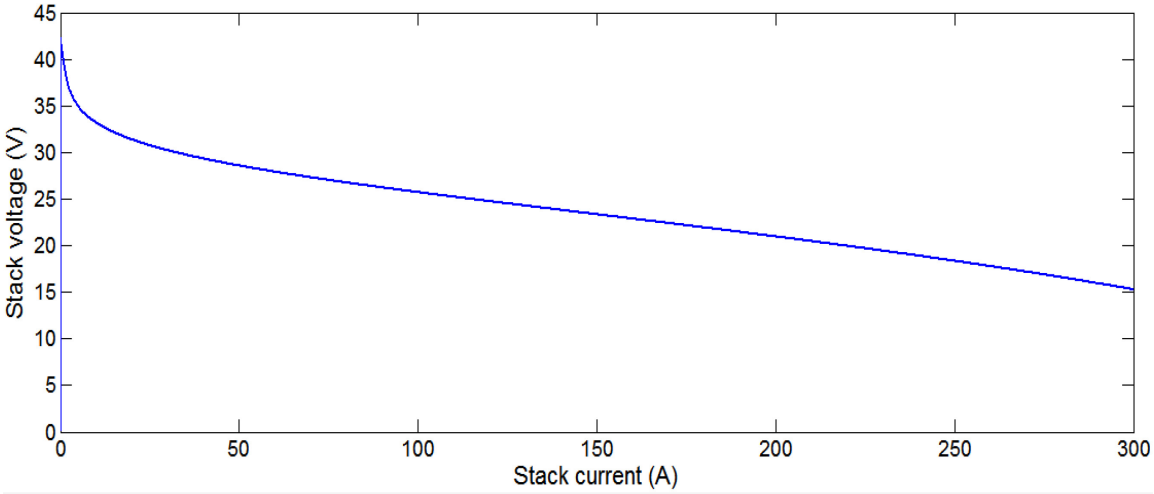

Fig. 2.8. I-V polarization curve

The values of the parameters associated with the cathode and anode flow modelling are tabulated in Table 2.3 [28].

Table 2.3: Parameters for the PEMFC reactant flow models

Symbol	Parameter	Value	Unit
V_{cc}	Cathode volume	0.01	m^3
f_c	Cathode flow constant	0.065	mol s^{-1} atm^{-1}
p_{BP}	Cathode outlet pressure	3	atm
V_a	Anode volume	0.005	m^3
f_a	Anode flow constant	0.065	mol s^{-1} atm^{-1}
p_{Bank}	Anode inlet pressure	3	atm

2.4 Validation of the PEMFC Model

The PEMFC model developed in Simulink using (2.1 – 2.23) is compared with experimental results of the Ballard MK5-E to validate the accuracy of the developed model. The validation of the developed PEMFC model plays an important role in determining the reliability of subsequent simulation results for the investigation of different tracking

techniques. The stack current and stack temperature from experimental results are taken into consideration [63]. The stack voltage output for the corresponding stack current and stack temperature is obtained from the developed Simulink PEMFC model. The simulated voltage versus experimental voltage plot of the PEMFC is shown in Fig. 2.9. From the figure, it can be seen that the developed model is accurate and the R^2 value for the stack voltage response is 0.98, which indicates a good fit.

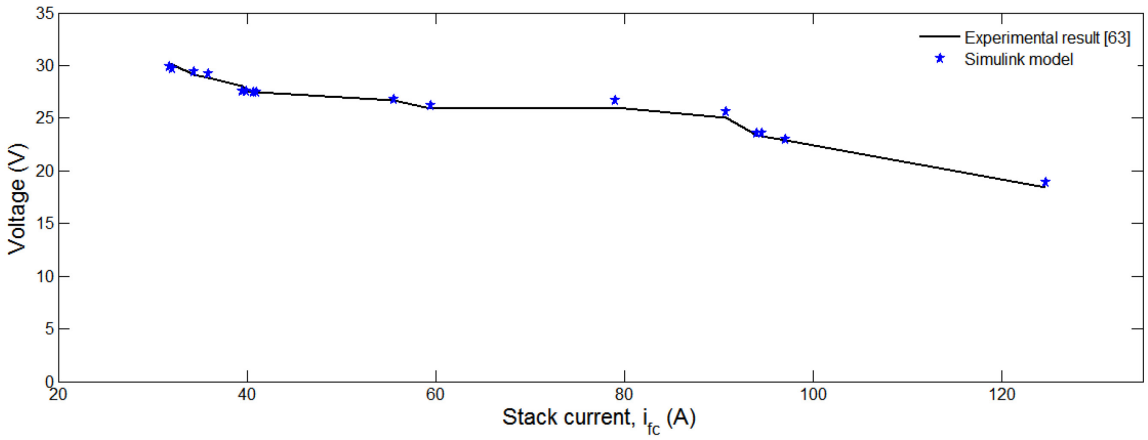

Fig. 2.9. Validation of developed PEMFC model

2.5 Model of Auxiliary Components

The PEMFC requires several auxiliary components to function properly, as shown in Fig. 2.3 [64]. The power consumed by auxiliaries is required for the accurate calculation of the net power (P_{net}) produced by the PEMFC. The power consumed by the auxiliary components of a 2 kW PEMFC system is shown using the Sankey diagram in Fig. 2.10. From the figure, it can be seen that the power required for the air compressor represents the major part of the power consumed by the auxiliary components. The power consumed by the other auxiliary equipment is very small and can be assumed constant. In many cases the

power consumed by other auxiliaries is assumed to be 2.75% to 3.5% of the rated power of the PEMFC considered [13], [52].

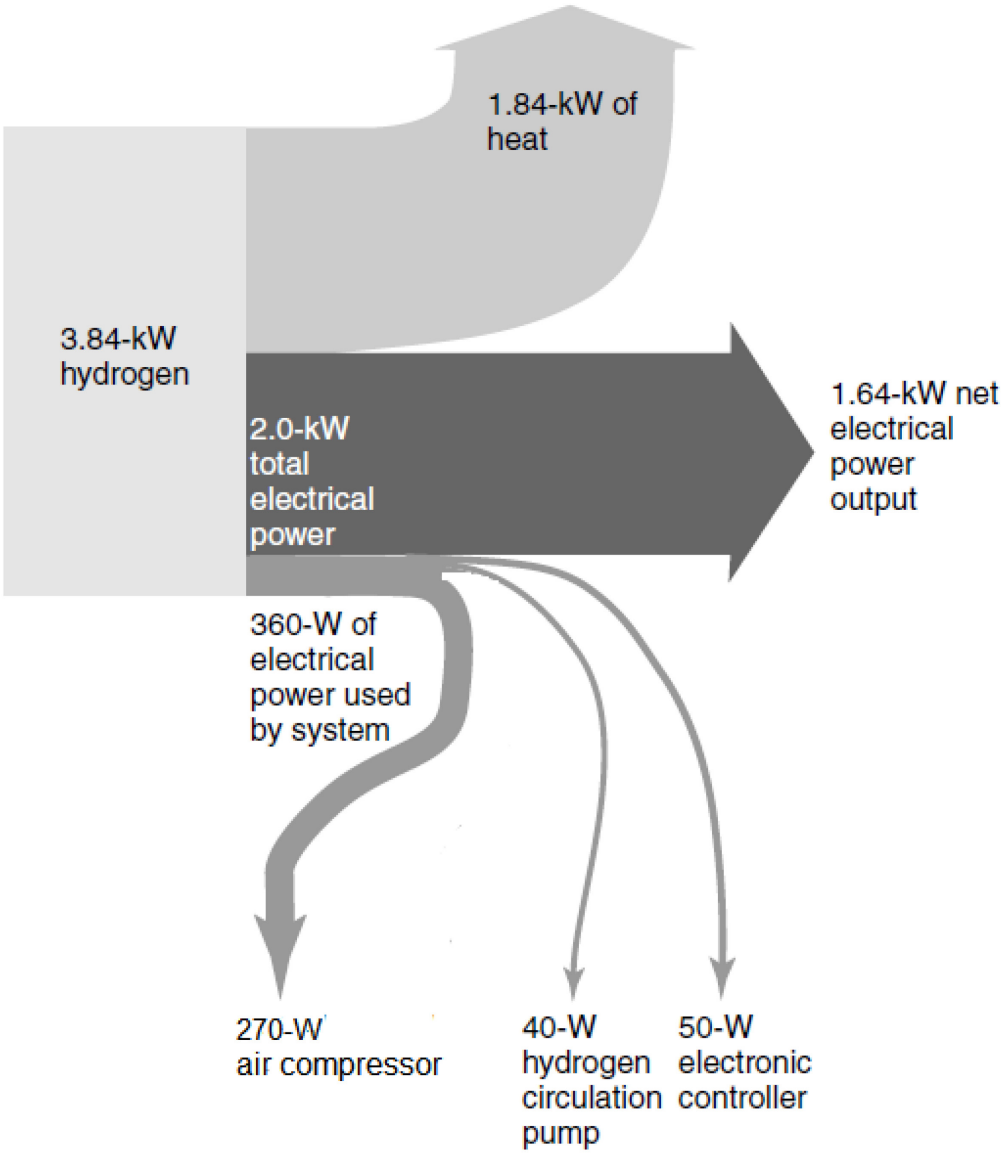

Fig. 2.10. Sankey diagram of a 2 kW PEMFC

The power consumed by the compressor depends on the stack current of the PEMFC [31]. A detailed compressor model is required to obtain the power consumed by the

compressor for a particular value of the stack current. The parameters and limitations of compressor models proposed in the literature are discussed in the following subsection.

2.5.1 Limitations of Air Compressor Models

The power consumed by the air compressor is obtained using a static motor equation, which is given by [13]

$$P_{compressor} = \frac{V_{cm}\left(V_{cm} - K_v \omega_{cp}\right)}{R_{cm}} \tag{2.24}$$

where, V_{cm} is the motor voltage (V); ω_{cp} is the rotational speed of the motor (rad/s); and K_v and R_{cm} *are* motor constants. The power obtained using (2.24) is valid for static models. Several other parameters are required to obtain an accurate compressor model. The curve fitting approach can be used to develop the compressor model, but this approach is sensitive to variation in more than one operating conditions and it is model-dependent.

To overcome this limitation, a complex compressor model has been developed using regression coefficients obtained from the compressor map [31]. This method involves detailed evaluation of the compressor parameters of a particular PEMFC and finding the required regression coefficients, which is highly complex and model-dependent. For all the above-mentioned reasons, a generic and simple compressor model is required to obtain the net power of the PEMFC. In this work, a generic compressor model using statistical design of experiment (DOE) methodology is developed.

2.5.2 Selection of a Statistical Design Methodology

The statistical design of experiment (DOE) methodology helps to identify the significant operating parameters to improve the performance of a system. The DOE methodology can also be used to build regression equations based on specified inputs. These regression equations are capable of representing the characteristics of a system with a high degree of accuracy.

In view of the complex and nonlinear nature of modern computer models, the classical response surface methodology (RSM) approaches, such as the central composite design (CCD) and Box-Behnken design (BBD), do not provide adequate coverage of the experimental area to provide an accurate model [65].

Space filling designs such as uniform design, Latin hypercube design, fast flexible filling design, and sphere packing design are able to generate a set of sample points that capture the maximum information between input-output relationships [65]. A review of different space filling designs presented in the literature shows that the fast flexible filling (FFF) design with maximum coverage of the design region, high accuracy, categorical factors, and constraints would be adequate for developing the net output power model [32].

2.5.3 Model of the PEMFC Net Power based on the Fast Flexible Filling Design

The fast flexible filling method forms clusters from random points in the design space [32]. Design points for the FFF design are generated by using large number of random points within the specified design region. These points are then clustered using a fast ward

algorithm into a number of clusters that equals the number of runs that are specified. The complex nonlinear characteristics of the PEMFC and the compressor can be well analyzed by using the FFF in the JMP statistical discovery software [32].

In order to develop a model-independent net power model, the regression equation is determined as a function of four factors, namely the membrane water content (λ), stack temperature (T), stack current (i_{fc}), and stack power (P_s). The levels of the factors considered in this FFF design are tabulated in Table 2.4.

Table 2.4: Factors and levels for net power FFF design

Factors	**Low level**	**High level**	**Unit**
T	323 (50˚C)	353 (80˚C)	K
λ	7	21	-
i_{fc}	0	300	A
P_s	0	10^5	W

Five thousand design points are used to accurately determine the net power equation. Design points (T, λ, i_{fc}) generated by the FFF design is considered as input to the PEMFC model in [31] to obtain the stack power (P_s). The stack power obtained for the corresponding combination of the design point is entered as the fourth factor in the net power FFF design. The scatter plot of the net power FFF design is shown in Fig. 2.11.

From the figure, it can be seen that the design points generated by the FFF design covers the entire design space of the PEMFC. The analysis of variance (ANOVA) is carried out based on p-values less than the value of $\alpha = 0.01$. The R^2 value for the net power response is 0.999995, which indicates a good fit.

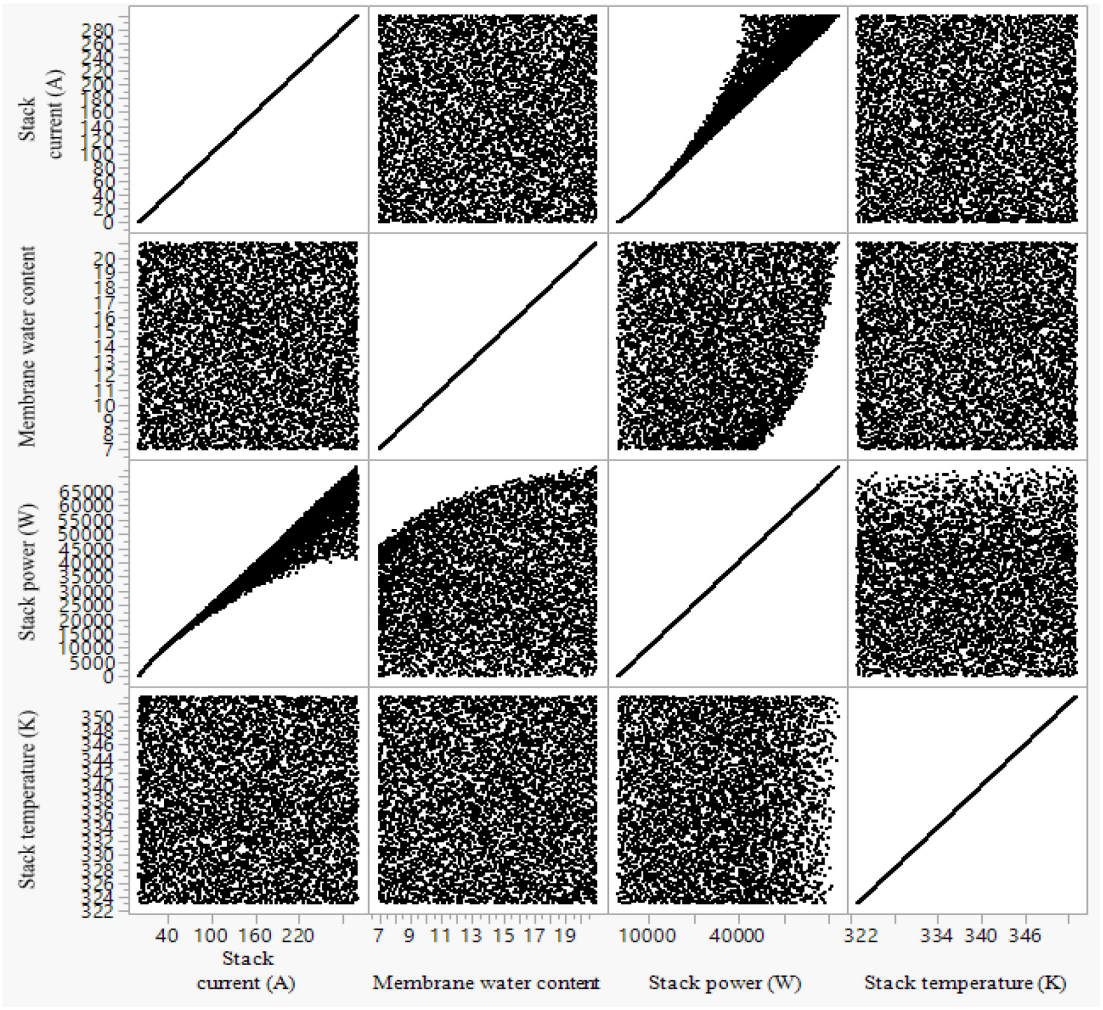

Fig. 2.11. Scatter plot matrix of the net power FFF design

The net power equation obtained using the FFF design is as follows:

$$\begin{aligned} Net\ power\ (P_{net}) &= a_1 + a_2 P_{sn} - a_3 I_n + a_4 L + a_5 T_n + a_6 P_{sn} I_n - a_7 I_n^2 \\ &+ a_8 P_{sn} L - a_9 I_n L + a_{10} T_n^2 - a_{11} I_n^2 P_{sn} - a_{12} P_{sn}^2 L - a_{13} I_n^2 T_n \end{aligned} \quad (2.25)$$

The variables P_{sn}, T_n, I_n, and L are the normalized values based on the median of factors, which are provided as input to the net power FFF design, which can be expressed as

$$T_n = \frac{(T - 338)}{15} \quad (2.26)$$

$$L = \frac{(\lambda - 14)}{7} \tag{2.27}$$

$$P_{sn} = h\frac{(P_s - 50000)}{50000} \tag{2.28}$$

$$I_n = \frac{(i_{fc} - 150)}{150} \tag{2.29}$$

$$scaling\ factor,\ h = \frac{75000}{Rated\ power\ of\ the\ PEMFC} \tag{2.30}$$

The net power required for any PEMFC can be obtained using the following expression

$$Net\ power\ of\ the\ required\ PEMFC = \left(\frac{1}{h}\right)P_{net} \tag{2.31}$$

The power consumed by the air compressor (P_{comp}) and other auxiliary equipment (P_{aux}) can be obtained using the following expressions:

$$Compressor\ Power\ (P_{comp}) = P_{stack} - P_{net} \tag{2.32}$$

$$Other\ auxiliary\ power\ (P_{others}) = 0.032 * rated\ power \tag{2.33}$$

The net output power (P_{out}) of the PEMFC can be obtained using the following expression

$$Net\ output\ power\ (P_{out}) = P_{net} - P_{others} \tag{2.34}$$

The value of the constants ($a_1 \ldots\ldots a_{13}$) are given in Appendix A. P_{others} is the power consumed by fans and other parasitic loads [5]. The actual net output power obtained form

the PEMFC model in [31] and the predicted net output power obtained from the regression equation (2.25) is shown in Fig. 2.12.

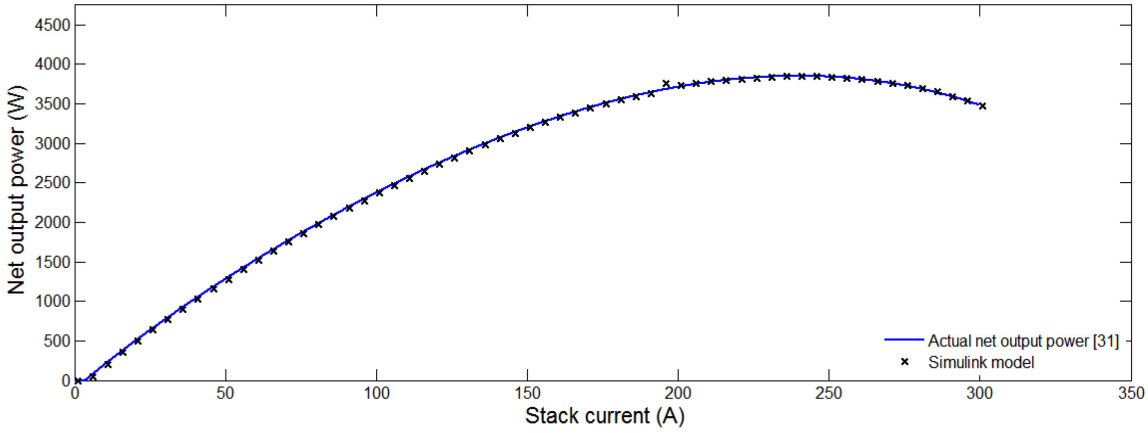

Fig. 2.12. Actual net power vs. predicted net power

The usefulness and versatility of the developed approach is that the net output power for any PEMFC can be obtained from (2.34) without knowing the parameters of the compressor. The net output power, stack power, and auxiliary power of Ballard MK5-E PEMFC obtained using the proposed approach are shown in Fig. 2.13.

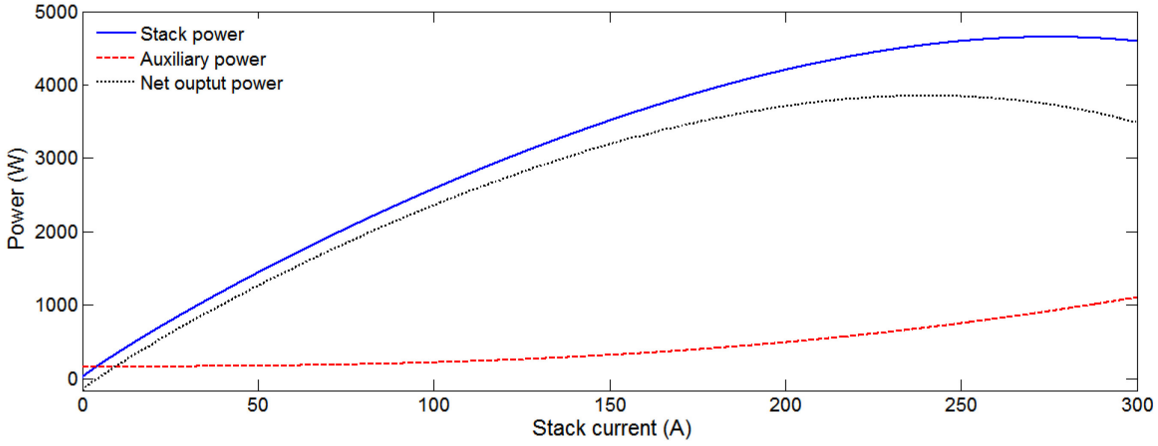

Fig. 2.13. Stack, auxiliary, and net output power of the PEMFC

2.6 PEMFC Efficiency Calculation

The efficiency of the FC is obtained by calculating the ratio between the electrical power and the supplied fuel power, which is given as [14]

$$\eta_s = \frac{Electrical\ power}{Fuel\ Power} \tag{2.35}$$

The electrical power of the PEMFC can be expressed as

$$Electrical\ power = i_{fc} * V_{out} \tag{2.36}$$

The chemical power obtained from the consumed fuel ($P_{fuel,c}$) can be expressed in terms of stack current (i_{fc}) and Faraday constant (F) as [13], [66]

$$P_{fuel,c} = \frac{\Delta H n i_{fc}}{2F} \tag{2.37}$$

where, ΔH is the low heating value of hydrogen, 241.98 (kJ mol^{-1}). The efficiency obtained based on (2.35 – 2.37) denote the efficiency of the stack (η_s). The process of obtaining electrical efficiency of the PEMFC based on hydrogen utilization is complex. Hence, for simplicity, the electrical efficiency of the PEMFC (η) is expressed in terms of net output power (P_{out}) and consumed fuel power, as given below [13], [66]

$$\eta = \frac{P_{out}}{\Delta H n i_{fc} / 2F} \tag{2.38}$$

The stack and electrical efficiency of the PEMFC are shown in Fig. 2.14. From the figure, it can be seen that the electrical efficiency of the PEMFC is low when compared with the stack efficiency. The power consumed by the auxiliaries accounts for the difference between the stack efficiency and electrical efficiency.

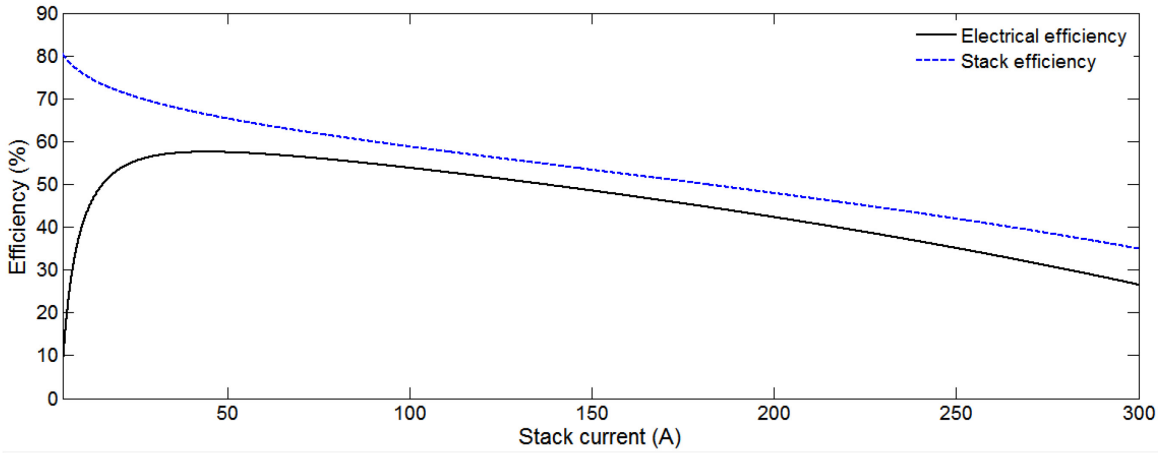

Fig. 2.14. Stack and electrical efficiency of the PEMFC

2.7 Performance of the PEMFC

The output of the PEMFC varies with changes in operating conditions, such as stack temperature (T), fuel flow, fuel pressure, and membrane water content (λ). The fuel pressure and fuel flow changes automatically in response to the stack current as discussed in previous sections. In this thesis, the performance of the PEMFC in terms of the stack voltage, output power, and electrical efficiency for changes in stack temperature and membrane water content are investigated using the developed model.

2.7.1 Response of the PEMFC for Variations in Stack Temperature

For this investigation, the value of membrane water content (λ) is set at 14 (100% humidified) and the stack temperature (T) is varied between 50˚C and 80˚C. At higher stack temperatures, the conductivity of the membrane and the speed of the electrochemical reaction increases, which results in increased output voltage, as shown in Fig. 2.15. The net

output power (P_{out}) of the PEMFC for variations in the stack temperature is shown in Fig. 2.16.

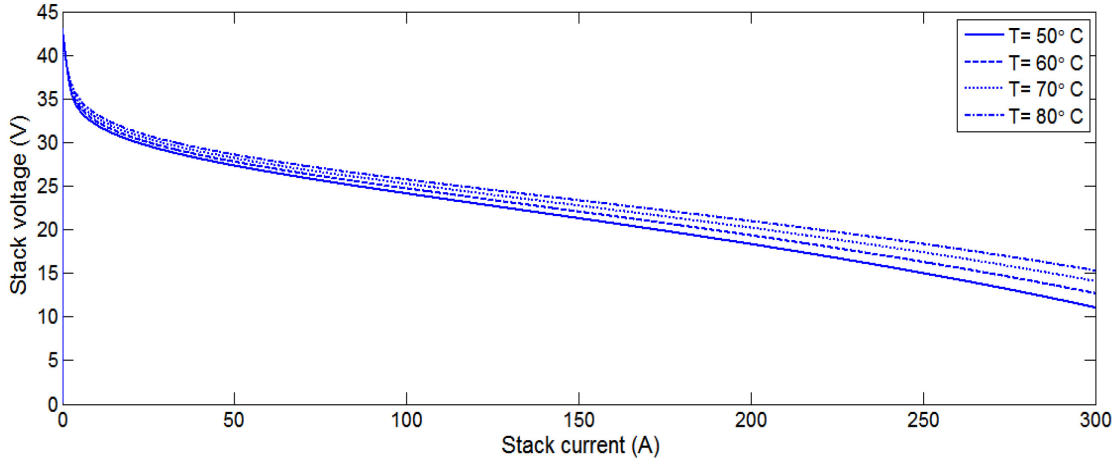

Fig. 2.15. Output voltage of the PEMFC for variation in stack temperature (λ = 14)

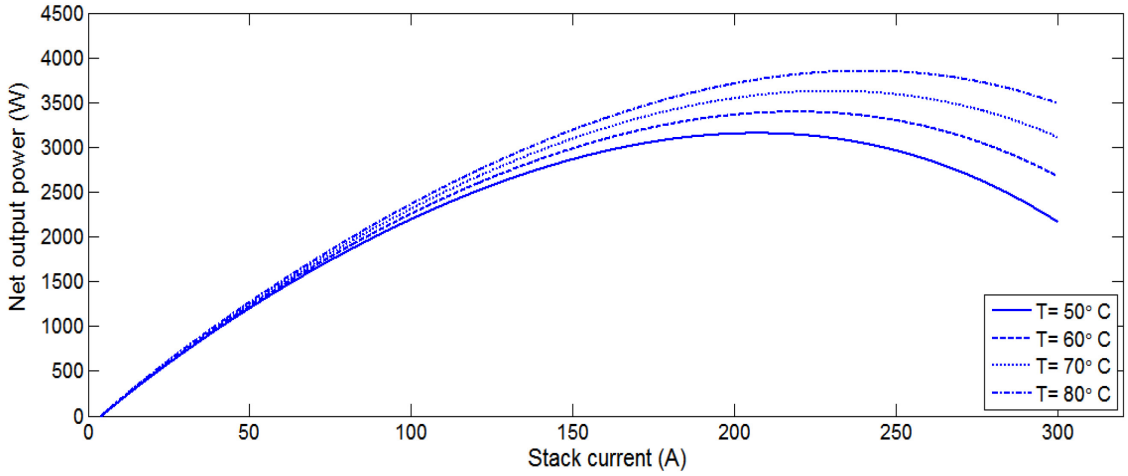

Fig. 2.16. Net output power of the PEMFC for variation in stack temperature (λ = 14)

From the figure, it can be seen that the net output power increases with increasing stack temperature. Hence, the efficiency (η) of the PEMFC also increases with increase in stack temperature, as shown in Fig. 2.17.

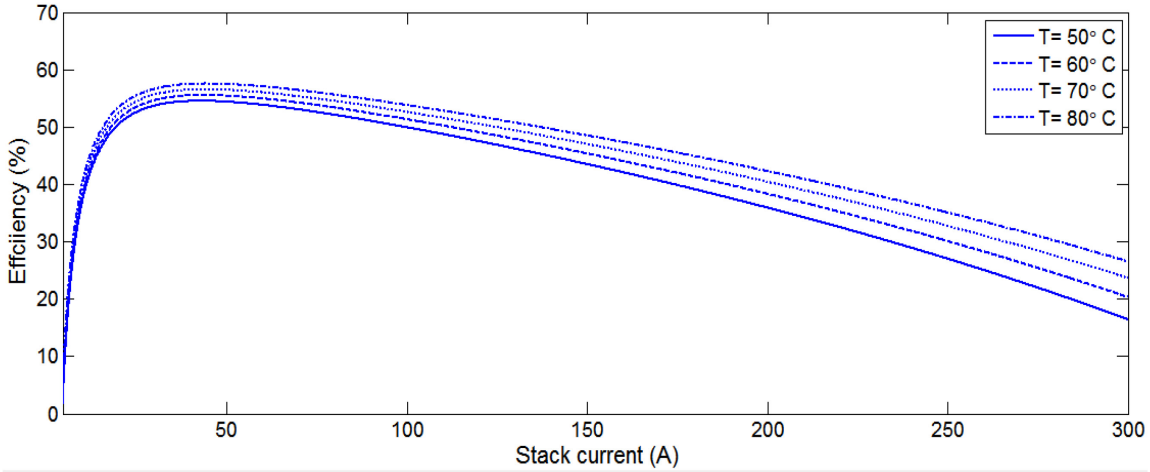

Fig. 2.17. Efficiency of the PEMFC for variation in stack temperature (λ = 14)

2.7.2 Response of the PEMFC for Variations in Membrane Water Content

For this investigation, the stack temperature (T) is maintained at 80˚ C and the value of the membrane water content (λ) is varied between 10.5 and 17.5, which corresponds to 75% and 125% of saturation, respectively. The proton conductivity of the PEMFC increases with increasing water content, which results in the reduction of ohmic losses in the PEMFC. This leads to the increase in the output voltage as shown in Fig. 2.18. However, high values of the membrane water content results in flooding, which degrades the life of the proton exchange membrane (PEM), while low values of membrane water content leads to dry PEM, which degrades the performance of the PEM. Hence, the membrane water content of the PEMFC should be maintained at an optimum value for proper operation of the PEM.

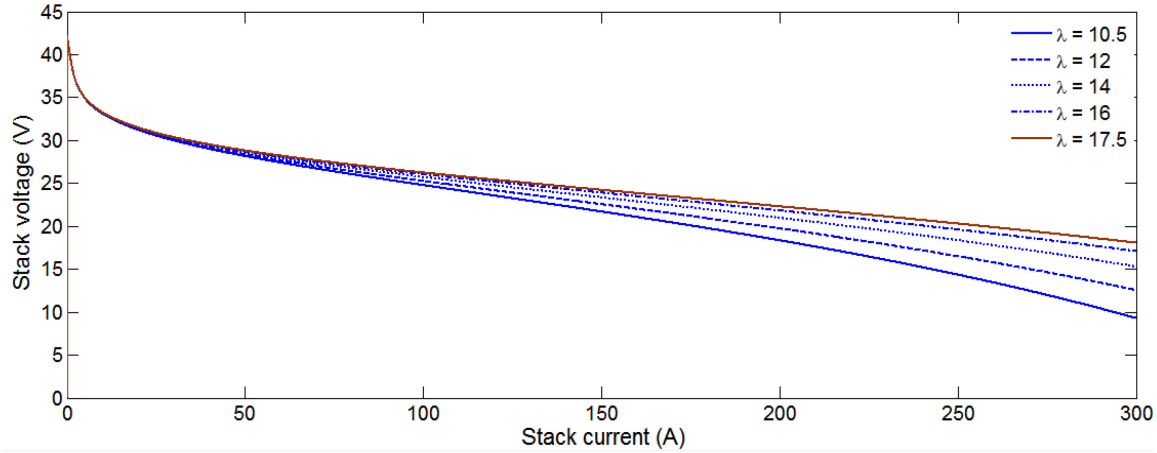

Fig. 2.18. Output voltage of the PEMFC for variation in λ ($T = 80^{\circ}$C)

As expected, the net output power (P_{out}) and efficiency (η) of the PEMFC increase with increasing membrane water content, as shown in Figs. 2.19 and 2.20.

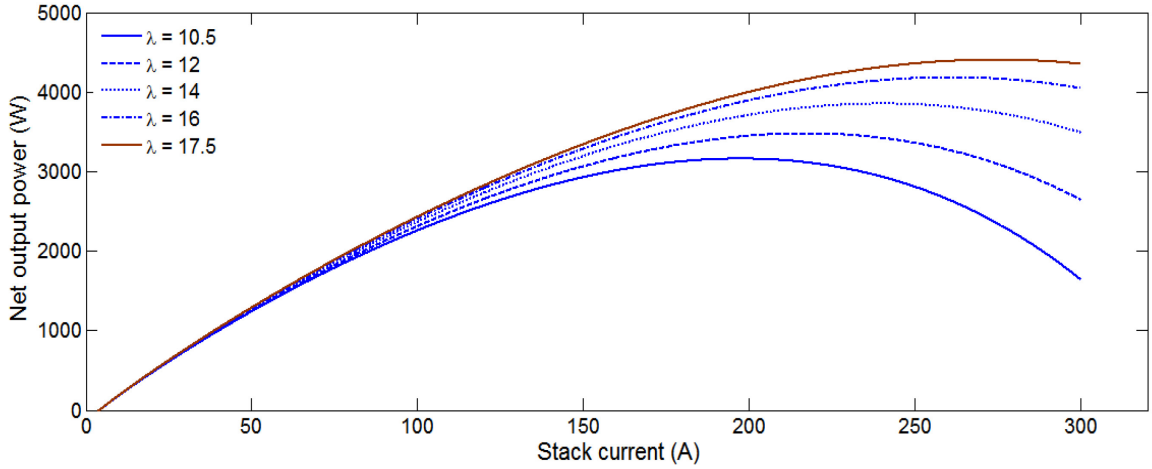

Fig. 2.19. Net output power of the PEMFC for variation in λ ($T = 80^{\circ}$C)

In order to obtain a relationship between the net output power (P_{out}) and efficiency (η) of the PEMFC for variations in λ and T, a surface plot is obtained, as shown in Fig. 2.21. From the figure, it can be seen that the maximum efficiency points and maximum power points occur at different regions of stack current.

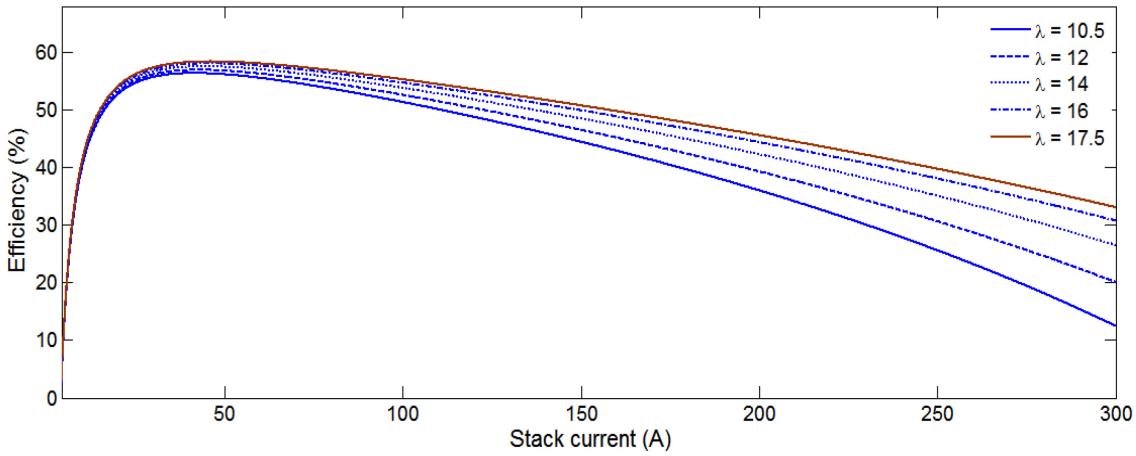

Fig. 2.20. Efficiency of the PEMFC for variation in λ (T = 80˚C)

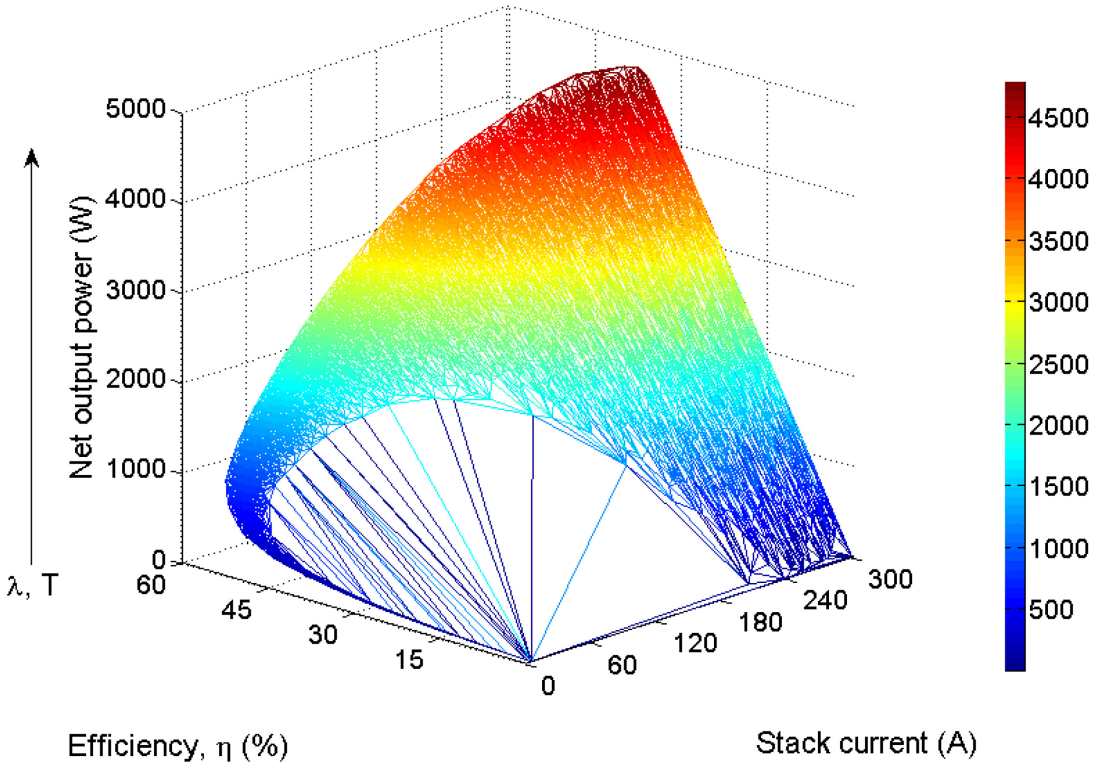

Fig. 2.21. Surface plot of PEMFC characteristics

2.8 Summary

A complete and versatile PEMFC Simulink model is described and developed. The model takes into account the stack and reactant flow models. The developed PEMFC stack model is validated with published experimental results, which indicate accurate fit. The power consumed by the auxiliaries required to run the PEMFC is described and a generic model to determine the net output power and compressor power is developed. The developed model is used to determine stack efficiency and electrical efficiency of the PEMFC. Finally, the behaviour of the PEMFC for changes in stack temperature (T) and membrane water content (λ) is discussed based on the simulation results from the developed PEMFC Simulink model. The variations of the maximum power point and maximum efficiency point for changes in the stack temperature and membrane water content require tracking techniques to operate the PEMFC at the required operating point (MPP or MEP). The MEP occurs at the lower region of the stack currents and the MPP occurs at the higher region of stack currents. Hence, at any given instance the PEMFC can be operated at the maximum power point or the maximum efficiency point. The analyses of the MPP and MEP tracking techniques are discussed in the following chapter.

Chapter 3

Tracking Techniques for the Proton Exchange Membrane Fuel Cell

The operating point of the PEMFC is at the intersection of the fuel cell power curve and load power curve and it should be selected to enhance the performance of the PEMFC. It is ideal to operate the PEMFC at a constant operating point to realize longer lifetime [67]. There exist two unique operating points, namely the maximum power point (MPP) and the maximum efficiency point (MEP). The PEMFC produces its maximum power at MPP and operates at maximum efficiency at MEP [14]. The MPP and MEP operating points are affected by changes in operating conditions, such as stack temperature (T), membrane water content (λ), fuel pressure, and fuel flow. Hence, a tracking technique is required to track changes and operate the PEMFC at the required operating point (MPP or MEP).

In this chapter, the maximum power point tracking (MPPT) and maximum efficiency point tracking (MEPT) techniques are presented and discussed. Several tracking algorithms are reported in the literature to track the maximum power point and maximum efficiency point [39]–[45]. The selection of a tracking algorithm is based on factors, such

as high tracking speed, high accuracy, and low complexity. The selected tracking algorithm should also satisfy the specific requirements of the PEMFC applications. The focus of this chapter is the selection of tracking algorithm to track the MPP and MEP for the simulation-based investigation of PEMFC system. The development of the DC-DC boost converter and the current controller for tracking techniques are presented. The performance of the selected tracking algorithm to track the MPP and MEP of the PEMFC system is analysed. Finally, the limitations of the MPPT and MEPT tracking techniques are discussed. The work described in this chapter regarding the selection of a suitable tracking algorithm to meet particular requirements of different PEMFC applications was presented at the IEEE Newfoundland Electrical and Computer Engineering Conference (NECEC) in 2015 [68].

3.1 Direct and Indirect Tracking Schemes

The tracking control of the maximum power point or maximum efficiency point of the PEMFC can be implemented directly in the PEMFC or indirectly by using a DC-DC power converter between the load and the PEMFC to track the required operating point. A comparison of the direct and indirect implementation of the tracking control scheme is shown in Table 3.1. The direct implementation of the tracking control scheme requires parameters, such as hydrogen pressure and oxygen pressure from the PEMFC model to track the required operating point. This approach leads to a model-dependent control [9], [47]. The direct tracking control scheme is also sensitive to load variations. An indirect control scheme implemented in a DC-DC power converter external to the PEMFC results in a model-independent tracking control.

In the indirect control scheme, the DC-DC power converter between the load and the PEMFC is controlled so as to maintain a constant value of equivalent resistance "seen" by the PEMFC, which corresponds to the operating point (MPP or MEP).

Table 3.1: Characteristics of the direct and indirect control schemes

Control Scheme	Model based	Sensitive to load variations	Advantages	Disadvantages
Direct	Yes	Yes	Simple control, prevents oxygen starvation and flooding	Dynamic load changes affect the fuel cell system and requires energy storage device to maintain constant PEMFC output voltage.
Indirect (with DC-DC power converter)	No	No	Dynamic Load control independent of the fuel cell model	Requires energy storage device to maintain constant PEMFC output voltage

For all of the above-mentioned reasons, the indirect control scheme is preferred over the direct control scheme [49]–[51], and it is therefore used in this thesis to implement the different tracking techniques.

3.2 DC-DC Power Converter

The configuration of the power converter connected between the load and the PEMFC unit plays a significant role in enhancing the performance of the PEMFC unit. The operating point of the PEMFC is based on the load connected to the PEMFC. In order to operate the PEMFC at the required point (MPP or MEP), the load resistance corresponding to the operating point is required. This leads to the operation of the PEMFC at a constant

load. However, in real-time the loads are not always constant. One possible solution is to use the impedance matching capability of the DC-DC power converter to maintain the equivalent resistance "seen" by the source (PEMFC) at the required value [69].

Several configurations of the DC-DC power converters have been presented in the literature [70], [71]. The selected power converter should have simple control to reduce complexity, less number of reactive elements to minimize cost, and less number of switches to minimize switching losses. In general, the buck, boost, and buck-boost DC-DC power converters are the most commonly used power converters to implement the tracking techniques [36]. However, the DC-DC buck-boost converter has limitations, such as negative output voltage for positive input voltage, absence of common ground, and requirement of opto-coupler for switching [37]. In the case of the DC-DC buck converter, the output voltage is less than the input voltage, which is not suitable for the PEMFC with low output voltage [38].

On the other hand, the DC-DC boost converter with high output voltage and blocking diode at the load end is suitable for implementing the tracking techniques for the PEMFC. The output voltage of the DC-DC boost converter is always higher than the input voltage. The blocking diode helps to prevent a battery connected at the output of the converter (for storage purposes) to discharge into the PEMFC. This feature is an added advantage when compared with the buck and buck-boost converters [11]. In this thesis, the DC-DC boost converter is considered to develop and implement the different tracking techniques.

3.2.1 DC-DC Boost converter

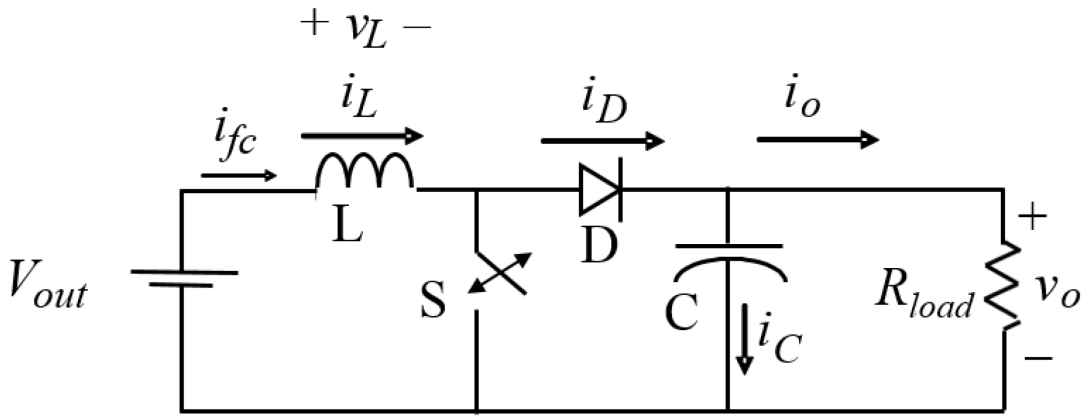

Fig. 3.1. DC-DC boost converter

The circuit diagram of the DC-DC boost converter is shown in Fig. 3.1. The working principle of the boost converter is based on the status of the switch (S). During the on-state, the switch (S) is turned on (closed) and the current through the inductor increases linearly. In the meantime, the capacitor discharges into the load. During the off-state, the diode (D) becomes forward biased and the inductor discharges through the diode to the load and charges the capacitor.

The DC-DC boost converter has the ability to control the resistance "seen" by the PEMFC (V_{out}), as shown in Fig. 3.2. From the figure, the equivalent resistance (R_{equiv}) "seen" by the source, assuming a lossless DC-DC boost converter, can be expressed as

$$R_{equiv} = \frac{V_{out}}{i_{fc}} = (1-d)^2 R_{load} \tag{3.1}$$

where, i_{fc} is the input current of the DC-DC boost converter and d is the duty ratio, which represents the fraction of the period during which the switch is turned on.

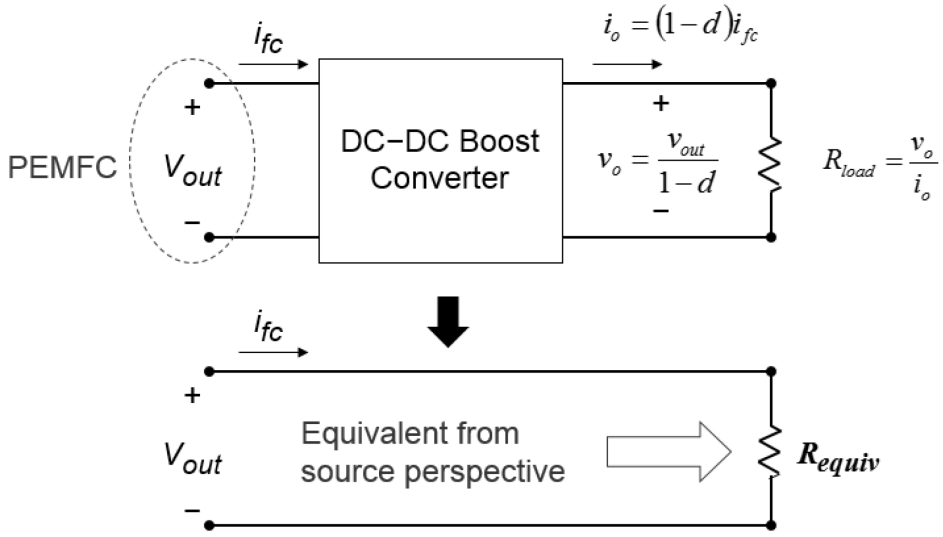

Fig. 3.2. Resistance matching of the DC-DC boost converter

From (3.1) and Fig. 3.2, it can be seen that the operating point of the PEMFC can be controlled by varying the current flowing though the inductor. The current flowing through the DC-DC boost converter can be controlled by using current control techniques. Several current control techniques have been presented in the literature [72]–[74]. A detailed comparison of current control techniques with the DC-DC boost converter implemented for tracking techniques is presented in Appendix B. In this thesis, the hysteresis current controller with variable frequency and less complexity is used to control the DC-DC boost converter [72].

3.2.2 Hysteresis Current Control

The hysteresis current control tracks the reference current generated by tracking algorithms within a hysteresis band [75]. The working principle of the hysteresis current controller is shown in Fig. 3.3.

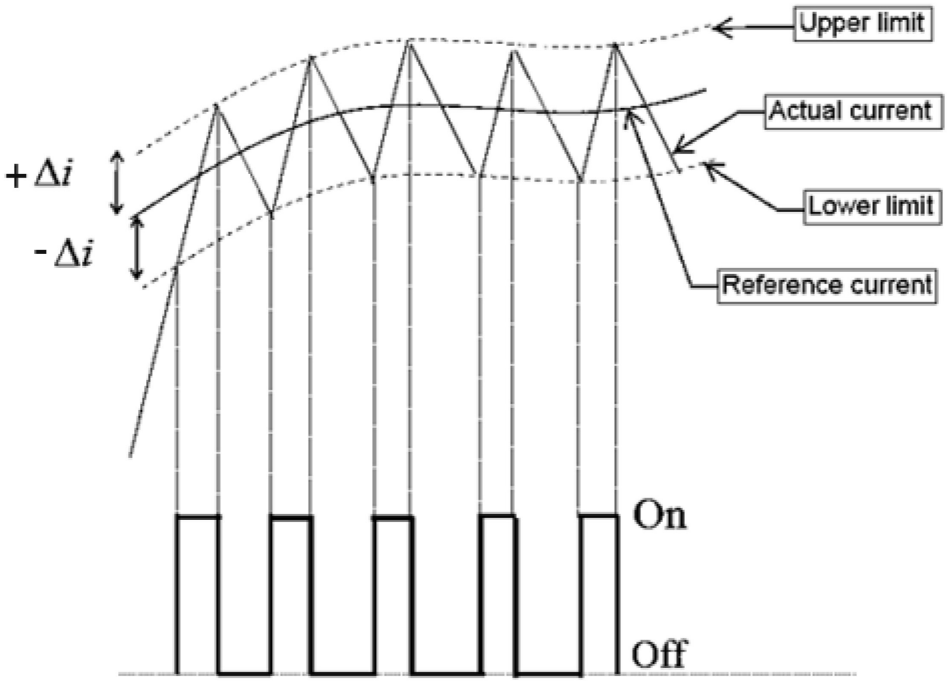

Fig. 3.3. Hysteresis current controller

If the current exceeds the upper limit (Δi_+) of the hysteresis band, the switch (S) of the DC-DC boost converter is turned off. As a result, the current starts to decrease. When the current reaches the lower limit (Δi_-) of the hysteresis band, the switch (S) is turned on and the current through the inductor increases. Hence, the actual current is forced to track the reference current within the hysteresis band, as shown in Fig. 3.3. The amplitude of the actual current oscillation around the reference current is based on the hysteresis band width. The hysteresis band width is defined by the term Δhys and is given by the equation

$$\Delta hys = \Delta i_+ - \Delta i_- \tag{3.2}$$

The hysteresis band width can be fixed to a constant value or to a fraction of the actual current. In this thesis, the hysteresis band width is set at $0.2i_{ref}$.

3.3 Tracking Algorithms

The selected tracking algorithm should be model-independent so that it can be used to develop a generalized indirect tracking technique for any required rating of the PEMFC. A review of the different tracking algorithms for maximum power point tracking in photovoltaic systems shows that model-independent tracking algorithms such as perturb and observe (P&O), incremental conductance (IncCond), dV/dI feedback control, extremum seeking control (ESC), and sliding mode control (SMC) are widely used [39]. In this thesis, three of the algorithms used for maximum power point tracking in photovoltaic arrays, namely P&O, ESC, and SMC are considered in the analysis of the PEMFC for stationary power applications.

3.3.1 Extremum Seeking Control

The ESC uses a periodic signal referred to as "dither" or perturbation signal to track the operating point near the maximum power point of the fuel cell system characteristics. Several types of ESC have been proposed in the literature [9], [47], [48], [76] for photovoltaic systems.

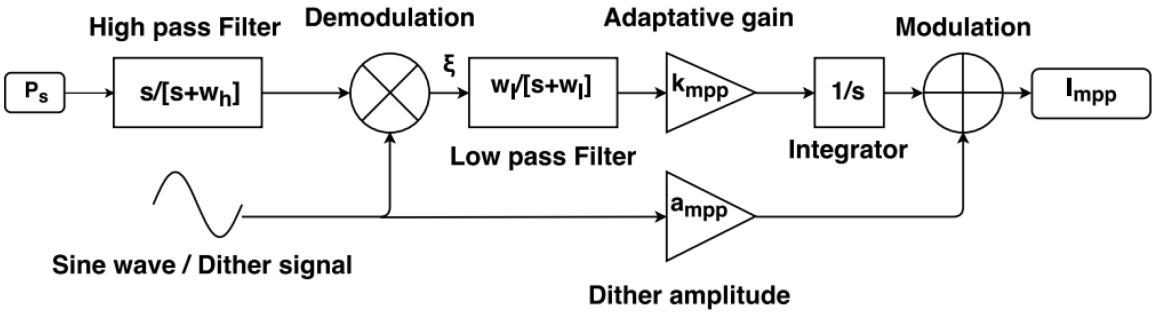

Fig. 3.4. Extremum seeking control algorithm for maximum power point tracking

A number of these techniques were analyzed and the technique with less complexity and good response, shown in Fig. 3.4, was selected and implemented in this thesis. The maximum point can be found by checking the sign of the gradient of the stack power (P_s) versus input current (I) characteristics. The gradient (ξ) is positive when the operating point is to the left of the MPP and the gradient is negative when the operating point is to the right of the MPP. At maximum point, the value of the gradient is zero. The reference signal (I_{mpp}) corresponding to the MPP of the non-linear PEMFC system obtained from the ESC block can be expressed as [11]

$$I_{mpp} = I_0 + \frac{k_{mpp} a_{mpp}}{2} P_s' t \tag{3.3}$$

Equation (3.3) provides the position of the operating point. If the initial current (I_0) is greater than I_{mpp}, the operating point is to the right of the MPP, and the current will decrease to move the operating point near the MPP, as shown in Fig. 3.5.

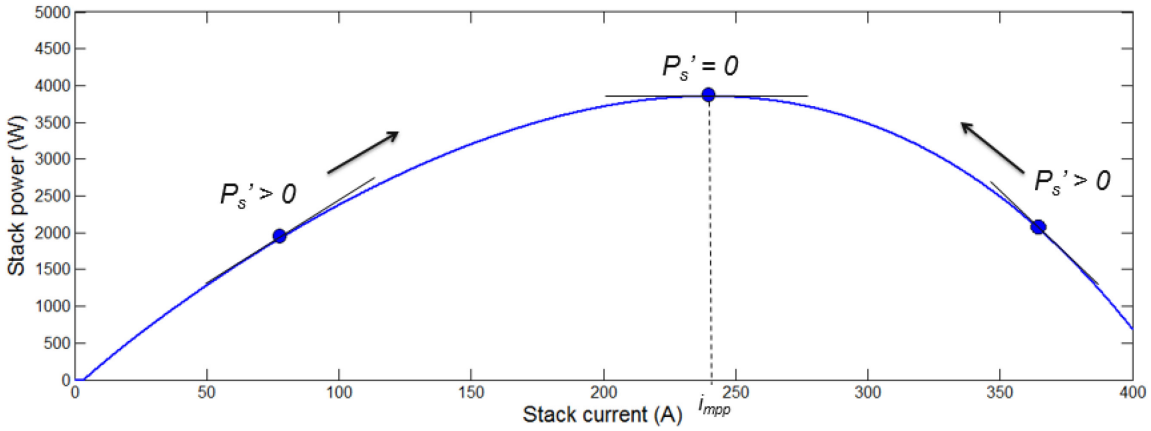

Fig. 3.5. Operation of the extremum seeking control

If I_0 is less than I_{mpp}, the operating point is to the left of the MPP, and the current will increase to move the operating point to the MPP. The value of the current step used for

the increment and decrement of the reference current is based on the value of the second term in (3.3).

The selection of the periodic sinusoidal perturbation signal frequency (ω), the high-pass filter cut-off frequency (ω_h) and the low-pass filter cut-off frequency (ω_l) in Fig. 3.4 influences the performance of the extremum seeking control. For example, a higher value of the periodic sinusoidal perturbation signal frequency can separate the dither signal from the response of the PEMFC system (P_s); however, a lower value of ω leads to low perturbation speed. Hence, the following criteria is taken into consideration in selecting the values of ω, ω_h, and ω_l [11]

$$\omega >> \omega_h >> \omega_l \tag{3.4}$$

The value of the adaptation gain (k_{mpp}) and the perturbation signal amplitude (a_{mpp}) have a significant effect on the system convergence speed. A small value of k_{mpp} slows down the convergence speed. Increasing k_{mpp} can improve the tracking speed; however, a high value of k_{mpp} can result in an inaccurate system response. An increase in a_{mpp} will increase the convergence speed, but the system becomes more sensitive and may not track the MPP [11]. The major constraints considered for selecting the tuning parameters of the tracking algorithms are as follows:

- The accuracy of the tracking algorithm should be maintained as high as possible.
- The overshoot in the output should be maintained as minimum as possible.

Optimum values of k_{mpp} and a_{mpp} are selected from simulating the ESC MPPT for different combinations of k_{mpp} and a_{mpp}. The optimum values selected are $k_{mpp} = 10$ and a_{mpp}

= 6.5. The cut-off frequency of the low pass filter (ω_l) and the high pass filter (ω_h) are set to 5 rad/s and 30 rad/s respectively. The frequency of the perturbation signal (ω) is set to 50 rad/s.

It is observed that the extremum seeking control (ESC) is a real-time optimization algorithm that involves a nonlinear dynamic system with feedback and adaptation. The model-independent and self-regulating characteristics improves the effectiveness of the extremum seeking control algorithm.

3.3.2 Perturb and Observe Algorithm

Perturb and observe (P&O) or Hill climbing involves a perturbation in the duty ratio of the DC-DC boost converter. With the PEMFC connected to a DC-DC boost converter, the DC-DC boost converter perturbs the PEMFC current to move the operating point to the maximum power point. From Fig. 3.5, it can be seen that increasing the current increases the power when operating on the left of the MPP and decreases the power when on the right of the MPP. Therefore, if there is an increase in power, the subsequent perturbation should be kept the same in order to reach the MPP and if there is a decrease in power, the perturbation should be reversed [77]. The process is repeated periodically until the MPP is reached. The system then oscillates about the MPP. The oscillation can be minimized by reducing the perturbation step size (dI). However, a smaller perturbation size slows down the MPPT. Hence, there is a trade-off in choosing the step size of the perturbation. The P&O algorithm is summarized in the form of the flow chart shown in Fig. 3.6.

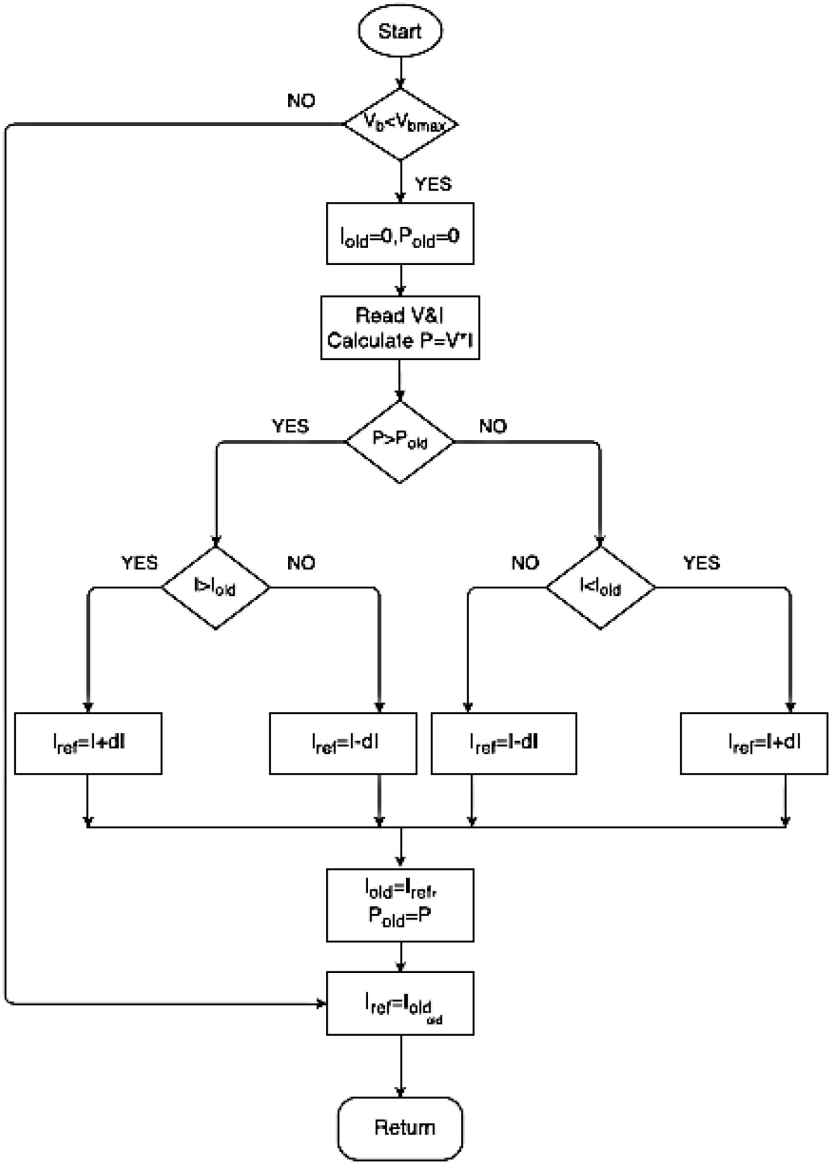

Fig. 3.6. Flowchart of the P&O algorithm

where, V_b is the voltage of the battery (V); V_{bmax} is the battery voltage limit (V); I_{old} is the previous value of stack current (A); V_{old} is the previous value of stack voltage (V); P_{old} is the previous value of stack power (W); $I_{old_{dd}}$ is the stack current at the beginning of the perturbation (A). During rapidly changing conditions, the operating point diverges from the

maximum point [39]. Hence, P&O method is not suitable under rapidly changing conditions. In this thesis, the value of the current step (dI) is set at 0.01A.

3.3.3 Sliding Mode Control

In the siding mode control (SMC) method a sliding surface (ψ) is defined and is expressed as [44]

$$\psi = V_{out} + I_{fc}\frac{\partial V_{out}}{\partial I_{fc}} \tag{3.5}$$

where V_{out} is the fuel cell voltage (V); I_{fc} is the fuel cell current (A).

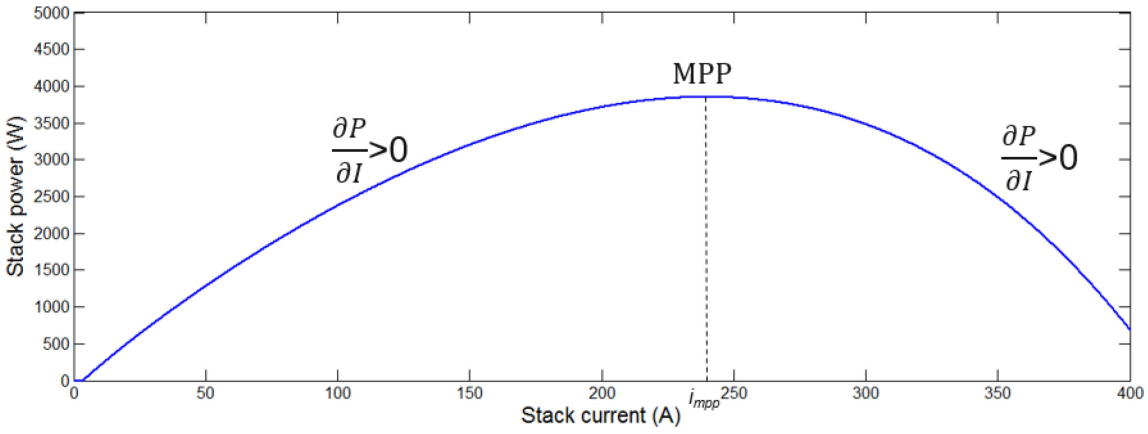

Fig. 3.7. Operation of the sliding mode control

The switching function of the converter is based on the fact that dP/dI>0 indicates an operating point to the left of the MPP and dP/dI<0 indicates an operating point to the right of the MPP as shown in Fig. 3.7. The switching function is expressed as

$$S = 0 \quad for \quad \psi \geq 0$$
$$S = 1 \quad for \quad \psi < 0 \tag{3.6}$$

where $S = 0$ means the switch is open and $S = 1$ means the switch is closed. The SMC tracking algorithm works well under rapidly changing environment and operational conditions [44]. The DC-DC boost converter is controlled by using PWM technique. The SMC tracking algorithm varies the value of the duty ratio of the DC-DC boost converter in order to track the MPP.

3.4 Simulation

The PEMFC system consisting of the MATLAB/Simulink model of the fuel cell discussed in Chapter 2, the tracking algorithms (ESC, P&O, and SMC) discussed in the previous section, the DC-DC boost converter with hysteresis current controller, and a battery load is implemented in Simulink. In this simulation, the temperature of the fuel cell is set to 80˚C. The inductor and capacitor values used in the DC-DC boost converter are 40 mH and 2000 µF, respectively. The battery load is rated at 200 V, 6.5 Ah. In order to compare the performance of the three MPPT algorithms, the simulation is carried out with varying membrane water content (λ) as shown in Fig. 3.8.

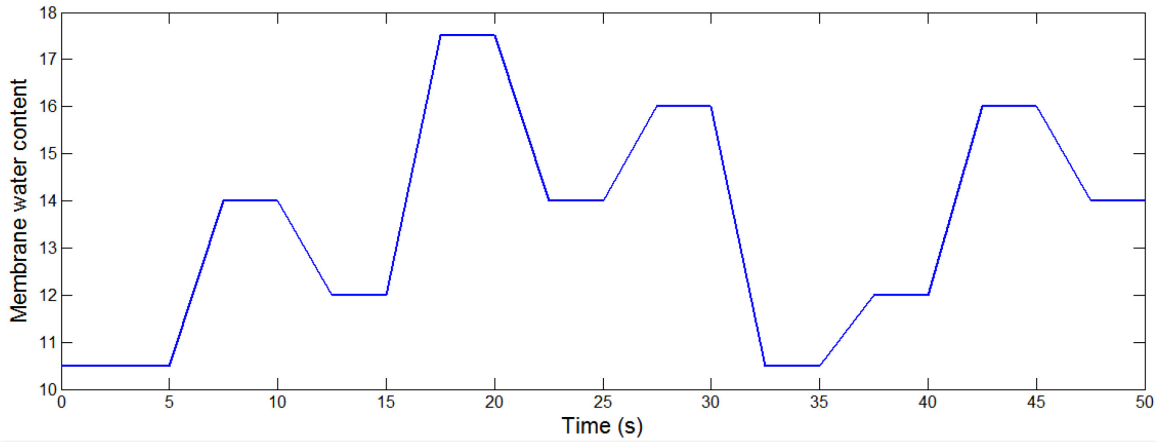

Fig. 3.8. Variation of membrane water content

The maximum power points and the maximum power point currents corresponding to the variations in membrane water content are shown in Fig. 3.9 and Fig. 3.10.

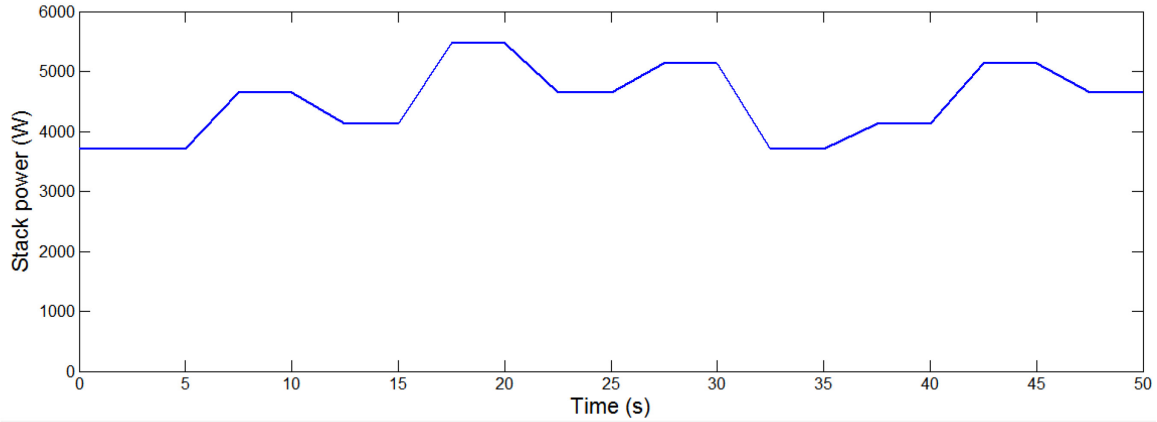

Fig. 3.9. Maximum power points for variation in membrane water content

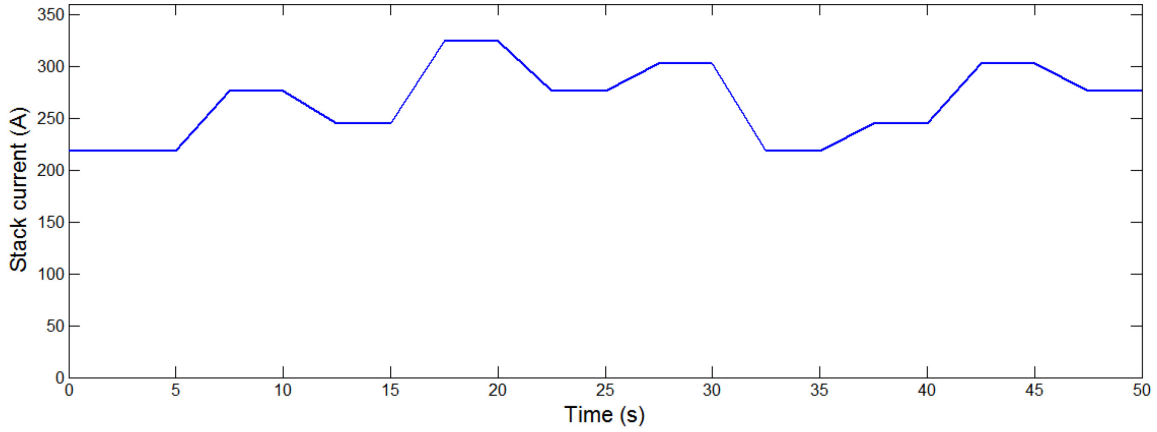

Fig. 3.10. Maximum power point currents for variation in membrane water content

If the MPPT algorithm tracks the MPP for varying membrane water content then it will also track the MPP for varying stack temperature, fuel flow, and fuel pressure.

3.4.1 Output Power of the Tracking Algorithms

The ESC MPPT tracking trajectory near the MPP for different values of membrane water content is shown in Fig. 3.11. From the figure, it can be seen that the ESC tracking

algorithm tracks the MPP of the PEMFC accurately for varying membrane water content (λ).

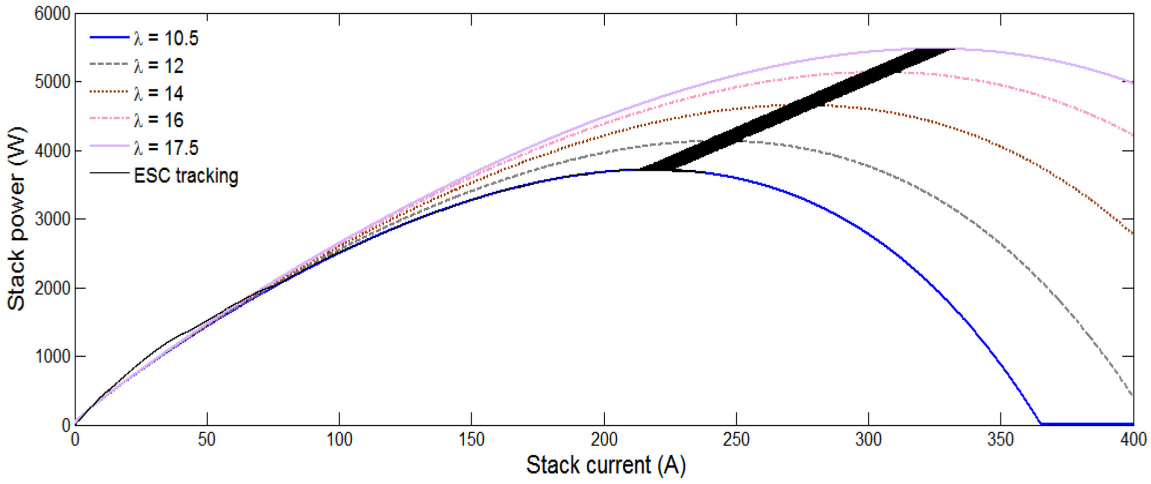

Fig. 3.11. MPP tracking using the ESC algorithm

Similarly, the tracking trajectory of the P&O tracking algorithm is shown in Fig. 3.12. From the figure, it can be seen that the P&O tracking trajectory tracks the MPP of the PEMFC, but it is associated with overshoots for random variations in membrane water content shown in Fig. 3.8. This is due to the oscillations associated with the P&O algorithm around the MPP.

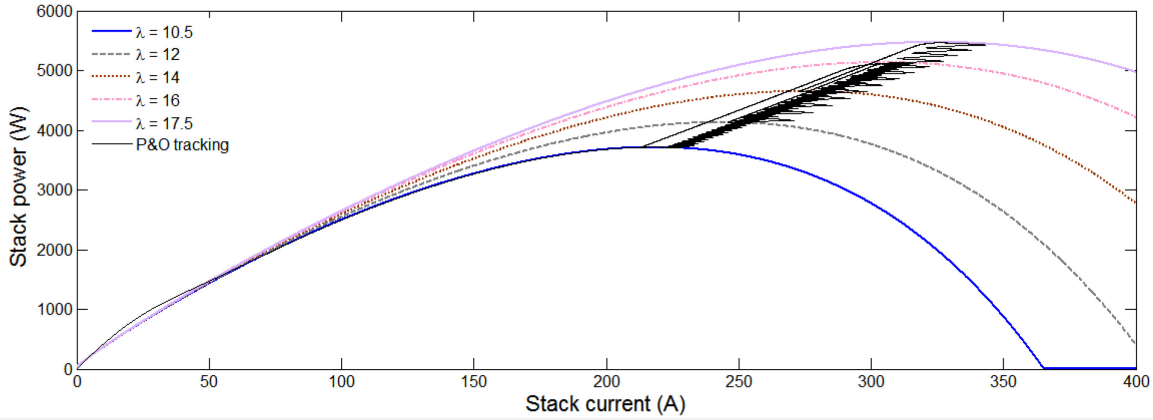

Fig. 3.12. MPP tracking using the P&O algorithm

In the case of the SMC tracking algorithm, the duty ratio of the DC-DC boost converter is controlled according to (3.6) until the stack current reaches the current corresponding to the maximum power point (i_{mpp}). Once the required operating point (i_{mpp}) is reached, the SMC algorithm will turn off the switch in the DC-DC boost converter as according to (3.6). This results in a decrease in current, which in turn reduces the power, causing the DC-DC boost converter to turn on to attain the MPP. This process continues, which results in the oscillation of the SMC tracking algorithm to the left of the MPP as shown in Fig. 3.13.

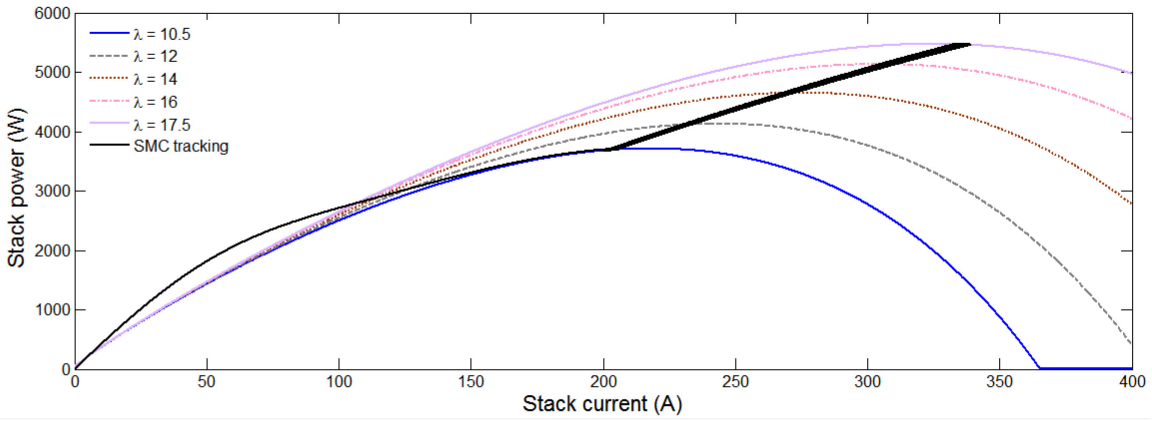

Fig. 3.13. MPP tracking using the SMC algorithm

3.5 Comparison of the Tracking Algorithms

In this section, a detailed comparison of the characteristics of the ESC, P&O, and SMC tracking algorithms based on accuracy and convergence speed is presented. The objective is to select a suitable tracking algorithm for maximum power point tracking of a fuel cell generation system.

3.5.1 Accuracy of the MPP Tracking Algorithms

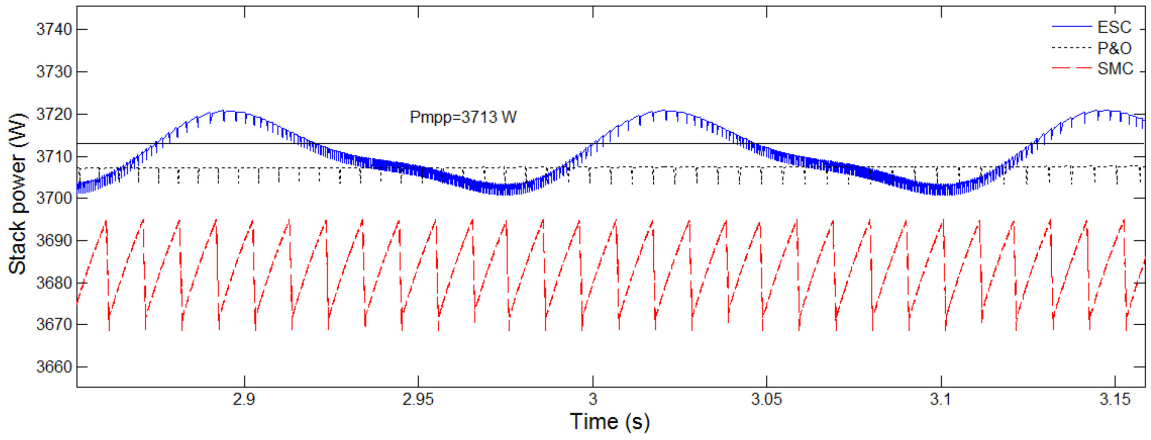

Fig. 3.14. Accuracy of the MPP tracking algorithms

The accuracy of the ESC, P&O, and SMC tracking algorithms for λ = 10.5 and T = 80˚ C is shown in Fig. 3.14. From the PEMFC P-I polarization curve for these conditions, the MPP attainable from these conditions is 3713 W. From the figure, it can be seen that the ESC tracking algorithm is more accurate in tracking the MPP when compared to the P&O and SMC tracking algorithms.

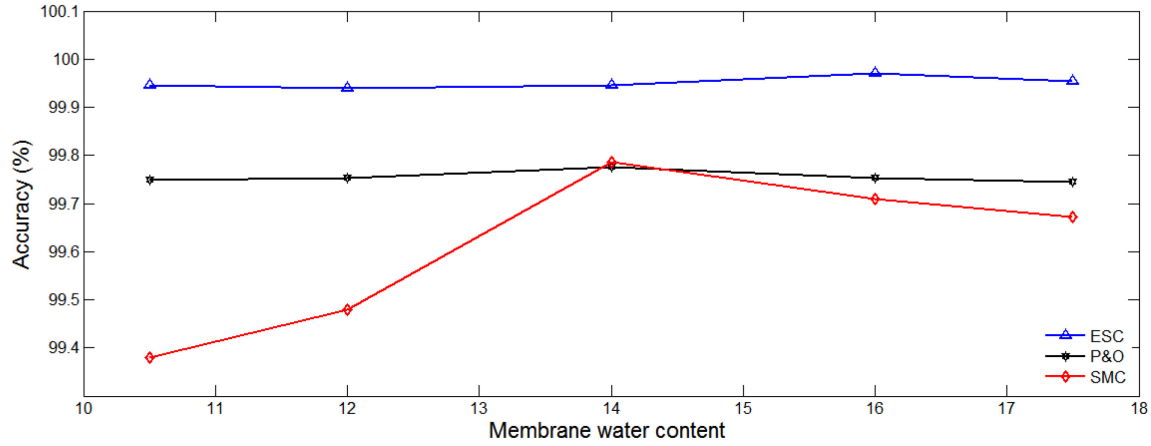

Fig. 3.15. Accuracy of the tracking algorithms

However, the accuracy of the P&O and SMC algorithm increases as the value of the membrane water content increases to 14, but the accuracy drops for values of membrane water content greater than 15 as shown in Fig. 3.15. This is due to the flat region of the MPP associated with the sub saturated region ($\lambda < 13$) and super saturated region ($\lambda > 15$) of the membrane water content.

3.5.2 Convergence Speed of the MPPT Tracking Algorithms

The convergence speed of the ESC, P&O, and ESC tracking algorithm is shown in Fig. 3.16. From the figure, it can be seen that the convergence speed of the SMC tracking algorithm is high compared with the ESC and P&O tracking algorithms, with the P&O algorithm being the most sluggish response. The convergence speed of the P&O can be increased by increasing the perturbation step size (dI). However, it increases the magnitude of oscillation around the MPP, which decreases the accuracy of the P&O algorithm.

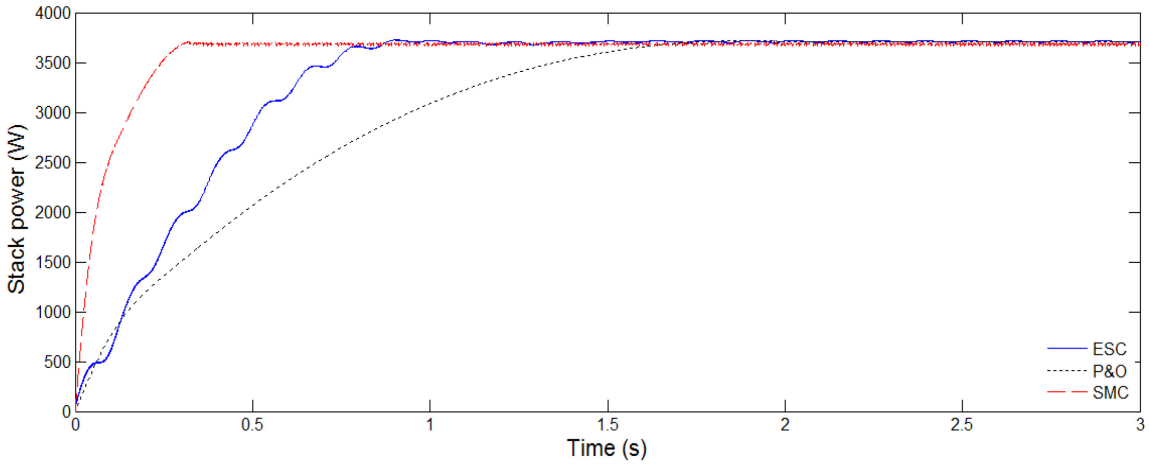

Fig. 3.16. Convergence speed of the MPPT tracking algorithms

In case of the ESC MPPT, the convergence speed can be increased by increasing the adaptation gain (k_{mpp}) and perturbation amplitude (a_{mpp}), but large value of k_{mpp} and a_{mpp}

result in large oscillations around the MPP and the system will become sensitive to noise or ripple content. The characteristics of the ESC, P&O, and SMC tracking algorithms discussed are tabulated as shown in Table 3.2.

Table 3.2: Characteristics of the tracking algorithms

Tracking Algorithm	**Accuracy**	**Convergence Speed**
ESC	High	Medium
P&O	Medium	Low
SMC	Low	High

From the above-mentioned points and Table 3.2, it can be seen that the ESC algorithm with high accuracy, and medium tracking speed would be adequate for maximum power point tracking of a PEMFC generation system and it is considered for comparative study of the maximum power point tracking and maximum efficiency point tracking techniques.

3.6 Maximum Power Point Tracking (MPPT) Technique

In general, the stack power of the PEMFC is considered for tracking the MPP of the PEMFC [11], [44], [48]. However, the net output power (P_{out}) is always less than the stack power (P_s) due to the parasitic power consumed by the auxiliaries connected to the PEMFC as discussed in Chapter 2. In order to account for the effect of the parasitic power in the tracking techniques, the net output power (P_{out}) of the PEMFC is considered in the following discussions. The input of the ESC control algorithm is therefore changed from P_s to P_{out}.

Using the ESC algorithm, the maximum power point of the net output power (P_{out}) obtained from (2.34) is shown in Fig. 3.17. From the figure, it can be seen that the ESC algorithm effectively tracks the maximum point of the net output power (P_{out}).

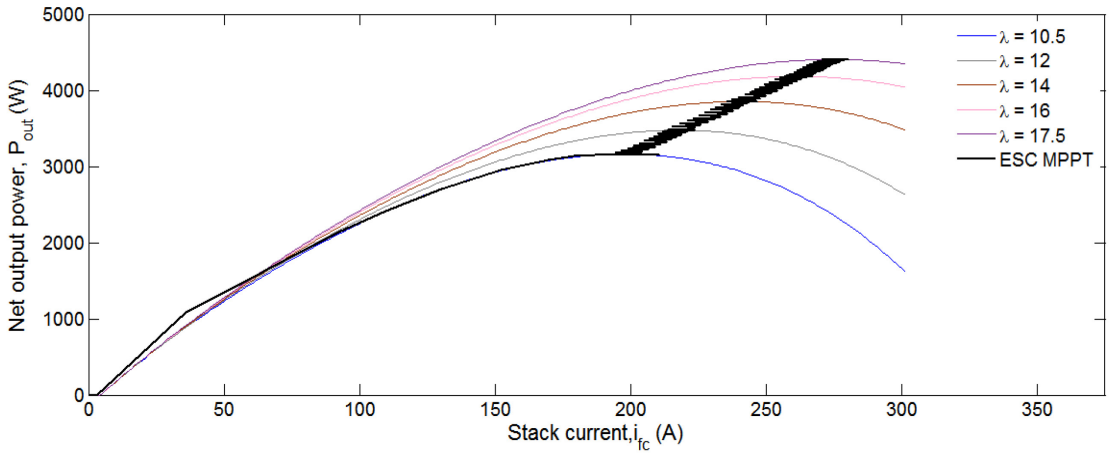

Fig. 3.17. Net output power of the MPPT technique with ESC algorithm

3.6.1 Simulation

The stack temperature of the PEMFC is maintained constant at 80˚C . The simulation is carried out with varying membrane water content (λ), as shown in Fig. 3.9 to investigate the performance of the system for the MPPT technique.

3.6.1.1 Efficiency of the MPPT Technique

The efficiency of the PEMFC for different values of membrane water content can be obtained using (2.38). The electrical efficiency (η) of the PEMFC with the MPPT technique is shown in Fig. 3.18.

From the figure, it can be seen that the efficiency of the PEMFC corresponding to the MPP operation of the PEMFC is low. This is due to the operation of the PEMFC in the high current region.

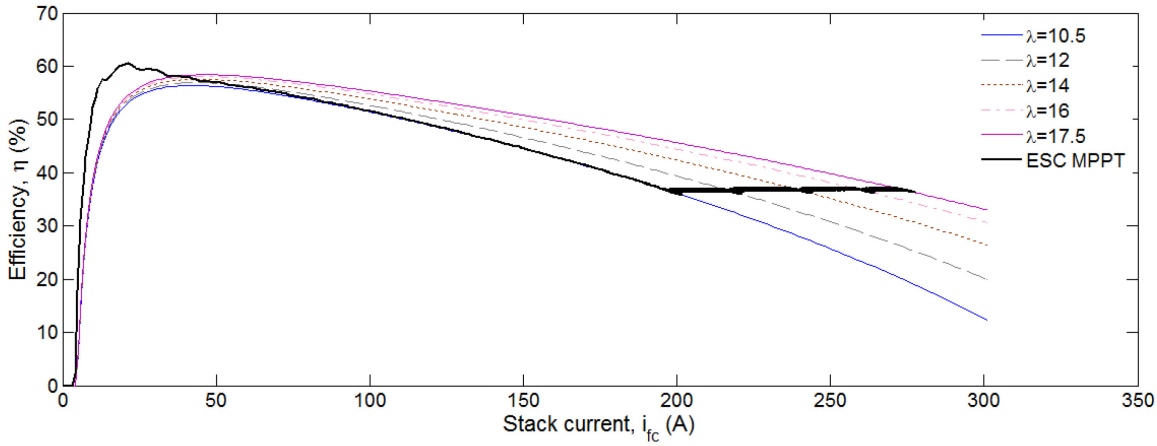

Fig. 3.18. Efficiency of the MPPT technique with ESC algorithm

3.6.1.2 Limitations of the MPPT Technique

The efficiency as a function of the net output power and membrane water content is shown in Fig. 3.19.

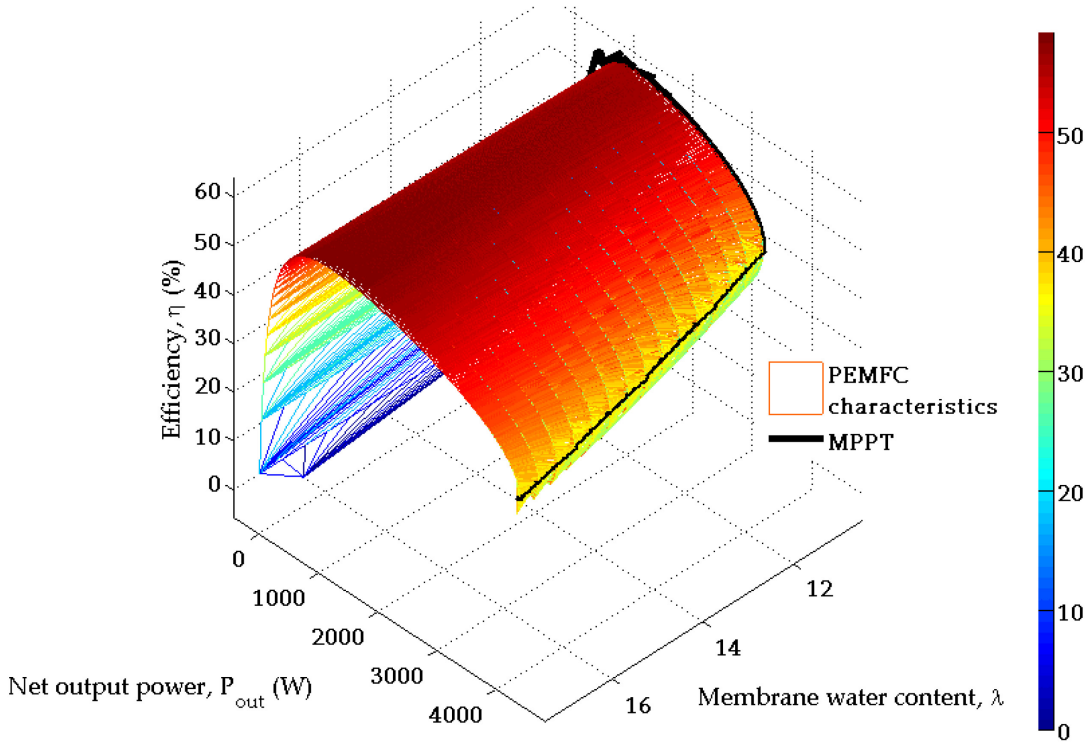

Fig. 3.19. Net output power and efficiency of the MPPT technique

It is observed that the efficiency of the PEMFC at the MPP is low (~35 to 40%). The low efficiency operation at the MPP leads to increased fuel consumption.

3.7 Maximum Efficiency Point Tracking (MEPT) Technique

The MEPT technique is similar to the MPPT technique except the efficiency (η) of the PEMFC is given as input instead of the net output power (P_{out}) used in the MPPT technique. The development of the ESC MEPT technique is discussed below.

3.7.1 MEPT Technique with Extremum Seeking Control

The modified extremum seeking control algorithm for the maximum efficiency point tracking is shown in Fig. 3.20. The values of the adaptation gain and perturbation amplitude are different from that of the MPPT technique. A tuning process to determine optimum values for the MEPT algorithm is carried out, and the selected values for the ESC MEPT are k_{mep} = 600, a_{mep} = 2, ω_{le} = 3 rad/s, ω_{he} = 18 rad/s, and ω_e = 30 rad/s. A hysteresis current controller with i_{mep} as the reference current is used to generate the switching pulses for the DC-DC boost converter.

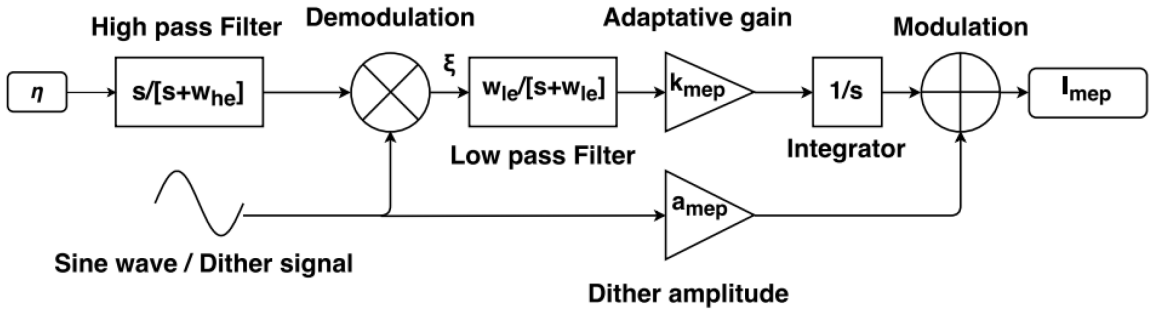

Fig. 3.20. Extremum seeking control based MEPT technique

3.7.2 Simulation

The stack temperature of the PEMFC is maintained constant at 80˚C. The simulation is carried out with varying membrane water content (λ), as shown in Fig. 3.8 to investigate the performance of the system for the MEPT technique.

3.7.2.1 Efficiency of the MEPT Technique

The MEPT tracking trajectory near the maximum efficiency point of the PEMFC for different values of membrane water content is shown in Fig. 3.21. The variation of the MEP for different values of λ is small. From the figure, it can be seen that the ESC MEPT tracks the maximum efficiency point of the PEMFC accurately. It is observed that the maximum efficiency point occurs in the low current region, which requires fuel consumption.

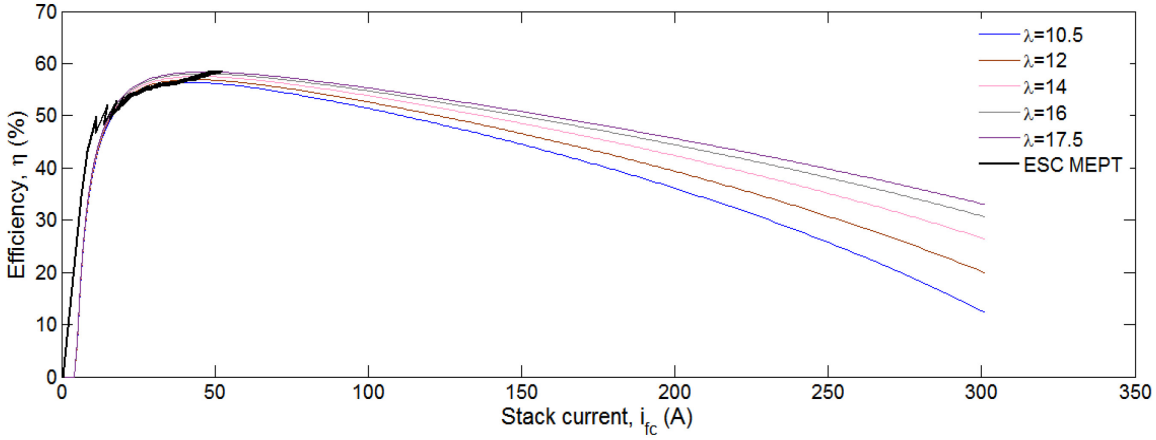

Fig. 3.21. Efficiency of the ESC MEPT technique

3.7.2.2 Net Output Power of the MEPT Technique

The net output power obtained using the PEMFC with MEP tracking technique is shown in Fig. 3.22. From the figure, it can be seen that the net output power of the PEMFC

corresponding to the MEP operation of the PEMFC is low. This is due to the operation of the PEMFC in the low current region.

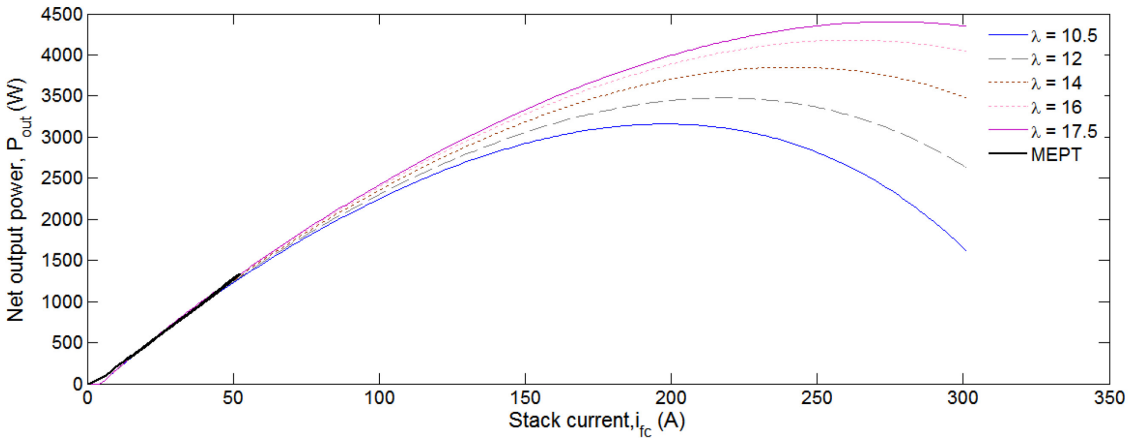

Fig. 3.22. Net output power of the ESC MEPT technique

3.7.2.3 Limitations of the MEPT Technique

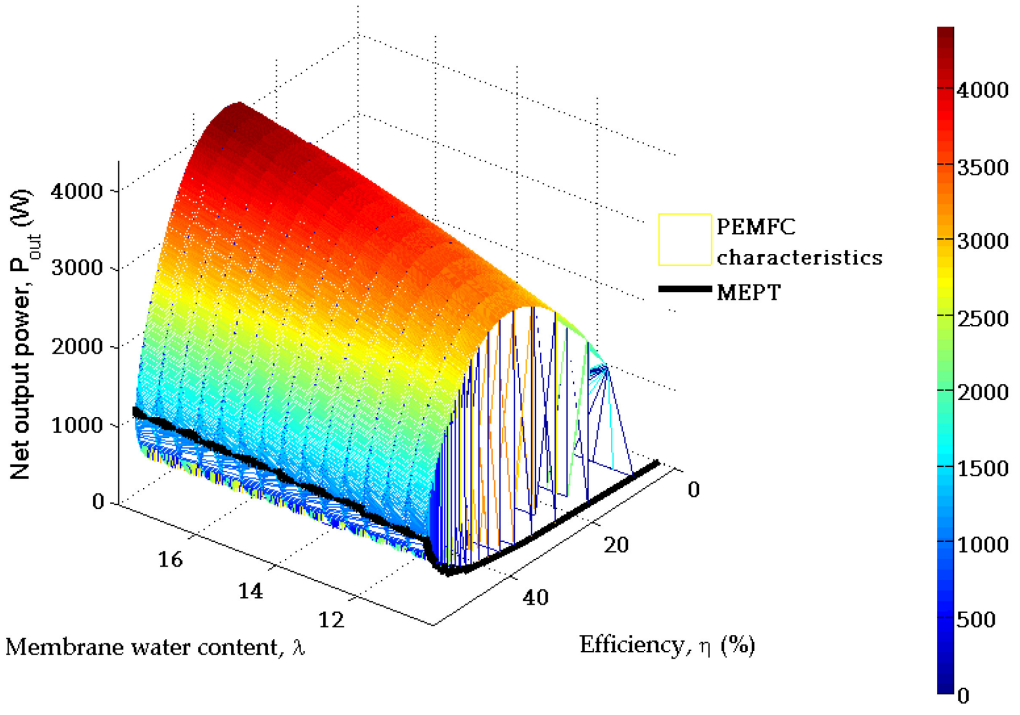

Fig. 3.23. Net output power and efficiency of the MEPT technique

The fuel consumption rate is low at the MEP due to the operation of the PEMFC in the low current region. However, the net output power (P_{out}) of the PEMFC with the MEPT technique is very low, as shown in Fig. 3.23. The results obtained from the MPPT and MEPT techniques are considered for further investigation in the next chapter.

3.8 Summary

Comparison of the different methods of implementing tracking control revealed that, the indirect method of tracking control is preferred because of the model-independent feature and load insensitivity. The DC-DC boost converter with hysteresis current control technique required for the power conditioning stage of the indirect control method was described and developed in Simulink. The working principle and development of three tracking algorithms, namely the extremum seeking control, the perturb and observe, and the sliding mode control used in photovoltaic systems, were presented with respect to their application in fuel cell systems. Simulation of a PEMFC system using the three tracking algorithms was carried out. A comparative analysis of the simulation results showed that the extremum seeking control algorithm accurately tracked the MPP of the PEMFC with high accuracy and high tracking speed. The extremum seeking control algorithm was selected for further comparative study of the maximum power point tracking and maximum efficiency point tracking techniques. The results confirmed the limitation of the MPPT technique, namely high fuel consumption rate (corresponding to high stack current) and low efficiency of the PEMFC at the MPP. On the other hand, the maximum efficiency point tracking technique was characterized by low fuel consumption (corresponding to low stack current) and low output power at the maximum efficiency point.

Chapter 4

Midpoint Tracking Technique

The PEMFC has the advantages of high power density and high efficiency when compared with internal combustion (IC) engines. However, the efficiency and net output power of the PEMFC are inversely related, so operating at maximum efficiency results in low net output power and operating at maximum net output power results in low efficiency. In order to overcome these limitations, a new tracking technique called the midpoint tracking (MDT) technique, which tracks the trade-off operating point, is proposed in this chapter.

The selection of a trade-off operating point plays a significant role in determining the effectiveness of the proposed tracking technique. The proposed tracking technique should satisfy the requirements, such as model-independency, high convergence speed, and high accuracy. Several possible methods to develop the midpoint tracking technique are discussed. The simulation-based investigations of the proposed tracking technique are carried out and the results are presented and discussed. A detailed comparison of the MPPT, MEPT, and MDT techniques for stationary PEMFC applications is presented. The work described in this chapter has been accepted for presentation at the IEEE Canadian Conference on Electrical Power and Energy Conference (EPEC) in October, 2016 [78].

4.1 Trade-off Operating Point

The net output power-efficiency characteristics of the PEMFC for varying membrane water content (λ) is shown in Fig. 4.1. In the case of operating points to the right of the MPP, the efficiency and net output power of the PEMFC are low. Similarly, the net output power and efficiency are low for operating points to the left of the maximum efficiency point. Hence, the region of the characteristics between the maximum efficiency point and maximum power point (identified by the ellipse) is considered to provide the trade-off operating point.

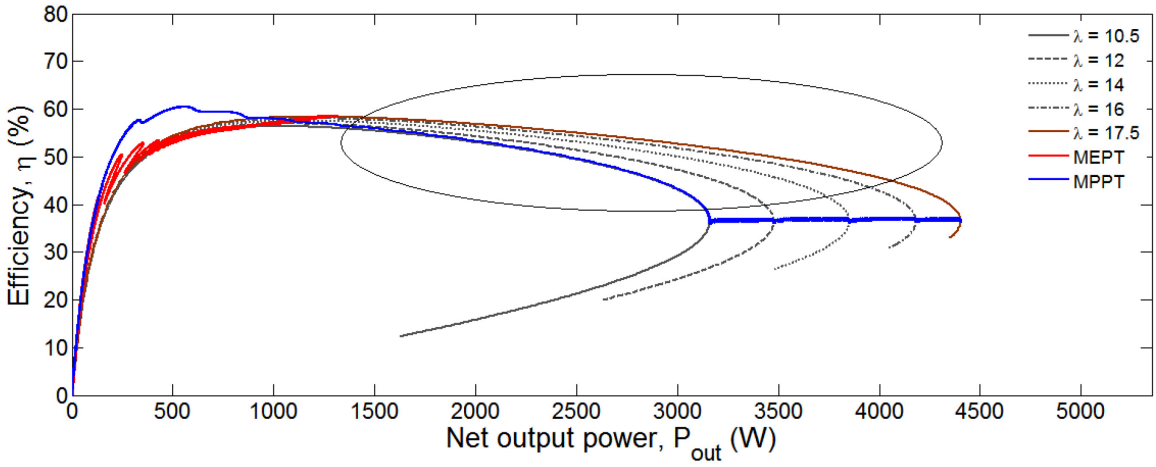

Fig. 4.1. PEMFC characteristics for the selection of trade-off operating point

Several possible trade-off operating points, namely the median of the net output power (M_P), the median of the efficiency (M_E), and the median of the stack current (M_I) can be considered within the region. The values of the net output power and efficiency corresponding to the above-mentioned operating points of the PEMFC are tabulated in Table 4.1.

Table 4.1: Net output power and efficiency of the PEMFC with different operating points at $\lambda = 14$

Operating points	MPP	M_E	M_I	M_P	MEP
Net output power, P_{out} (W)	3855.0	3365.0	3128.0	2477.5	1100.0
% of MPP	100.0	86.9	81.3	64.7	29.5
Efficiency, η (%)	36.4	46.9	49.0	53.3	57.4
% of MEP	63.8	81.9	85.4	92.5	100.0

For an operating corresponding to the median of efficiency (M_E), the net output power is high (86.9% of MPP), but the efficiency is low (46.9%). In the case of an operating point corresponding to the median of power (M_P), the efficiency is high (92.5% of MEP), but the net output power is low (64.7% of MPP). From the Table 4.1, it can be seen that the operating point corresponding to the median of current results in high net output power (81.3% of MPP), and high efficiency (85.4% of MEP). Hence, in this thesis, it is proposed to used the operating point corresponding to the median of current as the trade-off operating point (MD). The trade-off operating point varies with changes in the operating conditions, such as membrane water content, stack temperature, fuel pressure, and fuel flow. Hence, a tracking technique referred to as the midpoint tracking technique (MDT) is proposed to track changes in the trade-off operating point.

4.2 Midpoint Tracking Technique

The tracking algorithms reported in the literature are designed to track the maximum point (MPP or MEP) [39]–[45]. However, the objective of the midpoint tracking technique is to track the trade-off operating point, which occurs in the linear region of the

PEMFC characteristics shown in Fig. 4.2. The trade-off operating point depends on the maximum power point current (i_{mpp}), and the maximum efficiency point current (i_{mep}).

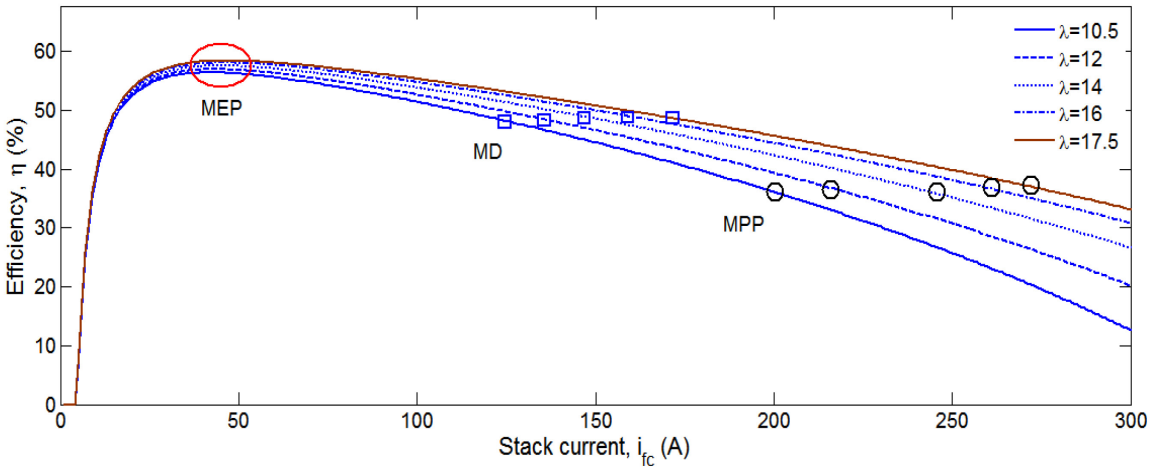

Fig. 4.2. Operating points of the PEMFC with the three tracking techniques

One possible solution for tracking the trade-off operating point is to define the boundary conditions of current by providing the maximum power point current (i_{mpp}) and maximum efficiency point current (i_{mep}) as inputs to the variation in operating conditions. However, this approach leads to a model-dependent control, and the accuracy of the control depends on the quality of inputs provided to define the boundary conditions (i_{mpp} and i_{mep}).

A simple curve fitting approach can also be used to track the trade-off operating point. However, this approach is sensitive to variations in more than one operating condition. This problem can be addressed by developing several regression equations incorporating the variations in operating conditions. However, this approach leads to a highly complex control technique with slow response.

In order to develop a model-independent MDT technique, a model similar to the PEMFC Simulink model, which provides the trade-off operating point (i_{mdt}) based on the net output power (P_{out}) is required. However, the development of the MDT model based

on this requirement is difficult due to the non-linear nature of the PEMFC. One possible solution is to employ statistical design approaches to develop the MDT technique. The statistical design approaches provide flexibility to add any number of inputs that influence the response. These approaches also lead to model-independent and accurate MDT technique. In this thesis, the MDT tracking algorithm based on the fast flexible filling (FFF) design [32] is proposed to track the trade-off operating point.

4.2.1 Fast Flexible Filling Design for the Midpoint Tracking Technique

The statistical response surface methodologies (RSM) can be used to develop the MD algorithm. However, the resulting algorithms would not be accurate due to the complex and non-linear nature of the PEMFC Simulink model. Space filling statistical designs are able to handle highly complex and nonlinear systems and is a suitable candidate for the development of the MD algorithm. Several statistical space filling designs have been reported in the literature [65]. As discussed in Chapter 2, the fast flexible filling (FFF) design generates design points based on the clusters from random points to cover the entire design space effectively when compared with other space filling designs [32]. Hence, the midpoint tracking algorithm based on the fast flexible space filling design using the JMP statistical discovery software is developed to track the trade-off operating point (i_{mdt}).

In order to develop a generic midpoint tracking algorithm for the PEMFC, the stack temperature, stack power and stack current corresponding to the trade-off operating point,

along with membrane water content are given as inputs to the PEMFC Simulink model to obtain the net output power corresponding to the trade-off current.

The stack temperature (T) and number of stacks (n) along with the net output power obtained in the previous step are considered as input factors in the MD FFF design to obtain the reference current (i_{mdt}). The levels of the factors considered for the MD FFF design are tabulated in Table 4.2.

Table 4.2: Factors and levels for MD FFF design

Factors	Low level	High level	Unit
P_{out}	0	5000	W
T	323 (50˚C)	353 (80˚C)	K
n	1	35	-

The analysis of variance (ANOVA) is carried out based on p-values less than the value of $\alpha = 0.01$. The R^2 value for the reference current is 0.99137, which indicates a good fit, as shown in Fig. 4.3. From the figure, it can be seen that the predicted stack current for the Ballard MK5-E obtained using the developed MD FFF is highly accurate.

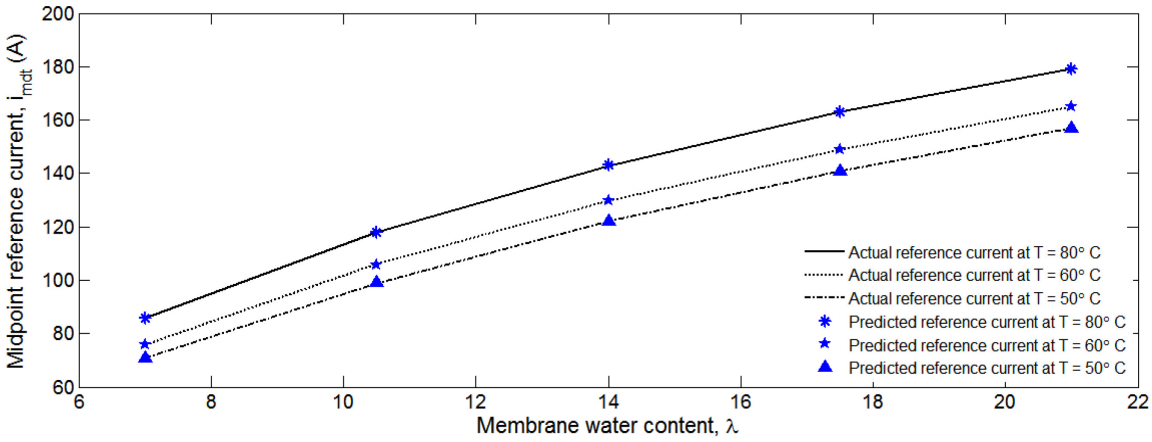

Fig. 4.3. Reference current actual vs. predicted

The regression equation obtained for the trade-off point reference current (i_{mdt}) is as follows:

$$\begin{aligned} \textit{Reference current } \left(i_{mdt}\right) \; = \; & b_1 + b_2 P_{on} - b_3 N - b_4 T_n - b_5 P_{on}^{\,2} - \\ & b_6 P_{on} N + b_7 N^2 - b_8 P_{on} T_n + b_9 N T_n + b_{10} N P_{on}^{\,2} + b_{11} N^2 P_{on} \end{aligned} \tag{4.1}$$

The variables P_{on}, T_n, and N are the normalized values based on the median of the factors, which are provided as input to the MD FFF design, which can be expressed as

$$P_{on} = u\frac{\left(P_{out} - 2500\right)}{2500} \tag{4.2}$$

$$T_n = \frac{T - 338}{15} \tag{4.3}$$

$$N = u\frac{\left(n - 18\right)}{17} \tag{4.4}$$

$$\textit{Scaling factor for MD FFF, } u = \frac{35}{n} \tag{4.5}$$

The values of the constant ($b_1 \ldots b_{11}$) are given in Appendix A. The reference current corresponding to the trade-off operating point for any required PEMFC can be obtained using (4.1). For example, the midpoint reference current (i_{mdt}) obtained using (4.1) for a 2.5 kW PEMFC is shown in Fig. 4.4. In order to obtain a 2.5 kW version from the 5 kW PEMFC Simulink model discussed in Chapter 2, the area of cross section (A) is changed from 232 cm^2 to 140 cm^2. From the figure, it can be seen that the predicted current obtained using (4.1) for a 2.5 kW PEMFC is highly accurate. This confirms the generic property of the developed midpoint tracking algorithm.

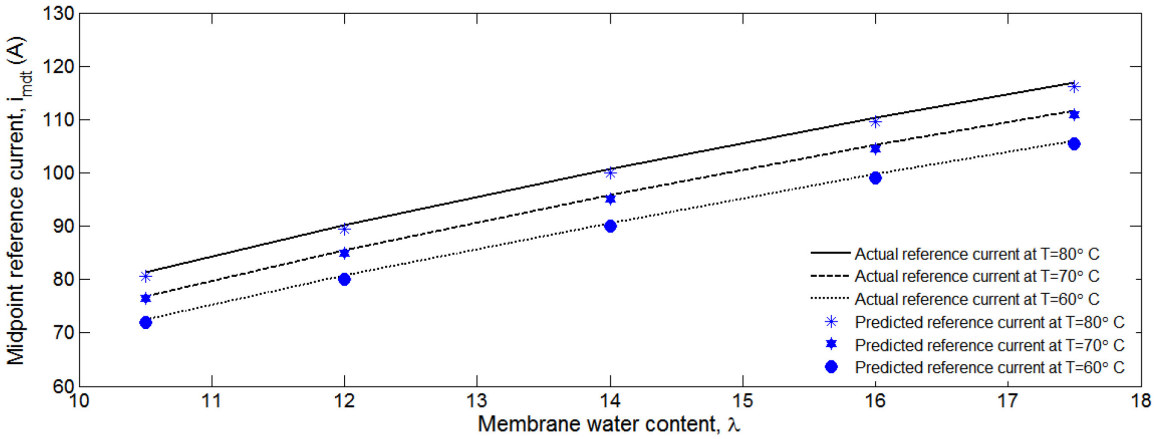

Fig. 4.4. Reference current actual vs. predicted for a 2.5kW PEMFC

4.3 Simulation

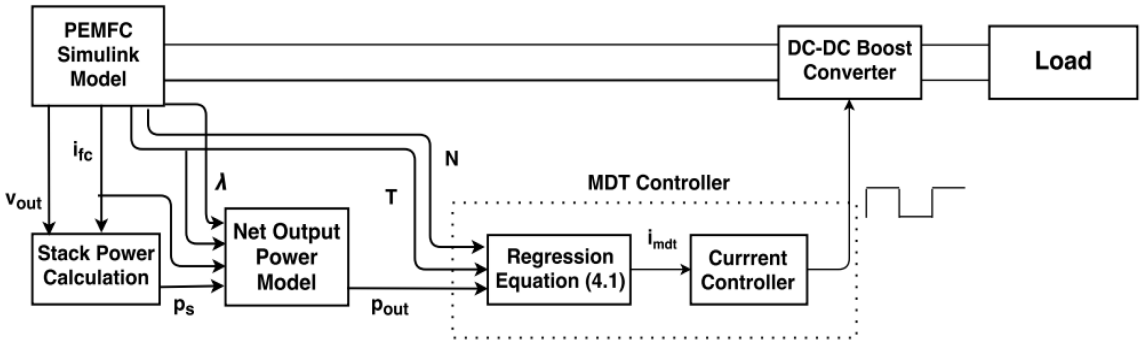

Fig. 4.5. PEMFC system with the MDT technique

In this simulation, the stack temperature of the fuel cell is maintained at 80˚C. The performance of the PEMFC system with the MDT technique is evaluated using the same range of variation of the membrane water content as in the analysis of the MPPT and MEPT techniques. The block diagram of the PEMFC system with MDT technique is shown in Fig. 4.5. The reference current obtained from (4.1) is fed to the hysteresis current controller which controls the DC-DC boost converter to track the trade-off operating point.

4.3.1 Output Power and Efficiency of the MDT Technique

The net output power and efficiency of the PEMFC with the MDT technique are shown in Fig. 4.6. From the figure, it can be seen that the developed MDT technique accurately tracks the net output power and efficiency corresponding to the trade-off operating points shown in Tables 4.1 and 4.2. The tracking speed of the MPPT and MEPT techniques can be varied by tuning the parameters associated with the tracking algorithm. However, the MD tracking algorithm does not have any tuning parameters to control the tracking speed. As a result, overshoot is observed in the tracking trajectory, as shown in Fig. 4.6.

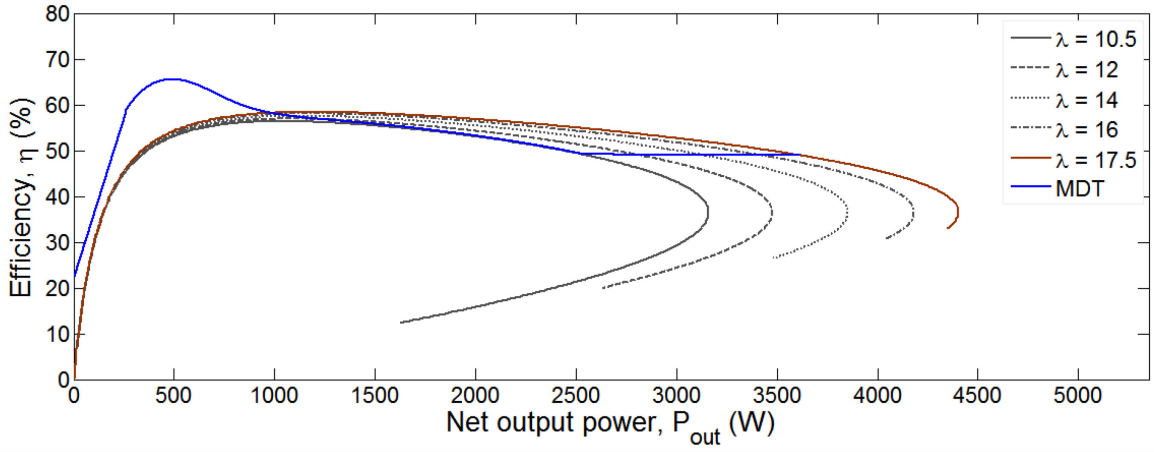

Fig. 4.6. Net output power and efficiency of the MDT technique

4.4 Comparison of the Tracking Techniques

A detailed comparison based on the simulation results obtained for the PEMFC with the MPPT and MEPT techniques using the ESC algorithm to track the maximum point, and the MDT technique to track the trade-off operating point is presented. The goal of the

comparison is to characterize three tracking techniques in relation to various operational requirements of stationary PEMFC applications.

4.4.1 Output Power of the Tracking Techniques

The tracking trajectories near the MPP, MEP, and MD for different values of membrane water content are shown in Fig. 4.7. From the figure, it can be seen that the developed tracking techniques accurately track the required operating points of the PEMFC (MPP or MEP or MD). As expected, the net output power of the MPPT technique is high when compared with the other tracking techniques. On the other hand, the net output power of the MEPT technique is very low due to the operation of the PEMFC in the lower stack current region. However, the MDT technique results in a trade-off operation with a 184% increase in output power when compared with the MEPT technique.

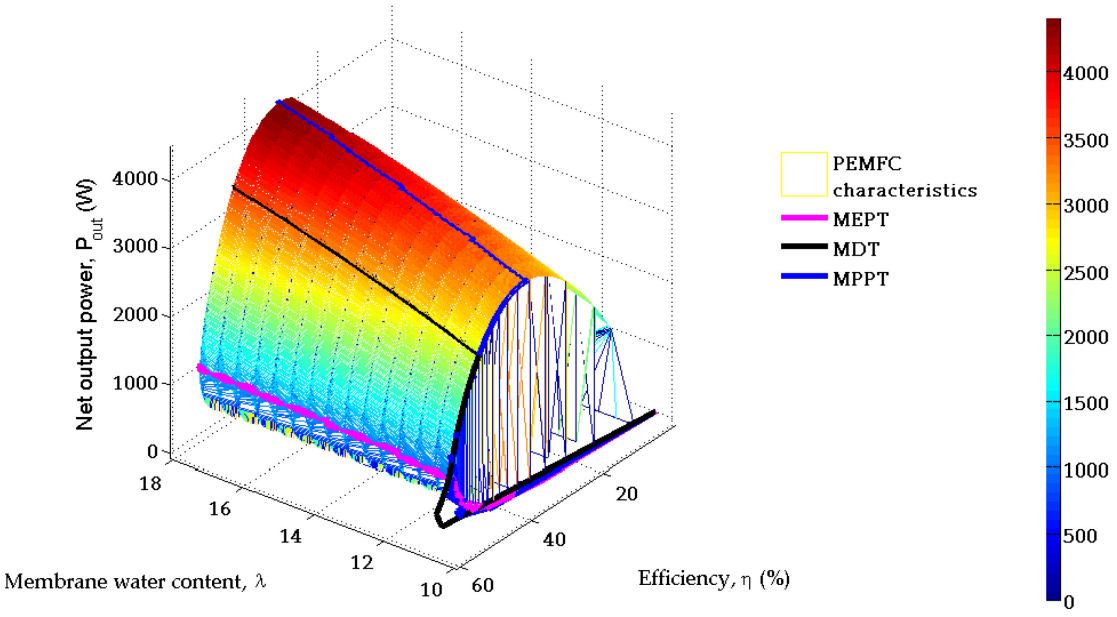

Fig. 4.7. Net output power of the PEMFC with the three tracking techniques

4.4.2 Efficiency of the Tracking Techniques

The efficiency of the PEMFC with the MPPT, MEPT, and MDT techniques is shown in Fig. 4.8. From the figure, it can be seen that the efficiency of the PEMFC with the MPPT technique is very low when compared with the other tracking techniques. The maximum power point of the PEMFC occurs in the higher stack current region with associated low efficiency. As expected, the MEPT technique tracks the maximum efficiency point, which ranges from 56.37% to 58.41% over a 60% change in membrane water content. However, the MDT technique tracks the trade-off operating point with a 25% increase in efficiency when compared with the MPPT technique.

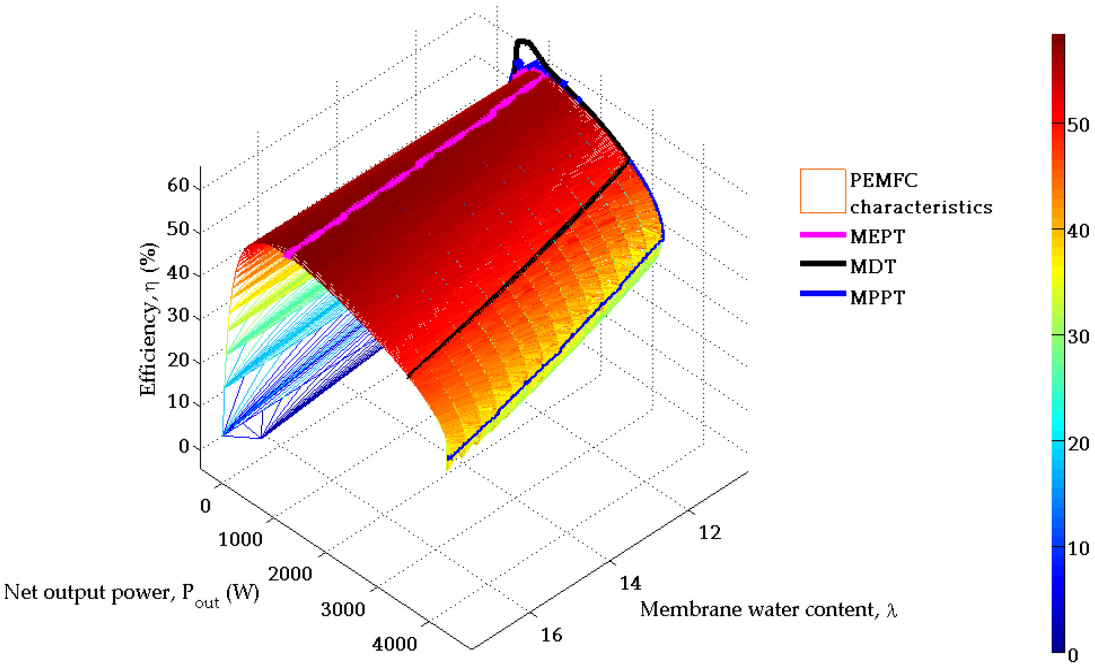

Fig. 4.8. Efficiency of the PEMFC with the three tracking techniques

4.4.3 Specific Power Density of the Tracking Techniques

One of the requirements of the stationary PEMFC applications is high specific power density (W/kg), and the tracking technique that meets this requirement is the preferred. In a PEMFC system, the humidifier and heat management system function to maintain the membrane water content and stack temperature at a constant predefined level. Hence, the membrane water content is assumed to be 100% humidified (λ=14) and the stack temperature is maintained at 80˚ C. The net output power of the tracking techniques corresponding to the specified operating conditions is considered in determining the specific power density. The specific power density of the PEMFC with the three tracking techniques is shown in Fig. 4.9.

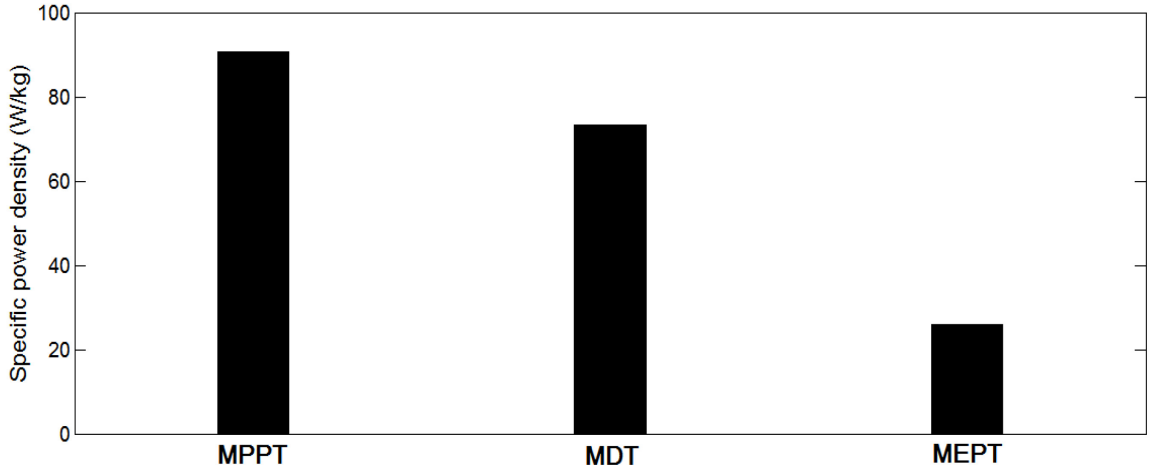

Fig. 4.9. Specific power density of the PEMFC with the three tracking techniques

From the figure, it can be seen that the specific power density of the MPPT technique is high when compared with the MEPT and MDT techniques due to high net output power at the MPP. The low net output power associated with the MEPT technique leads to a low value of specific power density. Consequently, for MEPT technique to

achieve the same net output power as the MPPT technique, a bigger PEMFC with more number of stacks is required. On the other hand, the MDT technique with trade-off operation results in increased specific power density (184%) when compared with the MEPT technique.

4.4.4 Stack Volume of the Tracking Techniques

Stack volume plays a significant role in stationary PEMFC applications. A low stack volume results in a PEMFC unit that is compact with reduced weight and cost. Therefore, a tracking technique that meets the requirement of low stack volume is preferred. Considering the net output power of the MPPT technique as the target power, additional stacks are required to meet the target power for the MDT and MEPT techniques. The number of additional stacks required for the MDT and MEPT techniques can be obtained using the following expression.

$$Number\ of\ additional\ stacks = \frac{P_{MPPT}}{\left(\frac{P_{MEPT/MDT}}{n}\right)} \tag{4.6}$$

These additional stacks are considered in calculating the stack volume of the PEMFC with the three tracking techniques. The stack volume obtained after stack modification is shown in Fig. 4.10.

From the figure, it can be seen that the stack volume of the MEPT technique is very high due to the low net output power at the MEP. On the other hand, the stack volume of the MPPT technique is low when compared with the other two tracking techniques. The

MDT technique operating at the trade-off operating point results in a 75% reduction in stack volume when compared with the MEPT technique.

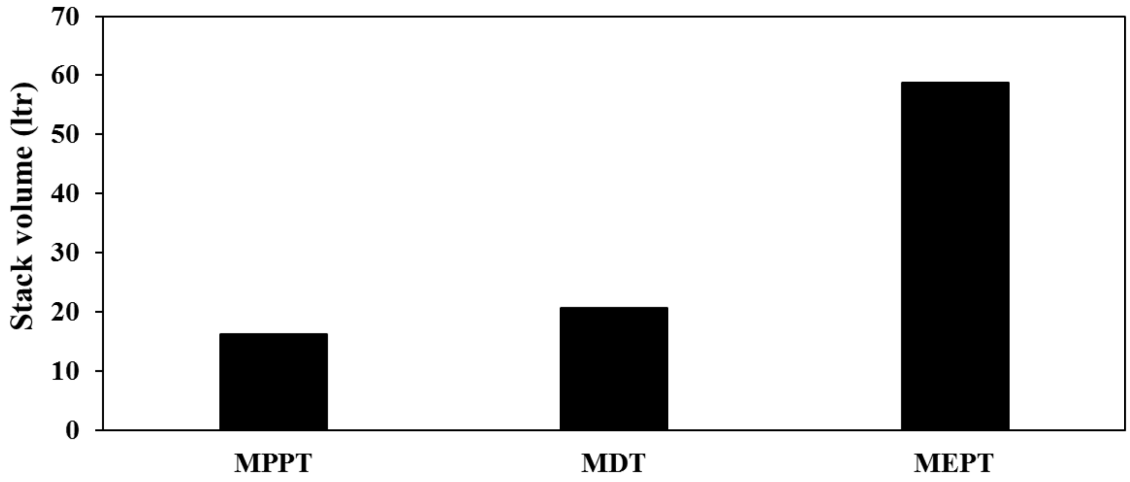

Fig. 4.10. Stack volume of the PEMFC with the three tracking techniques

4.4.5 Duration of Operation of the Tracking Techniques

The Ballard MK5-E PEMFC considered in this study is supplied with a 500 SL (standard litre) hydrogen tank. The duration of operation of the PEMFC with MPPT, MDT, and MEPT techniques is shown in Fig. 4.11.

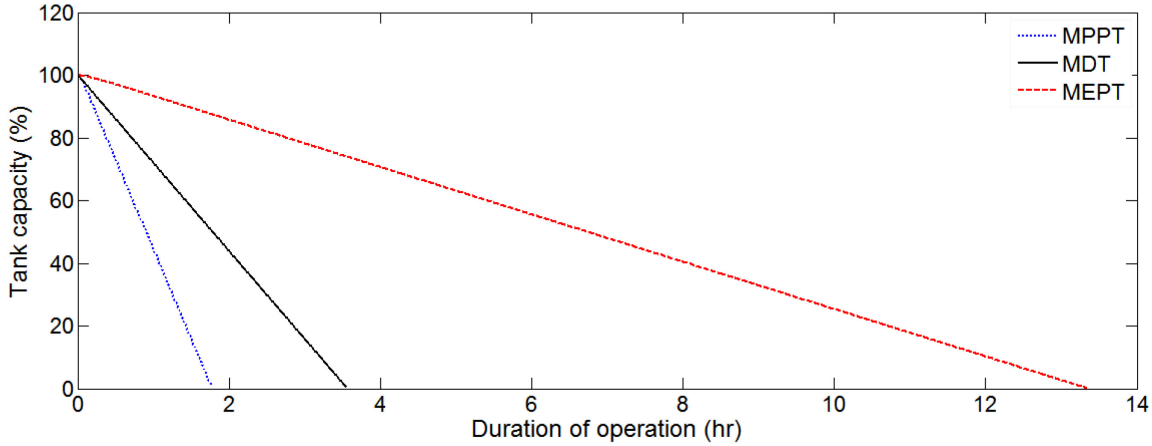

Fig. 4.11. Duration of operation of the PEMFC with the three tracking techniques

The duration of operation of the MEPT technique is very high because the PEMFC consumes less fuel when it operates at the maximum efficiency point. As discussed in previous sections, the efficiency of the MPPT technique is low, which contributes to increased fuel consumption. Hence, the duration of operation of the MPPT technique is short when compared with the other two tracking techniques, as shown in Fig. 4.11. The MDT technique with moderate efficiency results in an 80% increase in the duration of operation when compared with the MPPT technique.

4.4.6 Cost of the PEMFC with the Tracking Techniques

The cost of the PEMFC is calculated by taking the capital cost (C_c) of a 5 kW PEMFC system which is $22,000 [79] as the reference. The stack modification required for the MDT and MEPT techniques to meet the net output power of the MPPT technique is considered in calculating the cost of the PEMFC. The cost of the additional stacks ($C_{MDT/MEPT}$) is calculated based on the following expression

$$C_{MDT/MEPT} = \frac{C_c}{P_{MEPT/MDT}} P_{MPPT} \tag{4.7}$$

The cost of the PEMFC with the three tracking techniques is shown in Fig. 4.12. The MEPT technique results in high PEMFC cost due to the requirement of a large number of stacks to meet the P_{out} of the MPPT technique.

From the figure, it can also be seen that the MPPT technique with less number of stacks results in low cost of the PEMFC. Although the MDT technique requires additional

stacks to meet the MPPT technique, the cost of the PEMFC for the MDT technique compared with that of the MEPT technique is low (35.2% of MEPT).

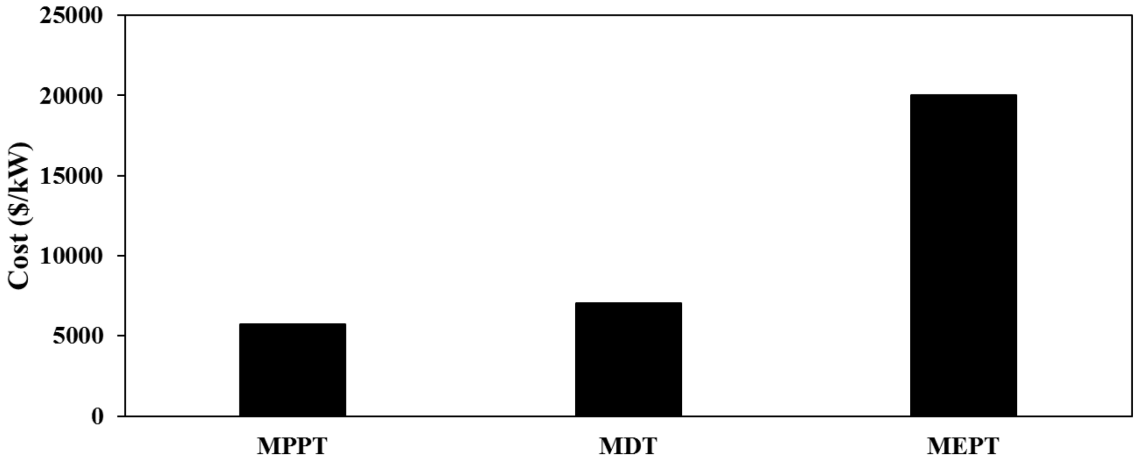

Fig. 4.12. Cost of PEMFC with the three tracking techniques

The characteristics of the three tracking techniques discussed above are summarized in Table 4.3

Table 4.3: Characteristics of the tracking techniques

Tracking Technique	MPPT	MDT	MEPT
Output Power	Very high	High	Low
Efficiency	Low	High	Very high
Specific power density	Very high	High	Low
Stack volume	Very low	Low	High
Duration of operation	Very low	Low	High
Cost of electricity	Very low	Low	High

From the above-mentioned points, it can be seen that the MDT technique results in reasonable high output power (81.3% of MPP), high efficiency (85.4% of MEP), high

specific energy density, small size, long duration of operation (180% of MPP), and low cost of electricity (35.2% of MEP). Hence, the MDT technique is the suitable technique to satisfy all the requirements of the stationary PEMFC applications.

4.5 Summary

The limitations of the maximum power point tracking and the maximum efficiency point tracking techniques were discussed. In order to obtain reasonable high net output power and high efficiency from the PEMFC, the midpoint of the maximum power point current and maximum efficiency point current was proposed as the trade-off operating point. The requirements of the tracking algorithm to track the trade-off operating points were discussed. Several possible methods to develop the midpoint tracking technique were taken into consideration and discussed. In order to develop a generic and model-independent midpoint tracking technique, the statistical fast flexible filling design was selected. The development of the midpoint fast flexible filling design to obtain the reference current corresponding to the trade-off operating point was presented. The reference current regression equation obtained from the developed design was implemented in Simulink to analyse the performance of the midpoint tracking technique. The simulation results showed that the developed midpoint tracking technique was effective in tracking the trade-off operating point for varying membrane water content. A detailed comparison of the performance of the MPPT, MEPT, and MDT techniques for various operational parameters, such as the net output power, efficiency, specific power density, stack volume, duration of operation, and cost of the PEMFC was presented and discussed. However, a detailed economic analysis to determine the effects of the tracking techniques on the cost

of electricity produced is required to select a suitable tracking technique for particular requirements of stationary PEMFC applications. A detailed economic analysis of the PEMFC system is presented in the following chapter.

Chapter 5

Economic Analysis of a Standalone PEMFC Generation System with Different Tracking Techniques

The PEMFC has the advantages of high power density, rapid start-up, moderate operating temperature, low maintenance cost, and zero carbon emission [54]. For all these reasons, PEMFCs are widely used in stationary, transportation, and portable applications [80]. Although PEMFCs have several advantages compared to conventional energy sources, the cost of electricity (COE) produced play a major role in determining the capability of PEMFCs to replace conventional energy sources. Yet accurate economic analysis to determine the cost of electricity of the PEMFC generation system is lacking in the literature.

In this chapter, a complete economic analysis of a standalone PEMFC system is presented. The economic analysis takes into account the capital cost, replacement cost and maintenance cost of the PEMFC, cost of hydrogen infrastructure, cost of power converters, cost of storage technique (electrolyzer and hydrogen tank) used to store excess electricity, effects of tracking techniques, and real time variations in load conditions. In addition, ten

load configurations are considered in order to investigate the effects of system size (rating) and combined heat and power (CHP) capability of the PEMFC system on the COE. Finally, based on economic considerations, a procedure to select a suitable tracking technique for particular requirements of a standalone PEMFC generation system is proposed. The work described in this chapter is under review for publication in the IET Renewable Power Generation [81].

5.1 System Configuration

In a PEMFC generation system, the heat management system and the humidifier system function to maintain the stack temperature (T) and membrane water content (λ) at a predefined constant level. In this economic analysis, the stack temperature is maintained constant at 80˚ C and the polymer electrolyte membrane is assumed to be 100% humidified (λ = 14). The net output power and efficiency values obtained for the maximum power point tracking, maximum efficiency point tracking, and midpoint tracking techniques as shown in Table 4.1 in Chapter 4 are considered as reference for configuring the systems considered for the economic analysis. In general, a standalone PEMFC system without a tracking technique consists of the PEMFC unit, power converter, hydrogen tank, and load. Incorporating tracking techniques to extract maximum power or operate at the maximum efficiency requires a storage technique to store the excess electrical energy produced by the PEMFC. This excess electricity is produced, when the operation of the PEMFC is at a constant operating point (MPP or MEP or MD), which results in higher output power than the load demand.

A review of different energy storage techniques presented in the literature shows that the modular, simple, and high energy density storage techniques, such as battery and hydrogen storage systems are widely used [82]–[84]. In this thesis, the hydrogen storage technique with less maintenance cost, low noise, and low CO_2 emissions is used to store the excess electrical energy produced by the PEMFC [85]. The electrolyzer in the hydrogen storage technique, converts the excess electricity to hydrogen and stores it in a hydrogen storage tank. The configuration of the system with hydrogen storage technique is shown in Fig. 5.1.

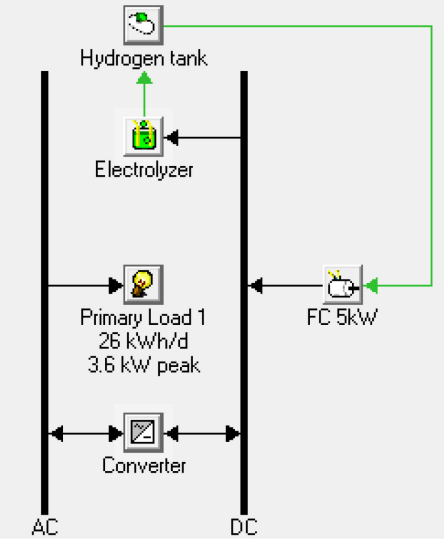

Fig. 5.1. System configuration

The electrical efficiency of the PEMFC varies from 35% to 60% depending on the type of tracking technique (Fig. 4.2). The remaining energy from the fuel is dissipated as heat. This heat can be utilized in a combined heat and power (CHP) configuration to supply a thermal load, thereby increasing the total efficiency of the PEMFC. For example, with a 50% heat recovery, the efficiency of the PEMFC unit can be increased from 67.5% (36.4% electrical efficiency + 31.1% thermal efficiency) to 80% (57.4% electrical efficiency +

22.6% thermal efficiency) depending on the type of tracking technique. In general, the heat recovery ratio varies from 40% to 60% [86]. Hence, an intermediate value of heat recovery ratio (50%) is chosen. The configuration of the system with CHP is shown in Fig. 5.2.

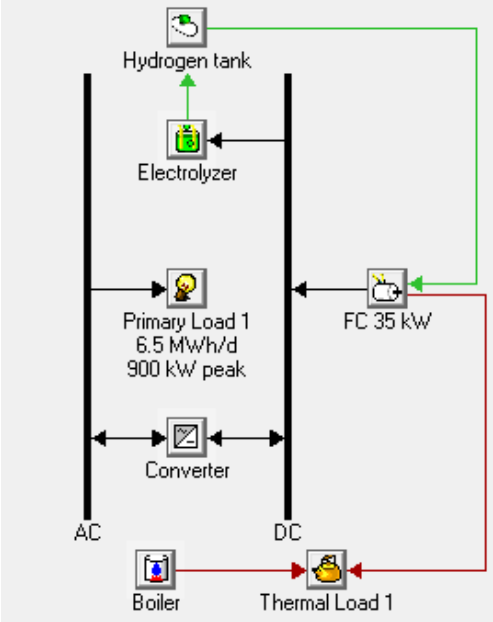

Fig. 5.2. System configuration with thermal load

5.2 Economic Terms

Several economic terms are used in the economic analysis of the PEMFC system in this thesis to describe the impact of the tracking techniques on the cost of electricity (COE). Economic terms such as total net present cost (C_{NPC}) and levelized cost of electricity (LCOE) are explained below.

5.2.1 Total Net Present Cost

The total net present cost (C_{NPC}) of a system is based on the present value of the components in the system. The total net present worth is obtained from the total annualized

capital cost, operation and maintenance cost, cost of fuel, and cost of depreciation of the components over the lifetime of the system or project. The expression used to calculate the total net present cost of the system is given as [87]

$$C_{NPC} = \frac{C_{an,tot}}{\left[\frac{i(1+i)^{N_{yr}}}{\left((1+i)^{N_{yr}}-1\right)}\right]} \tag{5.1}$$

where $C_{an,tot}$ is the total annualized cost, which includes the total annual cost of the components in the system ($/yr); N_{yr} is the lifetime of the project; i is the annual real interest rate (%). In this thesis, the annual real interest rate is set at 6% and the project lifetime is set at 25 years.

5.2.2 Levelized Cost of Electricity

The levelized cost of electricity (LCOE) provides the net present unit cost of electricity ($/kWh) over the lifetime of the project. A good project should have a low levelized cost of electricity. In the case of combined heat and power (CHP) configuration, the cost of energy supplied to the thermal load is deducted from the total cost of the electrical energy produced per kWh to achieve a realistic value of LCOE. The expression for calculating the LCOE is given as [87]

$$LCOE = \frac{C_{an,tot} - C_b E_t}{E_{AC} + E_{DC}} \tag{5.2}$$

where $C_{an,tot}$ is the total annualized cost of the system ($/yr); C_b is the marginal cost of the boiler ($/kWh); E_{AC} is the AC load (kWh/yr); E_{DC} is the total DC load (kWh/yr); E_t is the

total supplied thermal load (kWh/yr). In the absence of a thermal load, the value of E_t is set to zero. The LCOE can be used to determine the most suitable tracking technique for the PEMFC.

5.3 Case Studies

The cost of the PEMFC per kW decreases as the rating of the PEMFC increases [79]. In order to include this variation and its impact on the LCOE, ten different loads are considered. Table 5.1 shows the type and rating of the load.

Table 5.1: Load configuration.

Case No	Electrical load		Thermal load
	kWh/day	Peak kW	
1	25	3.5	No
2	158	22	No
3	325	45	No
4	650	90	No
5	1300	180	No
6	3420	450	No
7	6840	900	No
8	13000	1800	No
9	6840	900	Yes
10	13000	1800	Yes

The configuration shown in Fig. 5.1 is used for the cases without thermal load (cases 1-8) and the configuration shown in Fig. 5.2 is used for cases with thermal load (cases 9 and 10).

5.3.1 Electrical Load Profile

The load data from the Hybrid Optimization Model for Electrical Renewables (HOMER) example (Sicud village in the Philippines) is considered as reference for configuring the load used in the above-mentioned case studies [88]. The load profile used for all the case studies is shown in Fig. 5.3.

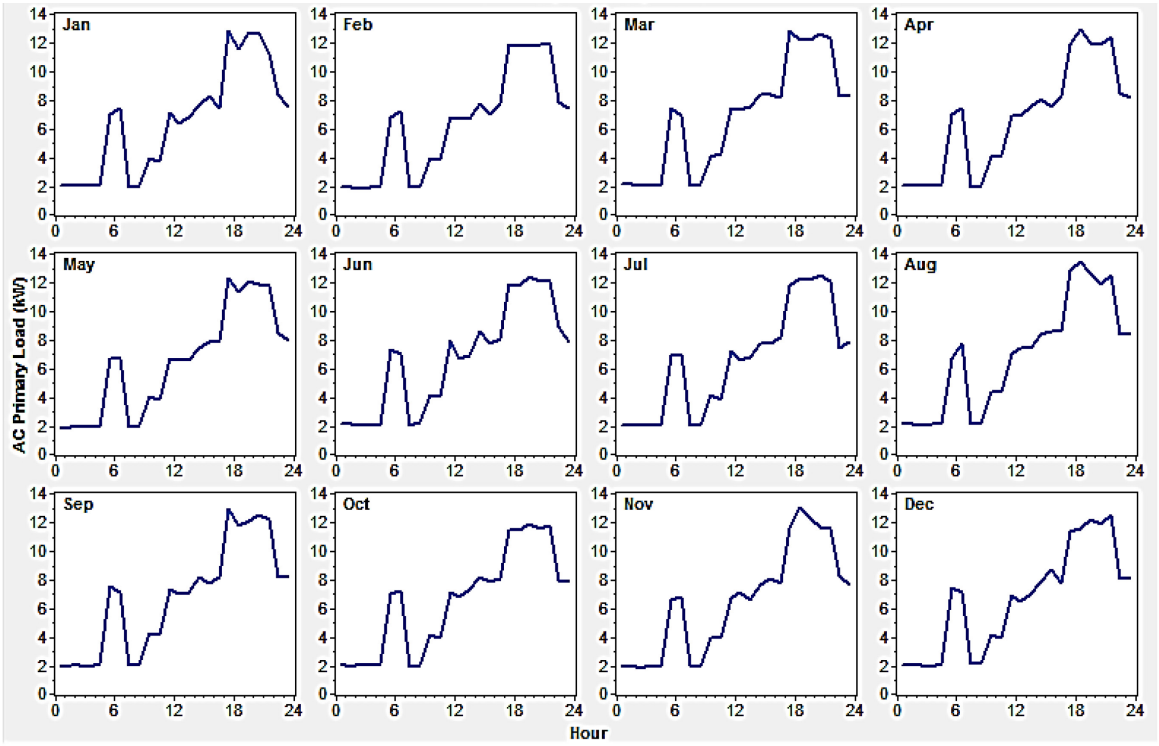

Fig. 5.3. Load profile

In order to include the seasonal and unexpected load variations, the random variability from day to day in a month is set at 10% and time step to time step (for every hour) variability is set at 20%. The load profile presented in Fig. 5.3 is considered as a reference and it can be scaled up or down according to the requirements of the load configuration in Table 5.1.

5.3.2 Thermal Load Profile

The thermal load profile used to analyze the effect of CHP configuration on the economics of the PEMFC for cases 9 and 10 is shown in Fig. 5.4. The thermal load is considered maximum during the daytime and minimum during nighttime. The day and time random variability is set at 10% and 20%. The renewable fraction of the system is set at 100%.

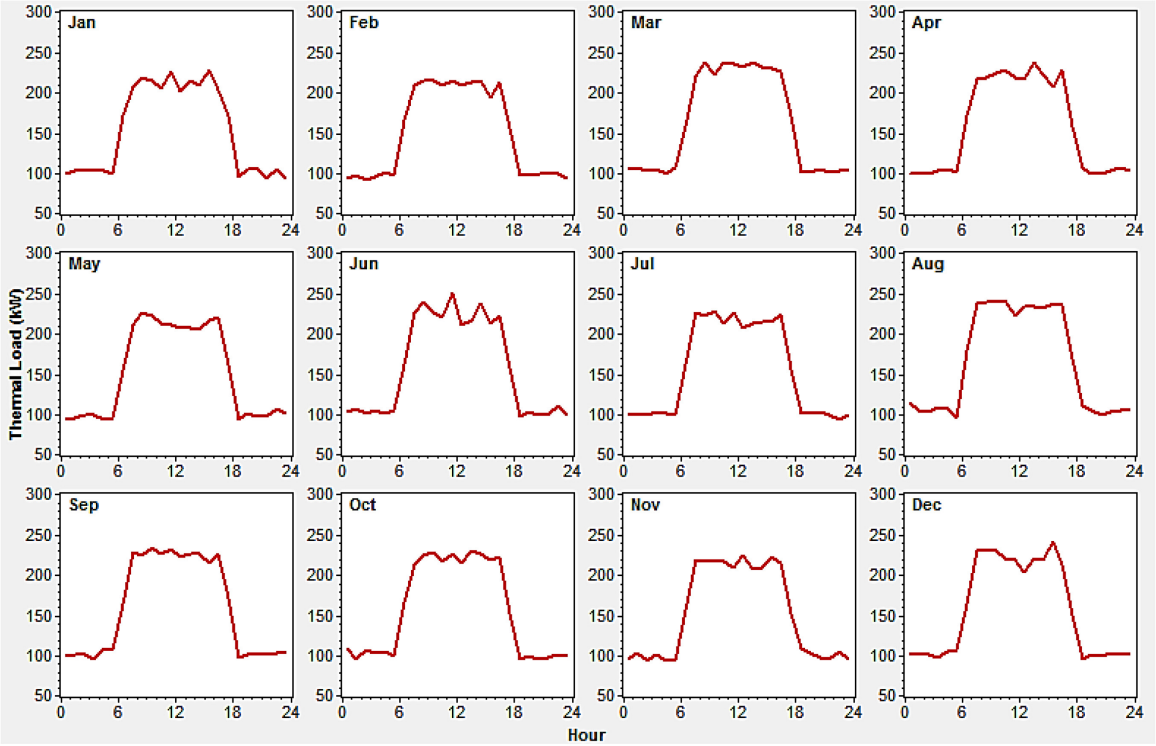

Fig. 5.4. Thermal load profile

HOMER includes the boiler running on diesel by default with the thermal load. The working schedule of the boiler is based on the cost of thermal energy supplied by the PEMFC ($C_{t,PEM}$) using combined heat and power configuration. In this thesis, the thermal

load supplied by the PEMFC is limited by the value of $C_{t,PEM}$ to satisfy the following condition:

$$C_{t,PEM} << C_{diesel} \tag{5.3}$$

where C_{diesel} is the cost of thermal energy supplied using a boiler running on diesel ($/kWh). The cost of diesel is set at $1.2/liter, and the efficiency of the boiler connected in-between the thermal load and diesel fuel is set at 85%.

5.4 Selection of Components

The selection of the component ratings plays an important role in measuring the influence of the tracking techniques on the economics of the PEMFC. The major constraints considered in this economic analysis are as follows:

- The system should be configured to meet the entire load demand (unmet load = 0)
- The excess electricity should be as minimum as possible (% of excess electricity ~ 0)
- The capacity shortage should be as minimum as possible (% of capacity shortage ~ 0)

5.4.1 Proton Exchange Membrane Fuel Cell

The load profile should be taken into consideration in determining the rating of the PEMFC to ensure that the maximum power required by the load (P_{load}) is always less than the rating of the PEMFC. The rating of the PEMFC also depends on the efficiency of the power converters connected between the load and the PEMFC. Hence, the following condition is used to determine the rating of the PEMFC to meet all the required conditions.

$$P_{rating} >> P_{out} >> P_{load} \tag{5.4}$$

In (5.4),

$$P_{rating} = P_{out} + P_{aux} \tag{5.5}$$

$$P_{out} = P_{load}\left(100 + \left(100 - \eta_p\right)\right) \tag{5.6}$$

where, η_p is the efficiency of the power converter. The fuel consumption curve for different ratings of the PEMFC [89] is used to determine a general relationship between the hydrogen consumption rate (kg/hr) and the net output power (P_{out}) of the PEMFC (kW) based on the curve fitting approach as shown in Fig. 5.5.

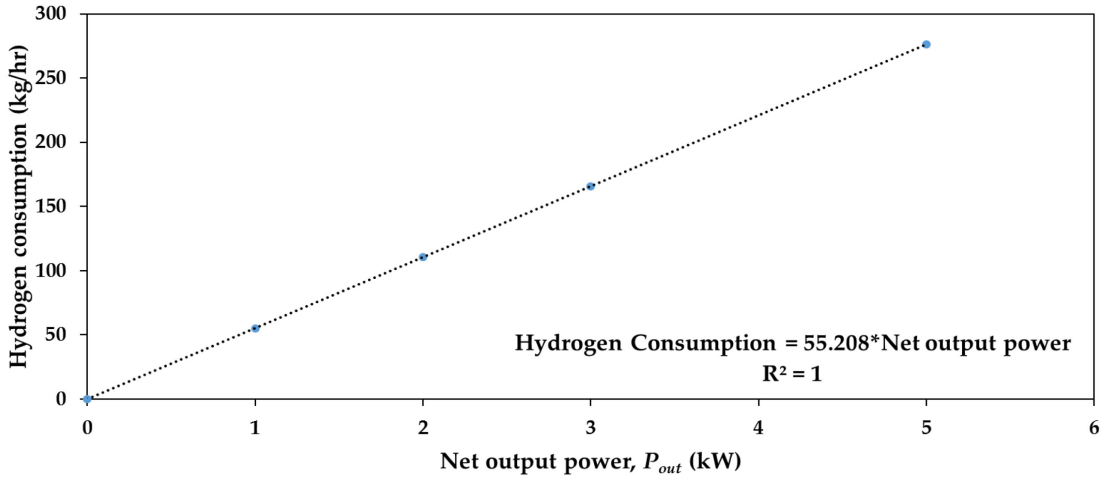

Fig. 5.5. Hydrogen consumption rate per kW power of PEMFCs

The cost of PEMFCs for different ratings obtained from a fuel cell store [79] is used to determine a general relationship between the cost per kW ($/kW) and the rating of PEMFC (kW) based on curve fitting approach as shown in Fig. 5.6.

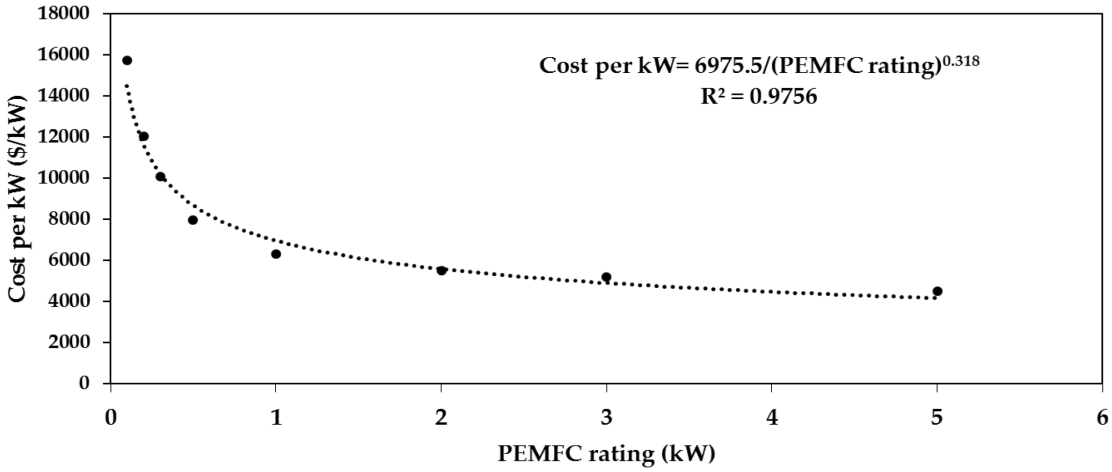

Fig. 5.6. Cost per kW rating of PEMFCs

The lifetime of the PEMFC is assumed to be 40000 hr (~4.566 yr) while the replacement cost is assumed to be 65% of the capital cost [8].

5.4.2 Inverter

The rating of the inverter ($P_{inverter}$) that supplies the AC load can also impact the value of the unmet electricity. The following condition is considered in order to keep the unmet load contributed by the inverter to zero.

$$P_{inverter} \geq P_{load} \tag{5.7}$$

The capital cost and replacement cost for different ratings of an inverter are shown in Fig. 5.7 [90]. From the figure, it can be seen that the capital and replacement cost of any required size of the inverter can be obtained.

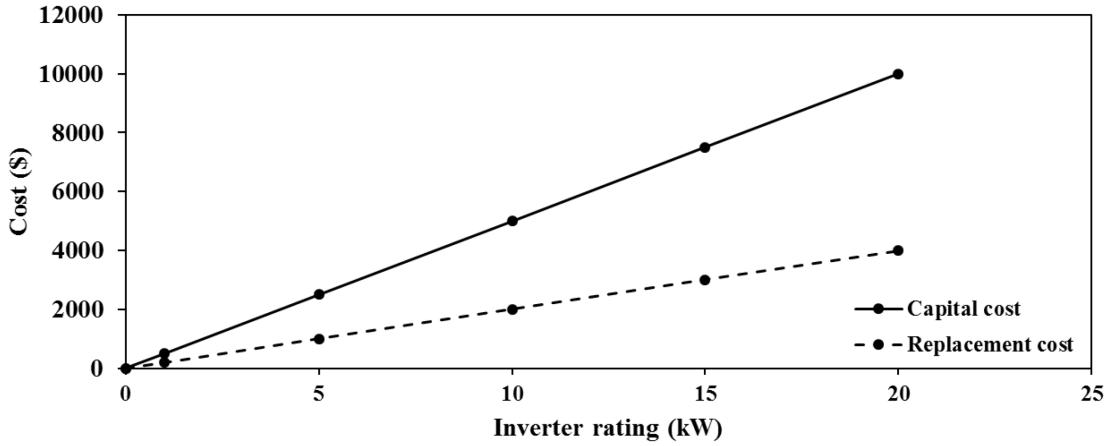

Fig. 5.7. Capital and replacement cost of inverter

In this economic analysis, the operational and maintenance (O&M) cost of the inverter is assumed to be $10/yr and the lifetime of the inverter is assumed to be 15 years.

5.4.3 Electrolyzer

The rating of the electrolyzer (P_{elec}) is selected so as to utilize the entire output power of the PEMFC in the case of very low load demand (~0), which occurs at short intervals. During these intervals, the PEMFC can be turned off, but frequent turn-off and turn-on will degrade the life of the membrane. It is therefore preferred to operate the PEMFC continuously and use the excess power to produce hydrogen for storage. The following condition is taken into consideration while selecting the rating of the electrolyzer.

$$P_{elec} \leq P_{out} \tag{5.8}$$

In this thesis, the net output power of the PEMFC is considered as the rating of the electrolyzer. The capital cost and replacement cost of an electrolyzer of different ratings are shown in Fig. 5.8 [91].

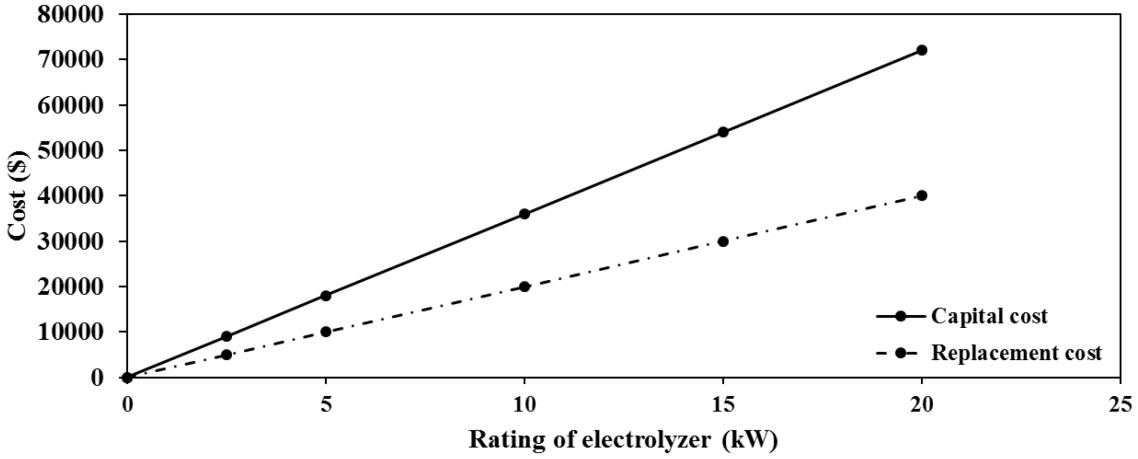

Fig. 5.8. Capital and replacement cost of electrolyzer

The operation and maintenance cost of the electrolyzer is assumed to be $10/yr and the lifetime of the electrolyzer is assumed to be 15 years.

5.4.4 Hydrogen Tank

Hydrogen storage tanks are included in the system to store the required amount of hydrogen for the PEMFC and to store the hydrogen produced by the electrolyzer. Using the capital cost of the hydrogen tanks corresponding to 2123 kg and 24733 kg hydrogen as reference [92], the capital cost of the hydrogen storage tank for different capacities is extrapolated and shown in Fig. 5.9. The replacement cost of the hydrogen tanks is assumed the same as the capital cost shown in Fig. 5.9. Initially, the hydrogen tank is considered to be at 100% of its capacity. At the beginning of every year, the cost of hydrogen refueling and transportation required for each configuration is added to the O&M cost of the corresponding hydrogen tank in that configuration. The quantity of hydrogen fuel (H_r) required by the PEMFC is determined based on the following expression:

$$H_r = H_t - H_p \tag{5.9}$$

where, H_t is the quantity of hydrogen remaining in the tank at the beginning of the year (kg); H_p is the quantity of hydrogen produced by the electrolyzer at the beginning of the year (kg). The cost of hydrogen fuel considered in this analysis is \$1.8/kg [93]. The transportation cost of hydrogen is assumed to be \$500/yr.

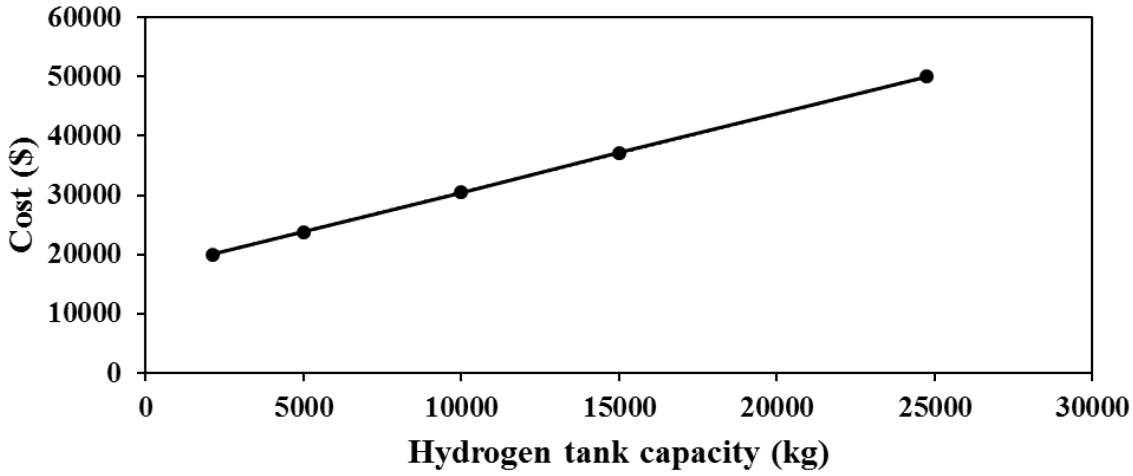

Fig. 5.9. Capital cost of hydrogen storage tank

The O&M cost of the hydrogen storage tanks is assumed to be 10% of the capital cost and the lifetime of the hydrogen storage tanks is assumed to be 25 years. The net output powers and efficiencies used in this economic analysis are tabulated in Table 5.2.

Table 5.2: Parameters considered for the economic analysis.

Efficiency of the components		**Net output power (P_{out})**	
Component	**Efficiency (%)**	**Net output power**	**Value**
PEMFC with MPPT	36.4	P_{MPPT}	77.04% of P_{rating}
PEMFC with MDT	49.0	P_{MDT}	81.20% of P_{MPPT}
PEMFC with MEPT	57.4	P_{MEPT}	28.55 % of P_{MPPT}
Inverter	90.0		
Electrolyzer	85.0		

5.5 Simulation Results

The configurations of the systems discussed in Figs. 5.1 and 5.2 are modelled in the HOMER energy analysis software to obtain a detailed economic analysis of the standalone PEMFC generation system. The simulation results obtained for ten different case studies are discussed in the following subsections.

5.5.1 Total Net Present Cost of the Case Studies

The total net present cost indicates the total cost required for the project including the predicted cash outflows and inflows. The total net present cost of the case studies considered in this analysis for the three tracking techniques are shown in Fig. 5.10.

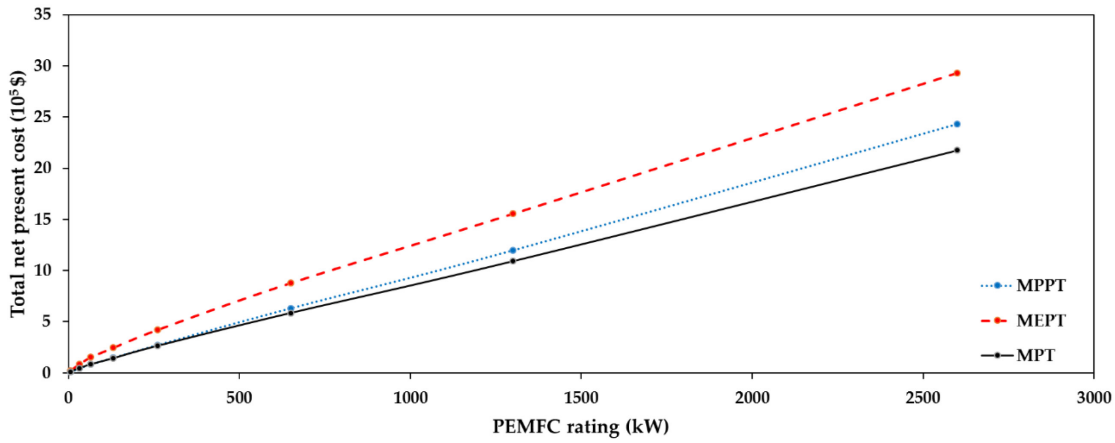

Fig. 5.10. Total net present cost

The preferred tracking technique is the one that meets the requirement of low total net present cost. As expected, the total net present cost of the PEMFC system with MEPT technique is too high due to the high capital cost associated with the PEMFC unit. From the figure, it can be seen that the total net present cost of the MDT technique is low when

compared with the other tracking techniques. The low capital cost for the PEMFC unit and the hydrogen storage equipment when compared with the MEPT and MPPT techniques is the main contributing factor to the low net present cost for the MDT technique. The total net present cost for all three techniques remains almost the same for power ratings less than 50 kW. From the point of view of the total net present cost, the MDT technique would be preferred for medium to high power applications.

5.5.2 Levelized Cost of Electricity of the Case Studies

The preferred tracking technique is the one that leads to a low value of levelized cost of electricity (LCOE). The value of LCOE for the case studies for three tracking techniques is shown in Fig. 5.11.

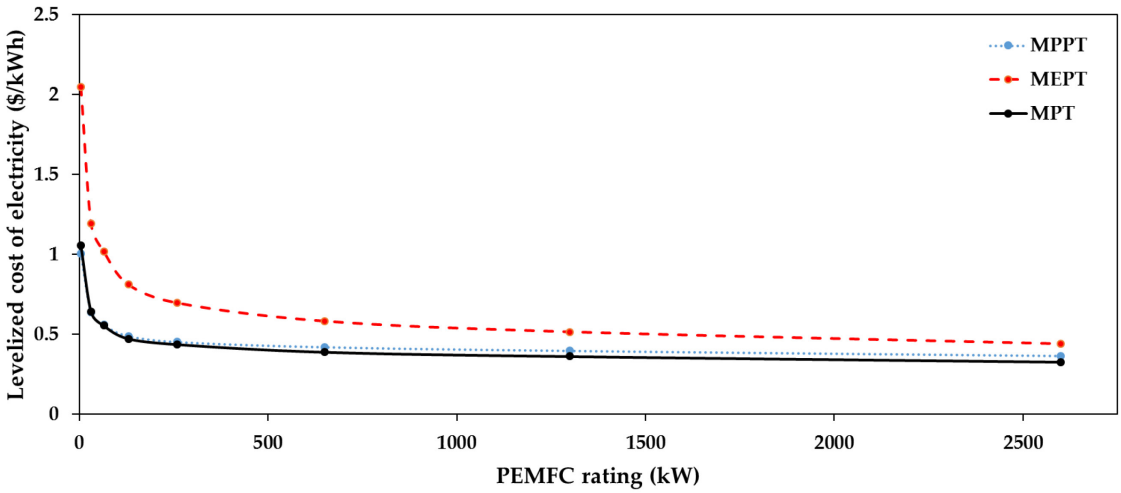

Fig. 5.11. Levelized cost of electricity

From the figure, it can be observed, that the LCOE decreases as the capacity of the system increases. Although the PEMFC with MEPT is highly efficient, its LCOE is about twice that of the MDT and MPPT for PEMFC ratings less than 100 kW. This is due to the

initial cost of the PEMFC, including the cost of the additional stacks required to meet the maximum power demand.

Since a low value of LCOE is preferred, the MPPT and MDT techniques would be favored for low PEMFC rating (< 50 kW). For PEMFC ratings greater than 500 kW, the LCOE for all three tracking techniques level off with the MDT technique giving a slightly lower value of the LCOE. The leveling off is due to the increase in the cost of hydrogen infrastructure required for the MPPT technique and increase in the capital cost of the PEMFC unit for the MEPT technique.

5.5.3 Hydrogen Consumption of the Case Studies

The hydrogen consumptions of the case studies are shown in Fig. 5.12. The hydrogen consumption is directly proportional to the stack current of the PEMFC. Hence, the MPPT technique, which operates in the high stack current region consumes a large amount of fuel when compared with other tracking techniques as shown in Fig. 5.12.

The MDT technique provides a trade-off operation by operating in the low current region when compared with the MPPT technique. As expected, the hydrogen consumption is low for the MEPT technique due to the operation of the PEMFC unit at high efficiency, which occurs in the low current region. However, the size and power density of the MEPT is low, and the MDT technique with reasonable fuel consumption rate, low capital cost, and small size would be preferred over the MEPT technique. The capacity of the hydrogen tank also follows the same trend as shown in Fig. 5.12.

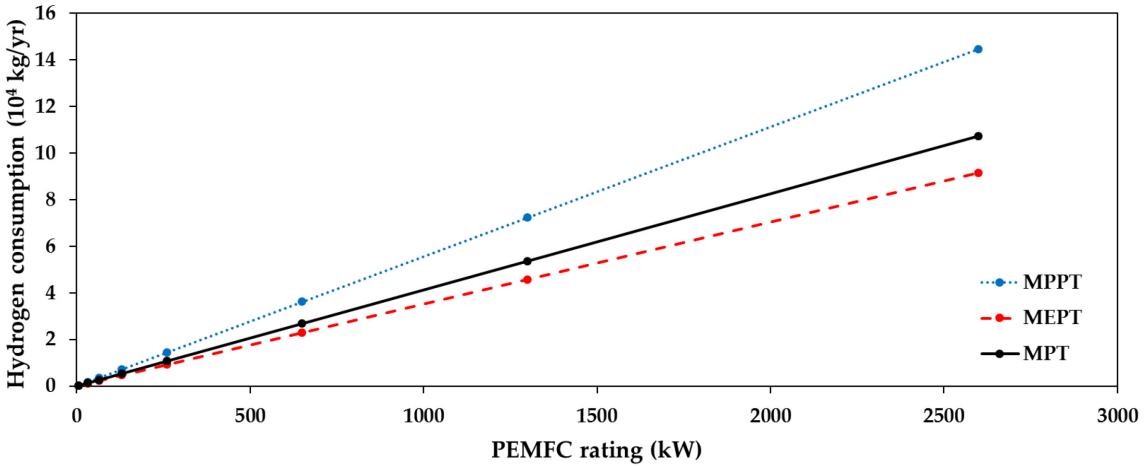

Fig. 5.12. Hydrogen consumption

5.5.4 Results of the Case Studies with Combined Heat and Power

The heat recovery ratio for the PEMFC is set at 50%, which means half of the heat energy generated by the PEMFC is used to supply the thermal load connected to the system. The temperature of hydrogen fuel and the stack temperature are assumed to be constant at 80˚C. The thermal load that the PEMFC can supply under different tracking techniques for case 9 and case 10 is tabulated in Table 5.3.

Table 5.3: Results for the CHP configuration.

Tracking Technique	**Thermal load supply capability (kWh/day)**		**Efficiency (%)**		
	Case 9	**Case 10**	η	η_{ther}	η_t
MPPT	7800	15600	36.4	31.8	68.2
MDT	4650	9300	49.0	25.5	74.5
MEPT	3750	7500	57.4	21.3	78.7

where, η_{ther} is the thermal efficiency of the system; η_t is the mean total efficiency of the system. From the table, it can be seen, that the electrical efficiency and thermal efficiency are inversely proportional. For example, with the MPPT technique the PEMFC converts 36.4% of fuel energy into electricity and the remaining 63.6% of fuel energy is converted into heat (31.8% in this case due to 50% heat recovery ratio). Hence, the thermal load supplied by the PEMFC with MPPT technique is high when compared with the PEMFC with MEPT and MDT technique. With the efficiencies for case 9 and case 10 remaining the same and the heat recovery ratio for both cases set at 50%, the thermal load supplied in case 10 is doubled. The results of the system with and without thermal load are identical except for the levelized cost of electricity as shown in Fig. 5.13.

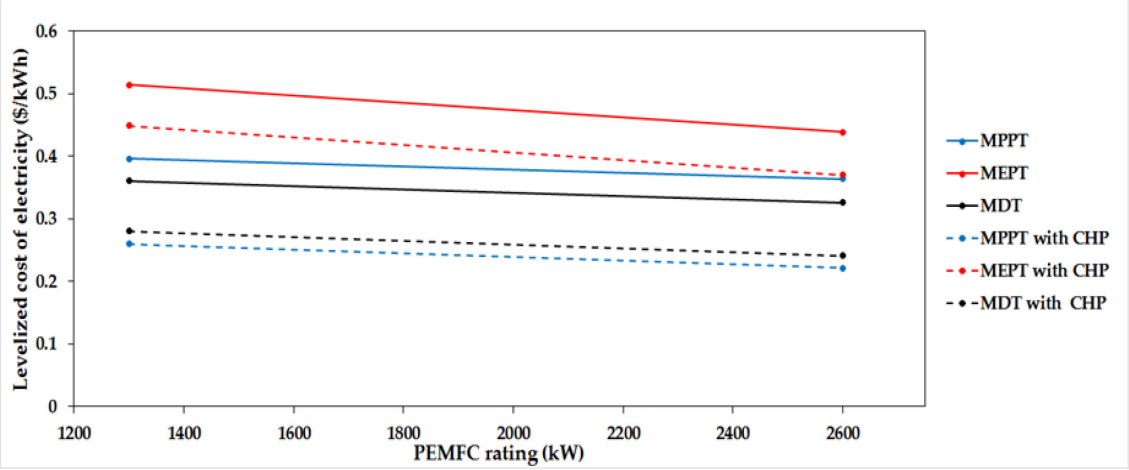

Fig. 5.13. Comparison of levelized cost of electricity

From the figure, it can be seen that the LCOE of the systems with thermal load is low when compared with systems without thermal load irrespective of the tracking technique. The MPPT technique is capable of supplying a large thermal load as shown in Table 5.3. This results in low LCOE for the MPPT technique when compared with other tracking techniques. The LCOE of the MEPT technique is very high due to the low thermal

efficiency and high capital cost associated with the PEMFC unit when compared with other tracking techniques. On the other hand, the MDT technique supplies a reasonable amount of thermal load with high electrical efficiency for the MPPT technique and low cost of electricity for the MEPT technique.

5.5.5 Effect of Electrolyzer Rating

The electrolyzer rating selected for the PEMFC system influences the levelized cost of electricity and the amount of excess electricity in the system. In order to study the effect of the electrolyzer rating, an electrolyzer ratio is used, which can be expressed as follows:

$$Electrolyzer\ ratio = \frac{Rating\ of\ electrolyzer}{P_{out}\ of\ PEMFC} 100\% \tag{5.10}$$

The effect of the electrolyzer rating on excess electricity is shown in Fig. 5.14. The electrolyzer ratio is used to determine the required rating of the electrolyzer for a particular rating of the PEMFC to meet the requirements of excess electricity and LCOE.

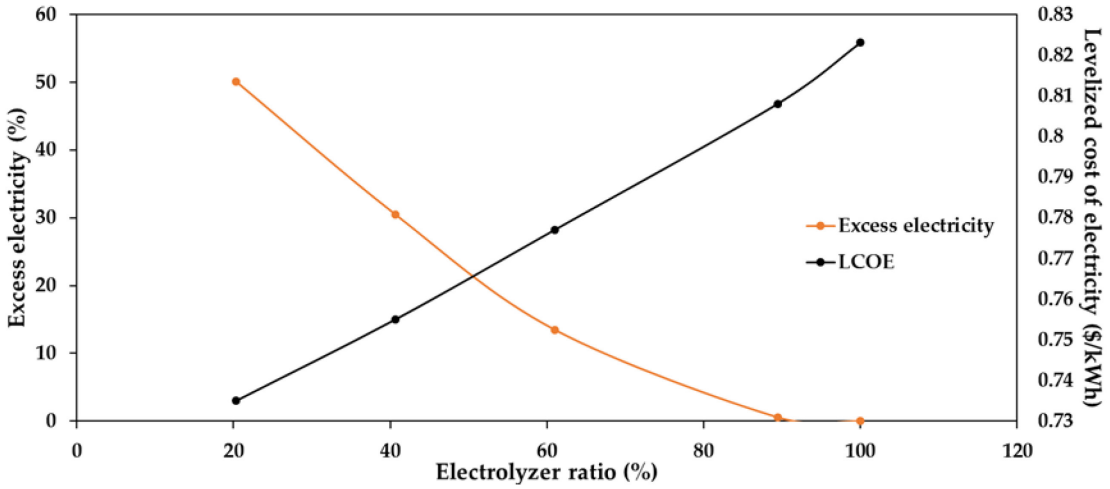

Fig. 5.14. Effect of electrolyzer rating

From the figure, it can be seen that the capital cost associated with the electrolyzer is directly influenced by LCOE. In order to achieve low LCOE, the rating of the electrolyzer should be kept at a minimum, which implies dumping excess electricity into a dump load.

5.6 Selection of Suitable Tracking Technique

Based on the simulation results discussed in the previous section, a flowchart for selecting a suitable tracking technique to achieve low levelized cost of electricity is presented in Fig. 5.15.

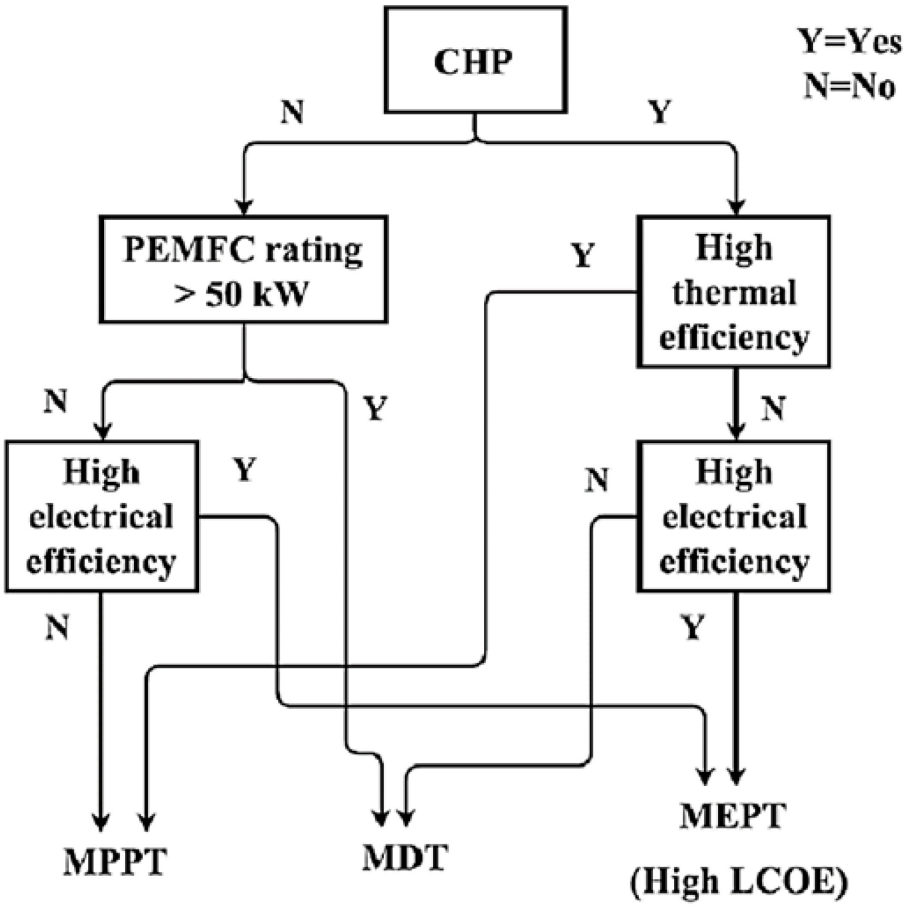

Fig. 5.15. Selection of tracking technique

From the flowchart, it is observed that for high electrical efficiency requirements, the MEPT technique would be the preferred tracking technique. It should be pointed out that the MEPT technique is associated with high LCOE. The common requirements of stationary power applications are low cost of electricity ($/kW), high power density (W/cm2), and high durability [67], with the cost of electricity being the major consideration. Based on this requirement, Fig. 5.15 shows that for PEMFC ratings less than 50 kW, MPPT would be the most suitable technique, while MDT would be preferred for PEMFC ratings higher than 50 kW. In the case of CHP configuration, the MPPT is expected to achieve low LCOE with high thermal efficiency. On the other hand, the MDT technique achieves low LCOE with high electrical and thermal efficiencies.

5.7 Summary

The economic analysis of the standalone PEMFC with maximum power point tracking, maximum efficiency point tracking, and midpoint tacking techniques is investigated. The configuration of the systems and the process of selecting required components for ten different load configurations were discussed. The assumptions and criteria considered for the economic analysis were presented and discussed. A detailed comparison of the simulation-based results obtained for the economic analysis of the PEMFC system with three tracking techniques using HOMER energy analysis tool is discussed.

It is found that the levelized cost of electricity of the PEMFC systems with combined heat and power is lower than that of the PEMFC systems without combined heat and power irrespective of the tracking techniques. Finally, based on the economic

considerations and simulation results, a procedure for determining a suitable tracking technique with low levelized cost of electricity for different power ratings of the PEMFC is developed and discussed. The results indicate that the MPPT technique is well suited for low power applications (<50 kW) and MDT technique would be preferred for medium and high power applications to achieve low levelized cost of electricity.

Chapter 6

Conclusion

The stationary fuel cell market for proton exchange membrane fuel cells is expanding rapidly. The cost of electricity produced, efficiency, and power density plays a significant role in determining the capability of PEMFCs in the stationary power generation industry.

This thesis has presented the development of a proton exchange membrane fuel cell model based on the electrochemical, electrical, and empirical equations in Simulink environment. The working principle and various components required to develop a PEMFC model were analyzed and discussed. The simulation results of the developed PEMFC model were validated with published experimental results, which showed a good fit.

The PEMFC requires several auxiliary components for proper operation, consume power and affects the net output power of the PEMFC stack. In order to obtain the net output power of the PEMFC, a simplified model based on the fast flexible filling statistical design was developed. The simulation results of the developed net output power model were validated to ensure high accuracy. In addition, an efficiency model was developed to obtain the electrical efficiency of the PEMFC. The simulation-based investigation confirmed the non-linear output characteristics of the PEMFC and the effect of the

operating parameters such as, stack temperature, membrane water content, fuel pressure, and fuel flow on the output characteristics.

The development of the maximum power point tracking technique and maximum efficiency point tracking technique was discussed in Chapter 3. The tracking control schemes, namely the direct and indirect tracking control were presented and discussed. The indirect tracking control scheme was preferred over the direct tracking control scheme. Several published tracking algorithms were analysed. The model-independent tracking algorithms, namely the extremum seeking control, perturb and observe, and the sliding model control were implemented in Simulink to track the maximum power point of the PEMFC. A detailed comparison of the three tracking algorithms was presented. The simulation-based investigation showed that the extremum seeking control algorithm is the suitable tracking algorithm with high tracking speed, and high accuracy. The low efficiency limitation of the maximum power point tracking technique was discussed. The maximum efficiency point tracking technique was introduced to operate the PEMFC at maximum efficiency, but the simulation results showed that the net output power of the maximum efficiency point tracking was low.

An alternative tracking technique referred to as the midpoint tracking technique was proposed in Chapter 4 to overcome the limitations of the maximum power point tracking and maximum efficiency point tracking techniques. The midpoint of the maximum power point current and maximum efficiency point current was selected as the operating point of the midpoint tracking technique. Several possible methods were considered to develop the midpoint tracking algorithm. The development of a generic and model-independent midpoint tracking algorithm based on the fast flexible filling (FFF) statistical design

approach was discussed. The simulation results of the developed midpoint tracking technique were validated, which resulted in a good fit. A detailed comparison of the tracking techniques based on the net output power, efficiency, power density, system size, fuel consumption, and cost per kW was presented. The simulation-based investigation showed that the midpoint tracking technique with high net output power, reasonably high efficiency, and smaller size compared with the maximum efficiency point tracking was the preferred technique for stationary applications of the PEMFC.

In order to address the effects of the tracking techniques on the economics of the PEMFC, a detailed economic analysis was carried out in Chapter 5. Ten different cases were considered to obtain the impact of the tracking techniques. A PEMFC generation system with hydrogen storage technique was taken into consideration. The HOMER energy system software was used to obtain the economics of ten different cases of the PEMFC with the tracking techniques. The configurations of the electrical loads and thermal loads for ten different cases were discussed. The criteria for the selection of different components, namely PEMFC unit, inverter, and electrolyzer were presented and discussed. The simulation-based investigation showed that the maximum power point tracking was characterized with low levelized cost of electricity for low power applications (<50kW) and midpoint tracking technique was characterized with low levelized cost of electricity for medium to high power applications. In the case of the combined heat and power configuration, the maximum power point tracking technique resulted in low levelized cost of electricity. Finally, a selection procedure based on the simulation results to determine a suitable tracking technique was presented.

6.1 Contributions

The major contribution from this thesis was to provide a procedure to select a suitable tracking technique for a proton exchange membrane fuel cell generation system. Several investigations were carried out to support the results discussed in the previous section.

A complete, versatile, and user-friendly PEMFC Simulink model with various components was developed in Chapter 2. A simple, accurate, and generic net output power model and efficiency model of a PEMFC were developed. The developed Simulink model can be used as a template for developing the model of a PEMFC of specified rating and configuration.

Several comparative analyses of tracking algorithms have been presented in the literature for photovoltaic systems. Yet accurate comparison of the tracking algorithms used for fuel cell systems was lacking in the literature. In order to address this issue, a detailed comparison of the tracking algorithm for the stationary PEMFC application was presented in Chapter 3. A detailed analysis of the maximum power point tracking and maximum efficiency point tracking of the PEMFC was carried out and their limitations were presented. This analysis provides a better understanding of the relationship between the net output power and efficiency of the PEMFC. The results of the investigations in Chapter 3 were published at a local IEEE conference [68].

In Chapter 4, the midpoint tracking (MDT) technique was proposed to overcome the limitations of the MPPT and MEPT techniques. The proposed technique is generic, model-independent, and less complex. A comparative analysis of the MPPT and MEPT

technique for fuel cell applications was lacking in the literature, and in this chapter, a detailed comparison of the MPPT, MEPT, and MDT techniques based on several characteristics was presented for stationary PEMFC applications. The results of the comparative analysis were presented at a national IEEE conference [78].

Several economic analyses of PEMFC systems have been presented in the literature, but an accurate economic analysis of a standalone PEMFC system, including the impact of the tracking techniques on the economics of the PEMFC is lacking. In order to address these issues, a detailed economic analysis of a PEMFC generation system with three tracking techniques for ten different cases was presented in Chapter 5. A selection procedure based on the simulation results of the economic analysis was developed to obtain a suitable tracking technique for particular requirements of a project. A manuscript based on the investigation in this chapter is under review for publication in an international journal [81].

6.2 Future Analysis

The research work presented in this thesis provides a comprehensive analysis of the PEMFC with tracking techniques. Although the work undertaken represents a complete and focused investigation, some aspects of the work require further investigation as follows:

1. *Improved PEMFC model:*

The PEMFC model can be improved to incorporate the effects of membrane degradation and aging on the output voltage of the fuel cell. Such a model would provide accurate analysis of the tracking techniques.

2. *Detailed model of the auxiliaries:*

Detailed analysis of the auxiliaries in a PEMFC system is required to develop a complete model to represent the power consumed by the control units, cooling fans, and heat exchanger pumps. An investigation of hardware implementations of a PEMFC with the auxiliaries for different applications (stationary, transportation, and portable) would be necessary.

3. *Complexity of the tracking techniques:*

It would be useful to investigate the complexity of the tracking algorithms for different tracking techniques. This study will add a new dimension or factor to the selection of tracking algorithm. The midpoint tracking technique reported in this thesis is based on the midpoint of the stack current, which resulted in the trade-off operation. However, it would be useful to study the optimum point operation of the PEMFC based on factors, such as output power, efficiency, stack volume, specific power density, and levelized cost of electricity.

4. *Experimental investigation of the PEMFC system with the tracking techniques:*

The results reported in this thesis are based on extensive simulation studies. Hardware implementation of the PEMFC system with the tracking techniques would be required to validate the approach presented in the thesis. The hardware implementation of the tracking algorithms would certainly help to identify new improvements and requirements.

5. *Extension of the approach to other PEMFC systems:*

The work presented in this thesis focused on the effect of the tracking techniques on the economics of a standalone PEMFC generation system. The approach developed in the thesis can be extended to portable and transportation applications of the PEMFC, which could lead to a set of new challenges and new contributions. It would be useful to incorporate the PEMFC in a hybrid system and analyse the effects of the tracking techniques on the economics of the entire hybrid system. In this thesis, the hydrogen storage technique was considered for storing the excess electricity. A detailed analysis and performance of the PEMFC with different storage techniques and their economics would lead to a complete economic analysis of the PEMFC system. In addition, the analysis of the combined heat and power operation of PEMFC could be carried out to address any new requirements and improvements. The procedure used in this thesis to analyse the PEMFC system can be extended to other fuel cell systems such as, solid oxide fuel cell system and direct methanol fuel cell system. These analyses would help to identify the suitable fuel cell system for particular requirements of an application.

References

[1] C. K. Dyer, "Fuel cells for portable applications," *J. Power Sources*, vol. 106, no. 1–2, pp. 31–34, Apr. 2002.

[2] S. Curtin and J. Gangi, "Fuel Cell Technologies Market Report 2014," *U.S. Department of Energy EERE*, pp. 1–58, 2013.

[3] M. Klippenstein, "Toyota Fuel-Cell 'Megafactory' Matches Tesla Gigafactory In Impact," 2015. [Online]. Available: http://www.greencarreports.com/news/1098818_toyota-fuel-cell-megafactory-matches-tesla-gigafactory-in-impact.

[4] "Nedstack wins China order for world's first 2 MW PEMFC plant," *Fuel Cells Bull.*, vol. 2015, no. 3, p. 6, Mar. 2015.

[5] G. McAree, "Ballard Reports Q4 , Full Year 2015 Results & 2016 Outlook," *Ballard Power Systems*, 2016. [Online]. Available: http://ballard.com/about-ballard/newsroom/news-releases/news02241601.aspx.

[6] A. T-Raissi, A. Banerjee, and K. G. Sheinkopf, "Current technology of fuel cell systems," in *IECEC-97 Proceedings of the Thirty-Second Intersociety Energy Conversion Engineering Conference*, 1997, pp. 1953–1957.

[7] P. P. Edwards, V. L. Kuznetsov, W. I. F. David, and N. P. Brandon, "Hydrogen and fuel cells: Towards a sustainable energy future," *Energy Policy*, vol. 36, no. 12, pp. 4356–4362, Dec. 2008.

[8] M. Smit, "Towards 40 000 hours of operation for Nedstack's FCS XXL PEM fuel cell stacks by," *Fuel Cells Bull.*, vol. 2014, no. 8, pp. 12–15, Aug. 2014.

[9] N. Bizon, "FC energy harvesting using the MPP tracking based on advanced extremum seeking control," *Int. J. Hydrogen Energy*, vol. 38, no. 4, pp. 1952–1966, Feb. 2013.

[10] F. A. Inthamoussou, R. J. Mantz, and H. De Battista, "Flexible power control of fuel

cells using sliding mode techniques," *J. Power Sources*, vol. 205, pp. 281–289, May 2012.

[11] Z. Zhong, H. Huo, X. Zhu, G. Cao, and Y. Ren, "Adaptive maximum power point tracking control of fuel cell power plants," *J. Power Sources*, vol. 176, no. 1, pp. 259–269, Jan. 2008.

[12] N. Bizon, "Tracking the maximum efficiency point for the FC system based on extremum seeking scheme to control the air flow," *Appl. Energy*, vol. 129, pp. 147–157, Sep. 2014.

[13] J. Lu and A. Zahedi, "Maximum efficiency point tracking control for fuel cell power systems," in *2010 International Conference on Power System Technology*, 2010, pp. 1–6.

[14] F. Barbir and T. Gomez, "Efficiency and Economics of Proton Exchange Membrane (PEM) Fuel Cells," *Int. J. Hydrogen Energy*, vol. 22, no. 10/11, pp. 1027–1037, Oct. 1997.

[15] M. S. Pandian, M. Anwari, and B. Y. Husodo, "Efficiency and Economics Analysis of Proton Exchange Membrane Fuel Cell," in *IPEC, 2010 Conference Proceedings*, 2010, pp. 875–880.

[16] D. Bezmalinović, F. Barbir, and I. Tolj, "Techno-economic analysis of PEM fuel cells role in photovoltaic-based systems for the remote base stations," *Int. J. Hydrogen Energy*, vol. 38, no. 1, pp. 417–425, Oct. 2013.

[17] S. Rahimi, M. Meratizaman, S. Monadizadeh, and M. Amidpour, "Techno-economic analysis of wind turbine-PEM (polymer electrolyte membrane) fuel cell hybrid system in standalone area," *Energy*, vol. 67, pp. 381–396, Feb. 2014.

[18] G. R. Ashari, M. a. Ehyaei, A. Mozafari, F. Atabi, E. Hajidavalloo, and S. Shalbaf, "Exergy, Economic, and Environmental Analysis of a PEM Fuel Cell Power System to Meet Electrical and Thermal Energy Needs of Residential Buildings," *J. Fuel Cell Sci. Technol.*, vol. 9, no. 5, pp. 51001–51001–11, Oct. 2012.

[19] C.-H. Lee and J.-T. Yang, "Modeling of the Ballard-Mark-V proton exchange membrane fuel cell with power converters for applications in autonomous underwater vehicles," *J. Power Sources*, vol. 196, no. 8, pp. 3810–3823, Dec. 2011.

[20] W. Choi, J. W. Howze, and P. Enjeti, “Development of an equivalent circuit model of a fuel cell to evaluate the effects of inverter ripple current,” *J. Power Sources*, vol. 158, no. 2 SPEC. ISS., pp. 1324–1332, Nov. 2006.

[21] D. Xue and Z. Dong, “Optimal fuel cell system design considering functional performance and production costs,” *J. Power Sources*, vol. 76, no. 1, pp. 69–80, Aug. 1998.

[22] V. Boscaino, R. Miceli, and G. Capponi, “MATLAB-based simulator of a 5 kW fuel cell for power electronics design,” *Int. J. Hydrogen Energy*, vol. 38, no. 19, pp. 7924–7934, May 2013.

[23] J. Jia, S. Yang, Y. Wang, and Y. T. Cham, “Matlab/simulink based-study on PEM fuel cell and nonlinear control,” in *2009 IEEE International Conference on Control and Automation, ICCA 2009*, 2009, pp. 1657–1662.

[24] A. Zaidi, P. Pokharkar, R. Krishnan, and D. Sonawane, “Dynamic Modeling and Simulation of A PEM Fuel Cell: MATLAB and LabVIEW Modeling Approach,” in *Proceedings of 2014 1st International Conference on Non Conventional Energy*, 2014, pp. 272–276.

[25] A. A. Abd El Monem, A. M. Azmy, and S. A. Mahmoud, “Effect of process parameters on the dynamic behavior of polymer electrolyte membrane fuel cells for electric vehicle applications,” *Ain Shams Eng. J.*, vol. 5, no. 1, pp. 75–84, Mar. 2014.

[26] Y.-X. Wang, D.-H. Yu, S.-A. Chen, and Y.-B. Kim, “Robust DC/DC converter control for polymer electrolyte membrane fuel cell application,” *J. Power Sources*, vol. 261, pp. 292–305, Mar. 2014.

[27] D. Zumoffen and M. Basualdo, “Advanced control for fuel cells connected to a DC/DC converter and an electric motor,” *Comput. Chem. Eng.*, vol. 34, no. 5, pp. 643–655, Nov. 2010.

[28] M. J. Khan and M. T. Iqbal, “Modelling and analysis of electrochemical, thermal, and recetant flow dynamics for a PEM fuel cell system,” *Fuel Cells*, vol. 5, no. 4, pp. 463–475, Nov. 2005.

[29] A. El, M. Aa, A. M. Azmy, and M. Sa, “Dynamic Modelling of Proton Exchange Membrane Fuel Cells for Electric Vehicle Applications,” *J. Pet. Environ.*

Biotechnol., vol. 5, no. 2, pp. 1–7, Apr. 2014.

[30] S. C. Lee, O. Kwon, and D. H. Lee, "Fuel cell simulation: Steady-state and dynamic case," in *ICCSE 2012 - Proceedings of 2012 7th International Conference on Computer Science and Education*, 2012, pp. 974–979.

[31] J. T. Pukrushpan, A. G. Stefanopoulou, and H. Peng, "Modeling and Control for PEM Fuel Cell Stack System," in *Proceeding of the American Control Conference*, 2002, pp. 3117 – 3122.

[32] R. Lekivetz and B. Jones, "Fast Flexible Space-Filling Designs for Nonrectangular Regions," *Qual. Reliab. Eng. Int.*, vol. 31, no. 5, pp. 829–837, Mar. 2015.

[33] Y.-X. Wang, D.-H. Yu, S.-A. Chen, and Y.-B. Kim, "Robust DC/DC converter control for polymer electrolyte membrane fuel cell application," *J. Power Sources*, vol. 261, pp. 292–305, Mar. 2014.

[34] Y. Huang, M. Shen, F. Z. Peng, and J. Wang, "Z-source inverter for residential photovoltaic systems," *IEEE Trans. Power Electron.*, vol. 21, no. 6, pp. 1776–1782, Nov. 2006.

[35] B. Somaiah and V. Agarwal, "Recursive estimation-based maximum power extraction technique for a fuel cell power source used in vehicular applications," *IEEE Trans. Power Electron.*, vol. 28, no. 10, pp. 4636–4643, Dec. 2013.

[36] T. Ramki and L. N. Tripathy, "Comparison of different DC-DC converter for MPPT application of photovoltaic system," in *International Conference on Electrical, Electronics, Signals, Communication and Optimization, EESCO 2015*, 2015, pp. 1–6.

[37] M. E. Basoglu and B. Cakir, "Hardware based comparison of buck-boost converter topologies in MPPT systems," in *ELECO 2015 - 9th International Conference on Electrical and Electronics Engineering*, 2016, pp. 1109–1112.

[38] A. Wiesner, R. Diez, and G. Perilla, "Design and implementation of a Buck converter with MPPT for battery charge from solar module," in *2013 Power Electronics and Power Quality Applications, PEPQA 2013 - Proceedings*, 2013, pp. 1–6.

[39] T. Esram and P. L. Chapman, "Comparison of photovoltaic array maximum power

point tracking techniques," *IEEE Trans. Energy Convers. EC*, vol. 22, no. 2, p. 439, Jun. 2007.

[40] O. Wasynczuk, "Dynamic behavior of a class of photovoltaic power systems," *IEEE Trans. Power App. Syst*, vol. 102, no. 9, pp. 3031–3037, Sep. 1983.

[41] B. M. Wilamowski, "Fuzzy system based maximum power point tracking for PV system," in *IEEE 2002 28th Annual Conference of the Industrial Electronics Society. IECON 02*, 2002, pp. 3280–3284.

[42] T. Hiyama, S. Kouzuma, T. Imakubo, O. O. Point, S. Member, and C. Science, "Identification of optimal operating point of PV modules using neural network for real time maximum power tracking control," *Energy Conversion, IEEE Trans.*, vol. 10, no. 2, pp. 360–367, Jun. 1995.

[43] M. Sarvi and M. Barati, "Voltage and current based MPPT of fuel cells under variable temperature conditions," in *Universities Power Engineering Conference (UPEC), 2010 45th International*, 2010, pp. 1–4.

[44] S. Abdi, K. Afshar, N. Bigdeli, and S. Ahmadi, "A Novel Approach for Robust Maximum Power Point Tracking of PEM Fuel Cell Generator Using Sliding Mode Control Approach," *Int. J. Elctrochemical Sci.*, vol. 7, no. 5, pp. 4192–4209, May 2012.

[45] C. A. Ramos, A. Romero, R. Giral, and L. Martinez-Salamero, "Maximum Power Point Tracking Strategy for Fuel Cell Power Systems," in *2007 IEEE International Symposium on Industrial Electronics*, 2007, pp. 2613–2618.

[46] S. Qin, M. Wang, T. Chen, and X. Yao, "Comparative analysis of incremental conductance and perturb-and-observation methods to implement MPPT in photovoltaic system," in *2011 International Conference on Electrical and Control Engineering, ICECE 2011 - Proceedings*, 2011, pp. 5792–5795.

[47] N. Bizon, "Optimal Filtering of the Fuel Cell Power Probing Signal for Maximum Power Point Robust Adaptive Tracking," in *Applied Electronics (AE), 2010 International Conference on*, 2010, pp. 1–4.

[48] N. Bizon, "On tracking robustness in adaptive extremum seeking control of the fuel cell power plants," *Appl. Energy*, vol. 87, no. 10, pp. 3115–3130, May 2010.

[49] N. Bizon, “A new topology of fuel cell hybrid power source for efficient operation and high reliability,” *J. Power Sources*, vol. 196, no. 6, pp. 3260–3270, Nov. 2011.

[50] M. A. Taghikhani and I. Soltani, “A new maximum power point tracking control method of proton exchange membrane fuel cell’s system,” in *Electrical Power Distribution Networks (EPDC), 2012 Proceedings of 17th Conference on*, 2012, pp. 1–7.

[51] K. Ettihir, L. Boulon, K. Agbossou, and S. Kelouwani, “MPPT control strategy on PEM Fuel Cell Low Speed Vehicle,” in *2012 IEEE Vehicle Power and Propulsion Conference*, 2012, pp. 926–931.

[52] D. Herrera Vega, N. Marx, L. Boulon, and A. Hernandez, “Maximum efficiency point tracking for hydrogen fuel cells,” in *2014 IEEE 27th Canadian Conference on Electrical and Computer Engineering (CCECE)*, 2014, pp. 1–6.

[53] J. Han, J. F. Charpentier, and T. Tang, “An energy management system of a fuel cell/battery hybrid boat,” *Energies*, vol. 7, no. 5, pp. 2799–2820, Apr. 2014.

[54] J. a. Smith, M. H. Nehrir, V. Gerez, and S. R. Shaw, “A broad look at the workings, types, and applications of fuel cells,” in *IEEE Power Engineering Society Summer Meeting,* 2002, vol. 1, pp. 70–75.

[55] G. Sasikumar, J. W. Ihm, and H. Ryu, “Optimum Nafion content in PEM fuel cell electrodes,” *Electrochim. Acta*, vol. 50, no. 2–3 SPEC. ISS., pp. 601–605, Aug. 2004.

[56] F. Laurencelle, R. Chahine, J. Hamelin, K. Agbossou, M. Fournier, T. K. Bose, and A. Laperrière, “Characterization of a Ballard MK5-E Proton Exchange Membrane Fuel Cell Stack,” *Fuel Cells*, vol. 1, no. 1, pp. 66–71, May 2001.

[57] K. K. Mankala and S. K. Agrawal, “Dynamic Modeling and Simulation of PEM Fuel Cells,” in *Modeling and Control of Fuel Cells:Distributed Generation Applications*, Wiley-IEEE Press, 2005, pp. 57–84.

[58] R. F. Mann, J. C. Amphlett, M. a. I. Hooper, H. M. Jensen, B. a. Peppley, and P. R. Roberge, “Development and application of a generalised steady-state electrochemical model for a PEM fuel cell,” *J. Power Sources*, vol. 86, no. 1–2, pp. 173–180, Mar. 2000.

[59] J. C. Amphlett, R. F. Mann, B. A. Peppley, P. R. Roberge, and A. Rodrigues, "A model predicting transient responses of proton exchange membrane fuel cells," *J. Power Sources*, vol. 61, no. 1–2, pp. 183–188, Jul. 1996.

[60] M. Wohr, K. Bolwin, W. Schnurnberger, M. Fischer, W. Neubrand, and G. Eigenberger, "Dynamic modelling and simulation of a polymer membrane fuel cell including mass transport limitation," *Int. J. Hydrogen Energy*, vol. 23, no. 3, pp. 213–218, Mar. 1998.

[61] N. Wagner, "Characterization of membrane electrode assemblies in polymer electrolyte fuel cells using a.c. impedance spectroscopy," *J. Appl. Electrochem.*, vol. 32, no. 8, pp. 859–863, Mar. 2002.

[62] M. Ceraolo, C. Miulli, and A. Pozio, "Modelling static and dynamic behaviour of proton exchange membrane fuel cells on the basis of electro-chemical description," *J. Power Sources*, vol. 113, no. 1, pp. 131–144, Sep. 2003.

[63] J. C. Amphlett, R. M. Baumert, R. F. Man, B. A. Peppley, P. R. Roberge, and A. Rodriguez, "Parametric modelling of the performance of a 5-kW proton exchange membrane fuel cell stack," *J. Power Sources*, vol. 49, no. 1–3, pp. 349–356, Apr. 1994.

[64] J. Larminie and A. Dicks, "Proton Exchange Memebrane Fuel Cell," in *Fuel Cell Systems Explained*, vol. 93, Wiley, 2001, pp. 67–118.

[65] L. Pronzato and W. G. Miiller, "Design of computer experiments: Space filling and beyond," *Stat. Comput.*, vol. 22, no. 3, pp. 681–701, Apr. 2012.

[66] D. Feroldi and M. Basualdo, "Description of PEM Fuel Cells System," in *PEM Fuel Cells with Bio-Ethanol Processor Systems*, vol. 87, 2012, pp. 49–72.

[67] K. S. Dhathathreyan and N. Rajalakshmi, "Recent Trends in Fuel Cell Science and Technology," in *Recent Trends in Fuel Cell Science and Technology*, no. 9, S. Basu, Ed. 2013, pp. 40–115.

[68] V. Karunamurthy Kumaraswamy and J. E. Quaicoe, "Comparison of Maximum Power Point Tracking Techniques for Different Fuel Cell Applications," in *2015 IEEE Newfoundland Electrical and Computer Engineering Conference (NECEC15)*, 2015, pp. 1–5.

[69] M. Dargahi, M. Rezanejad, J. Rouhi, and M. Shakeri, "Maximum power point tracking for fuel cell in fuel cell/battery hybrid systems," in *2008 IEEE International Multitopic Conference*, 2008, pp. 33–37.

[70] L. Wuidart, "Topologies For Switched Mode Power Supplies, " Application Note AN 513/0393, STMicroelectronics, 1999.

[71] T. Van Breussegem and M. Steyaert, "Converter Topologies and Fundamentals," in *CMOS Integrated Capacitive DC-DC Converters*, 2013, pp. 39–64.

[72] P. Bhatnagar and R. . Nema, "Control techniques analysis of DC-DC converter for photovoltaic application using SIMSCAPE," in *2012 IEEE 5th India International Conference on Power Electronics (IICPE)*, 2012, pp. 1–6.

[73] N. A. Keskar and G. A. Rincón-Mora, "A Fast, Sigma-Delta (∑Δ) Boost DC-DC Converter Tolerant to wide LC Filter Variations," *IEEE Trans. Circuits Syst. II Express Briefs*, vol. 55, no. 2, pp. 198–202, Feb. 2008.

[74] J. M. Galvez, M. Ordonez, F. Luchino, and J. E. Quaicoe, "Improvements in Boundary Control of Boost Converters Using the Natural Switching Surface," *IEEE Trans. Power Electron.*, vol. 26, no. 11, pp. 3367–3376, Apr. 2011.

[75] M. P. Kazmierkowski and L. Malesani, "Current Control Techniques for Three-Phase Voltage-Source PWM Converters: A Survey," *IEEE Trans. Ind. Electron.*, vol. 45, no. 5, pp. 691–703, Aug. 1998.

[76] B. Calli, W. Caarls, P. Jonker, and M. Wisse, "Comparison of extremum seeking control algorithms for robotic applications," in *IEEE International Conference on Intelligent Robots and Systems*, 2012, pp. 3195–3202.

[77] Y. K. Y. Kim, H. J. H. Jo, and D. K. D. Kim, "A New Peak Power Tracker for Cost-Effective Photovoltaic Power System," in *IECEC 96. Proceedings of the 31st Intersociety Energy Conversion Engineering Conference*, 1996, vol. 3, pp. 1673–1678.

[78] V. Karunamurthy Kumaraswamy and J. E. Quaicoe, "Tracking Techniques for the PEMFC in Portable Applications," in *Electrical Power and Energy Conference (EPEC), 2016 IEEE*, 2016, pp. 93–98.

[79] "100W to 5000W PEMFC stacks," 2016. [Online]. Available:

http://fuelcellstore.com/product/search&search=horizon&category_id=20&limit=25.

[80] J.-H. Wee, "Applications of proton exchange membrane fuel cell systems," *Renew. Sustain. Energy Rev.*, vol. 11, no. 8, pp. 1720–1738, Jan. 2007.

[81] V. Karunamurthy Kumaraswamy and J. E. Quaicoe, "A Standalone Fuel Cell Generation System with Different Tracking Techniques: Economic Analysis," *Renewable Power Generation, IET.*, pp. 1–20, 2016.

[82] T. M. Masaud, K. L. K. Lee, and P. K. Sen, "An overview of energy storage technologies in electric power systems: What is the future?," in *North American Power Symposium NAPS 2010*, 2010, pp. 1–6.

[83] S. Vazquez, S. M. Lukic, E. Galvan, L. G. Franquelo, and J. M. Carrasco, "Energy Storage Systems for Transport and Grid Applications," *IEEE Trans. Ind. Electron.*, vol. 57, no. 12, pp. 3881–3895, Dec. 2010.

[84] J. D. Boyes and N. H. Clark, "Technologies for energy storage. Flywheels and super conducting magnetic energy storage," in *2000 Power Engineering Society Summer Meeting*, 2000, vol. 3, pp. 1548–1550.

[85] A. Yilanci, I. Dincer, and H. K. Ozturk, "A review on solar-hydrogen/fuel cell hybrid energy systems for stationary applications," *Prog. Energy Combust. Sci.*, vol. 35, no. 3, pp. 231–244, Oct. 2009.

[86] T. G. Kreutz and J. M. Ogden, "Assessment of Hydrogen-Fueled Proton Exchange Membrane Fuel Cells for Distributed Generation and Cogeneration," in *2000 U.S. DOE Hydrogen Program Review*, 2000, pp. 1–43.

[87] T. Lambert, P. Gilman, and P. Lilienthal, "Micropower System Modeling with Homer," in *Integration of Alternative Sources of Energy*, F. A. Farret and M. G. Simões, Eds. Wiley, 2006, pp. 379–418.

[88] "Download Free Files Sample Data Files for HOMER Pro," *HOMER*, 2016. [Online]. Available: https://users.homerenergy.com/pages/file_download_pro.

[89] "1kW to 5kW Fuel Cell Stacks," *Fuel Cell Store*, 2016. [Online]. Available: http://fuelcellstore.com/fuel-cell-stacks/high-power-fuel-cell-stacks.

[90] "Inverter," *Alibaba*, 2016. [Online]. Available: https://www.alibaba.com/product-

detail/1MW-Solar-inverter-for-power-station_60366654887.html?spm=a2700.7724857.29.28.pF2y85&s=p.

[91] "HySolGenics' Hydrogen Fuel System," *SIlicon Valley Chapter of the American Hydrogen Assosciation*, 2016. [Online]. Available: http://www.ahasvc.org/page44.html.

[92] "Hydrogen Tank," *Alibaba*, 2016. [Online]. Available: https://www.alibaba.com/showroom/hydrogen-storage-tank.html.

[93] "Hydrogen Fuel Cost vs Gasoline," *Hydrogen Energy Systems*, 2016. [Online]. Available: http://heshydrogen.com/hydrogen-fuel-cost-vs-gasoline/.

Appendix A

FFF Design Constants

In this appendix, the value of the constants (a_1…..a_{13}) obtained from the FFF design of the net output power (2.34) and the value of the constants (b_1…..b_{11}) obtained for the FFF design of the midpoint reference current (4.1) of the midpoint tracking algorithm are tabulated in Table A.1.

Table A.1: Value of the constants for FFF design

Constant	Value	Constant	Value
a_1	47455.40	a_{13}	33.12
a_2	52243.28	b_1	219.85
a_3	7700.65	b_2	208.96
a_4	239.48	b_3	154.32
a_5	38.30	b_4	2.81
a_6	842.12	b_5	8.67
a_7	4719.44	b_6	144.16
a_8	1195.66	b_7	53.50
a_9	1091.14	b_8	1.21
a_{10}	15.12	b_9	0.62
a_{11}	913.27	b_{10}	6.81
a_{12}	162.40	b_{11}	49.77

Appendix B

Current Control Techniques

In this appendix, a detailed comparison of the current control techniques, namely the hysteresis current controller, sigma-delta (Σ-Δ) current controller [73], and natural switching surface (NSS) current controller [74] with the extremum seeking tracking algorithm based on accuracy and convergence speed is presented. For the simulation, the value of membrane water content (λ) is maintained at 14 and the stack temperature is set at 80˚ C. The parameters of the extremum seeking control algorithm used for the maximum power point tracking technique is considered in the investigation of the different current controllers.

B.1 Accuracy

The accuracy of the three current control techniques used with the extremum seeking control algorithm for tracking the maximum power point tracking is shown in Fig. B.1. From the figure, it can be seen that the accuracy of the three current controllers is almost identical. However, the natural switching surface current controller is associated with small oscillations. Hence, it is preferred over the hysteresis current controller and sigma delta modulated current controller.

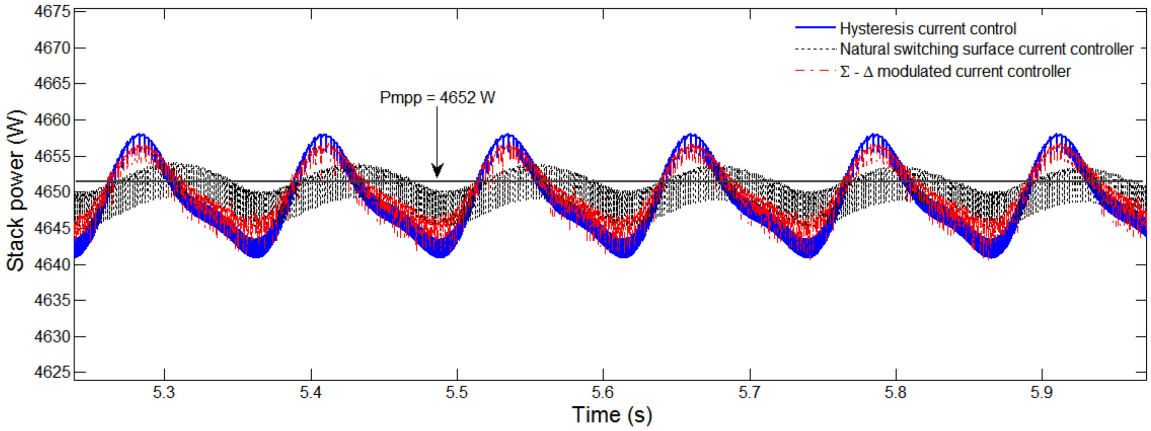

Fig. B.1. Accuracy of the tracking algorithm with three current controllers

B.2 Convergence Speed

The convergence speed of the extremum seeking control algorithm with three current controllers is shown in Fig. B.2.

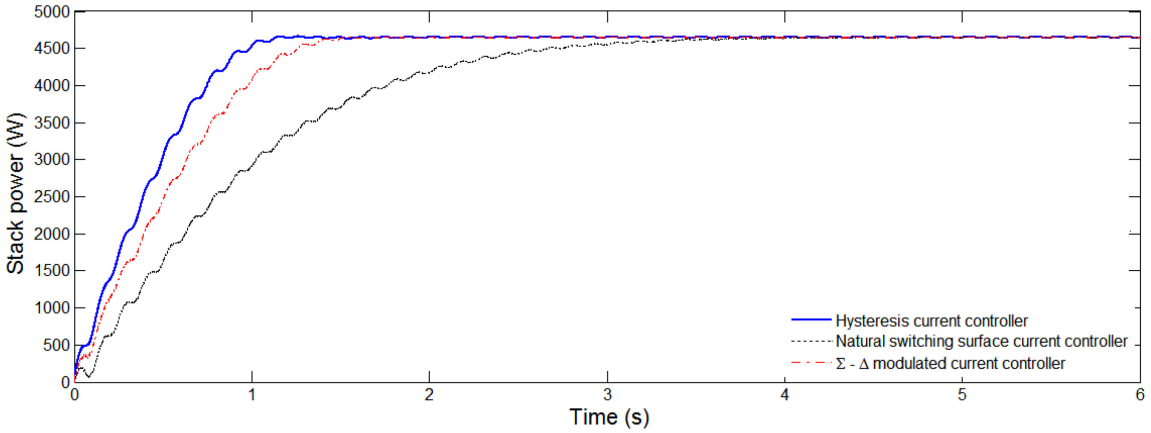

Fig. B.2. Convergence speed of the tracking algorithm with three current controllers

From the figure, it can be seen that the convergence speed of the extremum seeking control algorithm with hysteresis current controller is high when compared with the natural switching surface current controller. The high complexity associated with the sigma-delta modulated current controller and natural switching surface current controller resulted in

low convergence speed. The characteristics of the current controllers with the ESC tracking algorithm are tabulated in Table B.1.

Table B.1: Characteristics of the current controllers

Current Controller	**Accuracy**	**Convergence Speed**
Hysteresis	High	High
NSS	High	Low
Σ-Δ	High	Medium

From the above-mentioned points, the hysteresis current controller is the preferred current control technique with high accuracy and high convergence speed.

Appendix C

MATLAB-Simulink® Blocks

In this appendix, MATLAB/Simulink block diagrams for the PEMFC system discussed in Chapter 2, DC-DC boost converter and tracking techniques discussed in Chapter 3 and Chapter 4 are presented.

C.1 The PEMFC Generation System

The Simulink model of the entire PEMFC generation system consisting of a PEMFC unit, DC-DC boost converter, load, and tracking controller is shown in Fig. C.1.

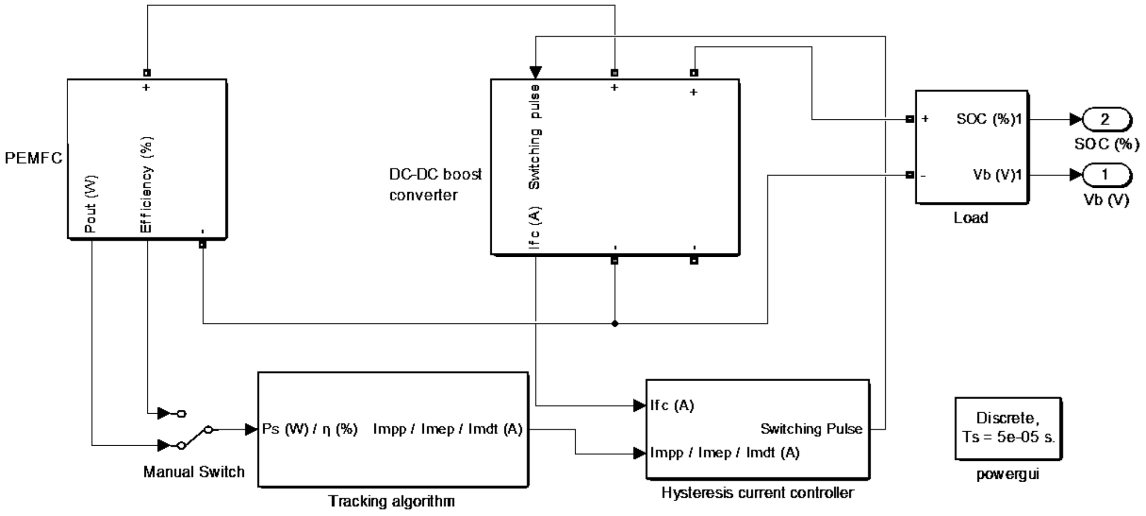

Fig. C.1. PEMFC generation system

C.2 PEMFC Simulink Model

The MATLAB/Simulink block diagrams of the PEMFC subsystems, namely stack model, reactant flow model, and net output power and efficiency model are presented in the following figures.

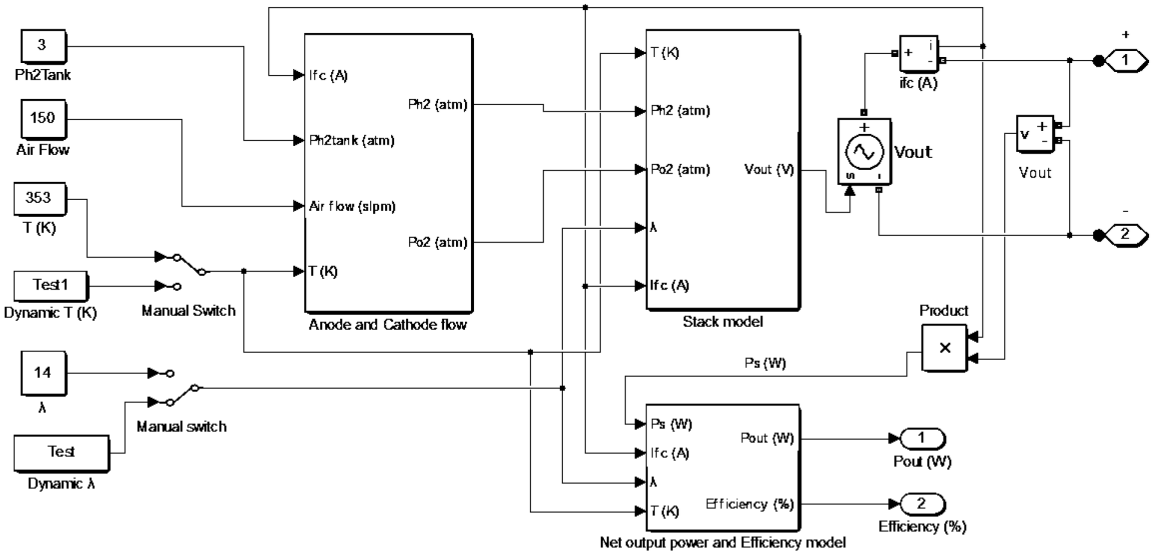

Fig. C.2. PEMFC Simulink model

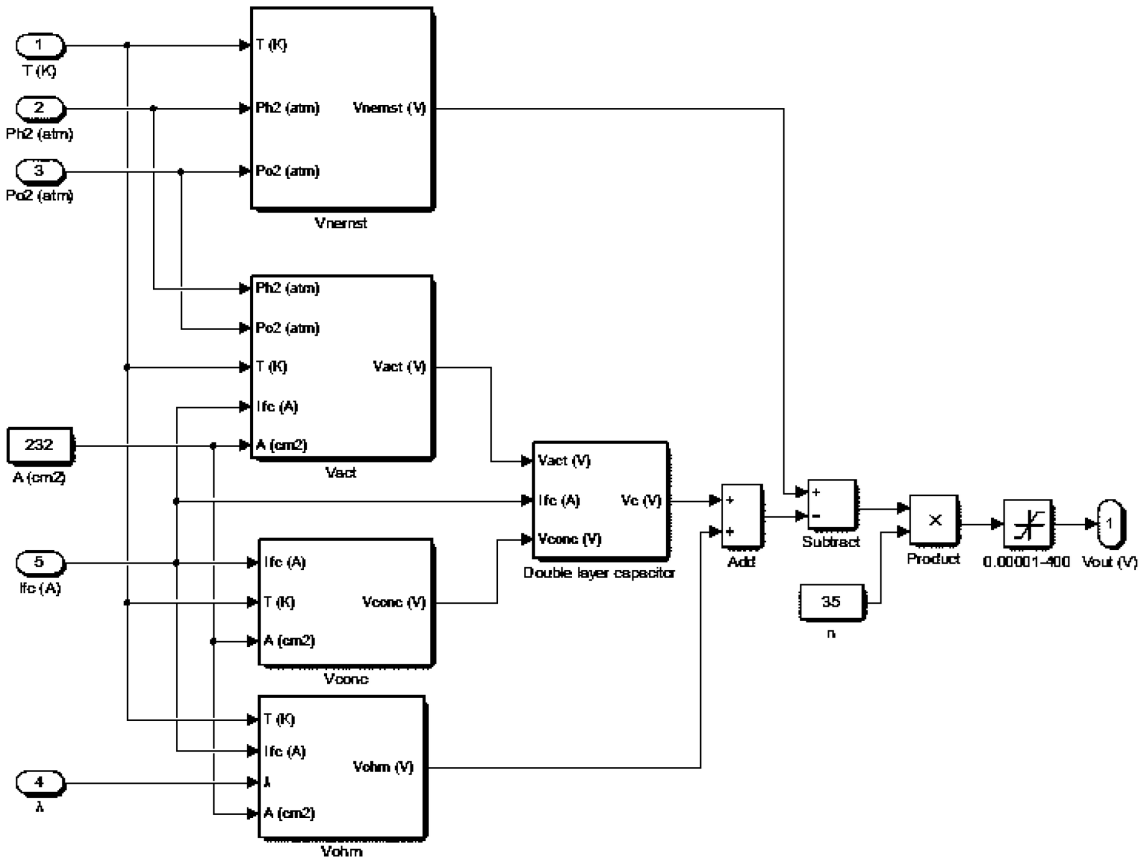

Fig. C.3. PEMFC stack model

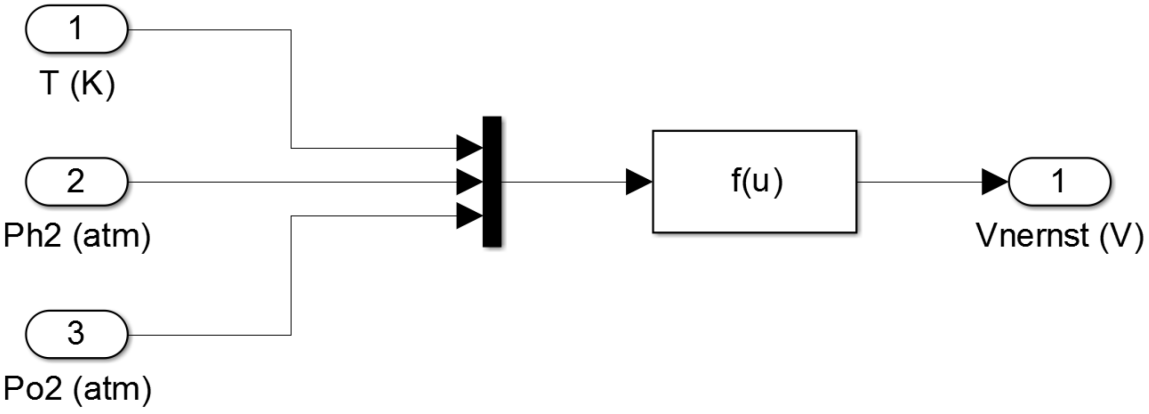

Fig. C.4. PEMFC Nernst output voltage model

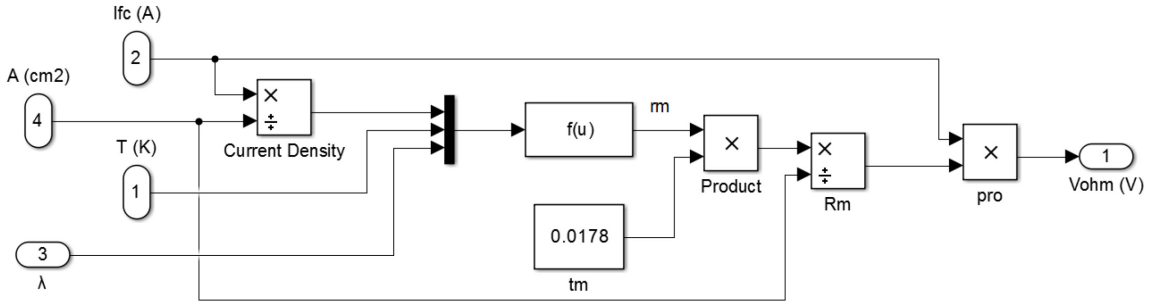

Fig. C.5. Ohmic voltage drop model

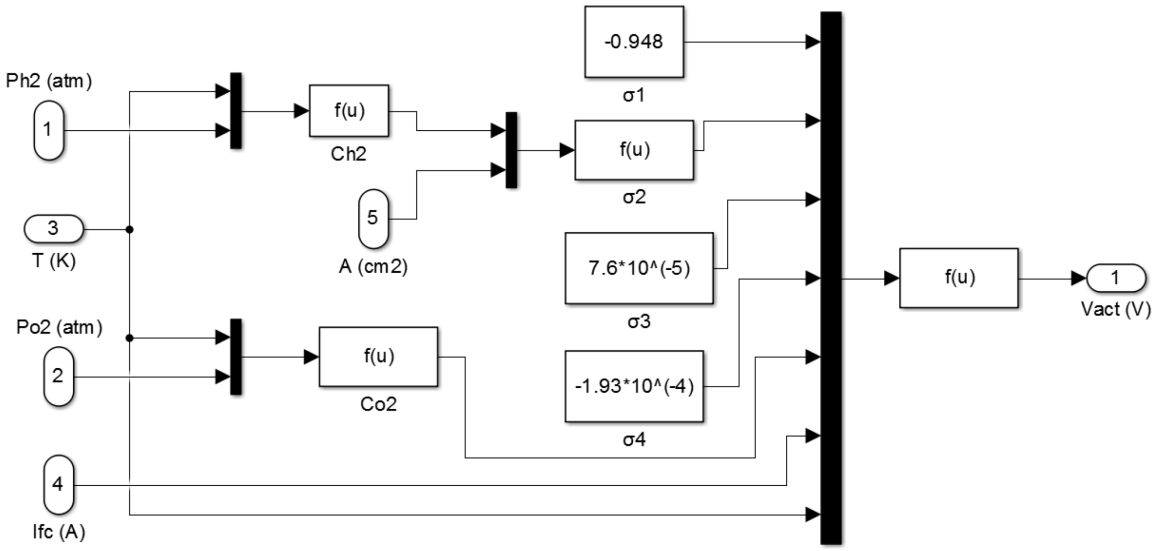

Fig. C.6. Activation voltage drop model

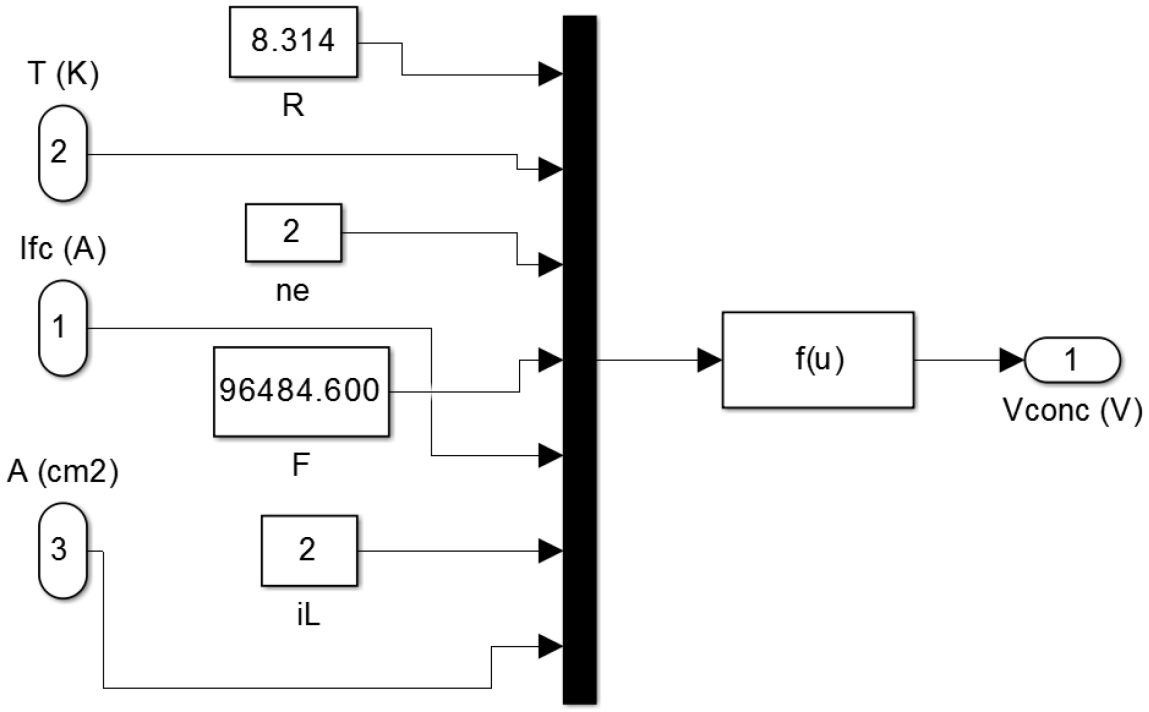

Fig. C.7. Concentration voltage drop

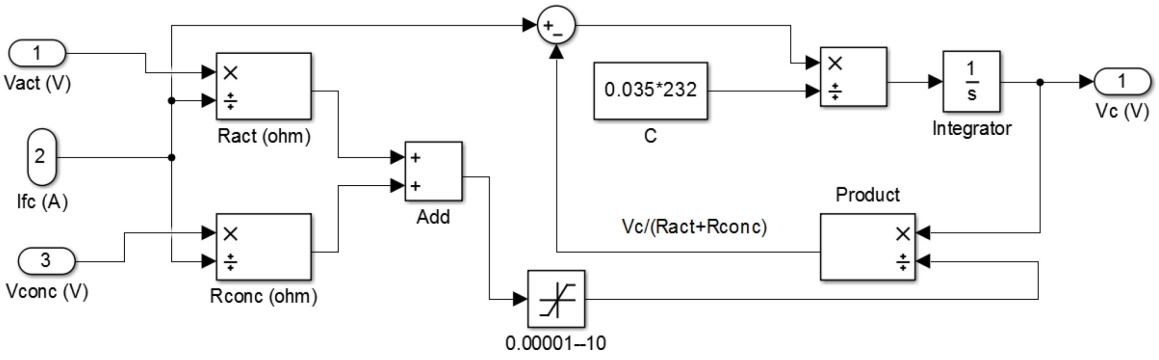

Fig. C.8. Double layer charge capacitance model

The reactant flow model consists of two subsystems, namely the cathode flow model and the anode flow model as shown in Fig. C.9.

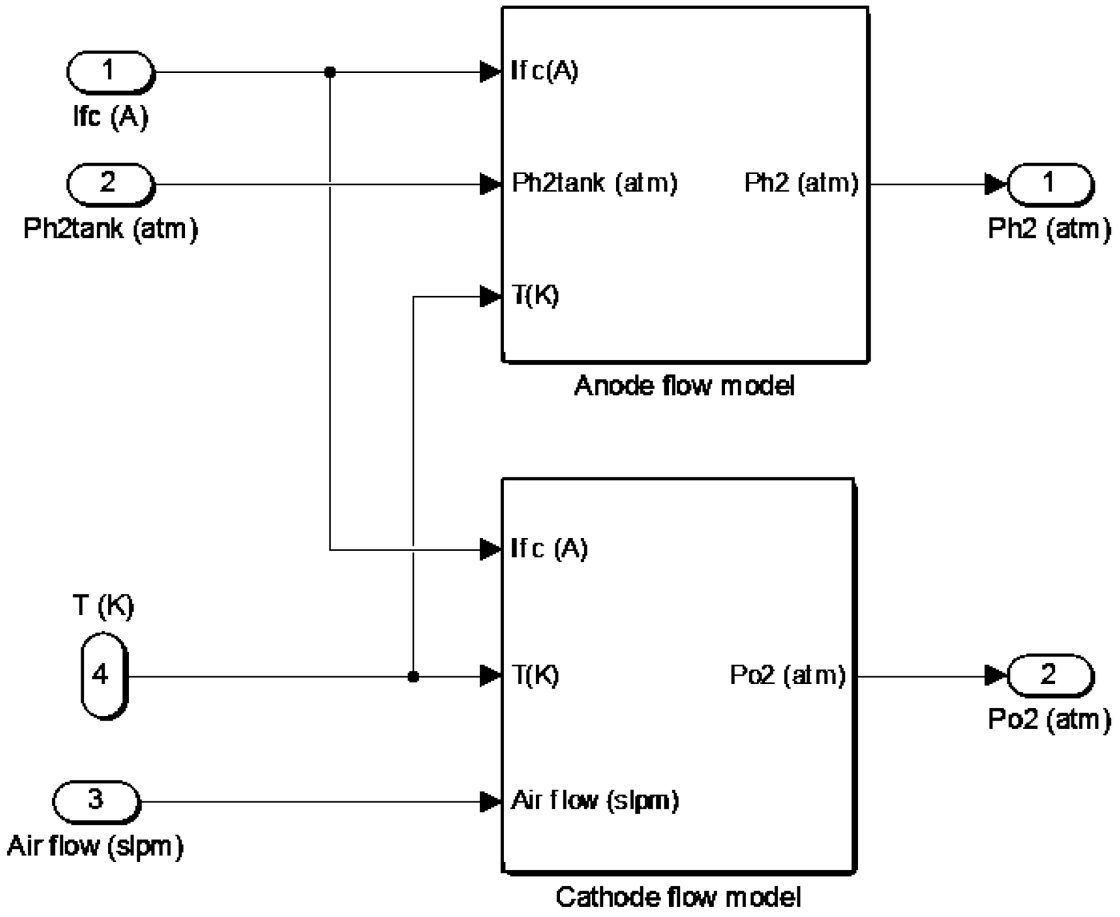

Fig. C.9. Reactant flow model

The Simulink block diagrams of the cathode and anode flow models are as follows:

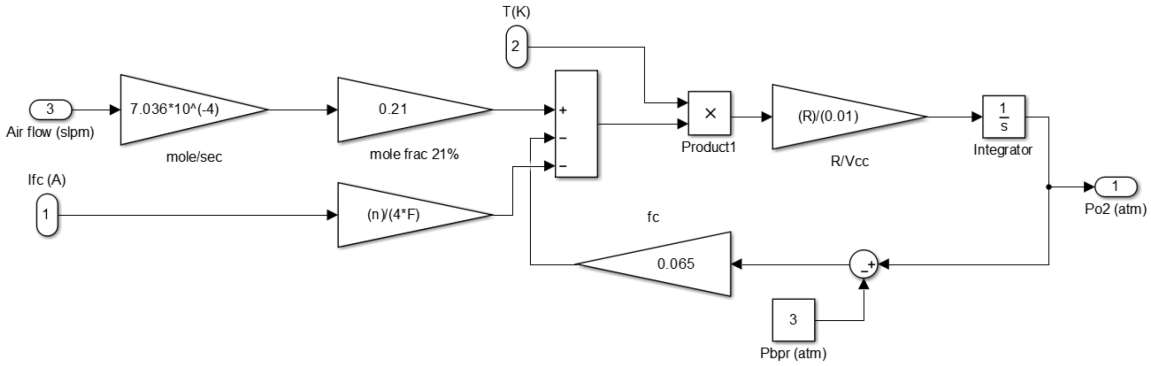

Fig. C.10. Cathode flow model

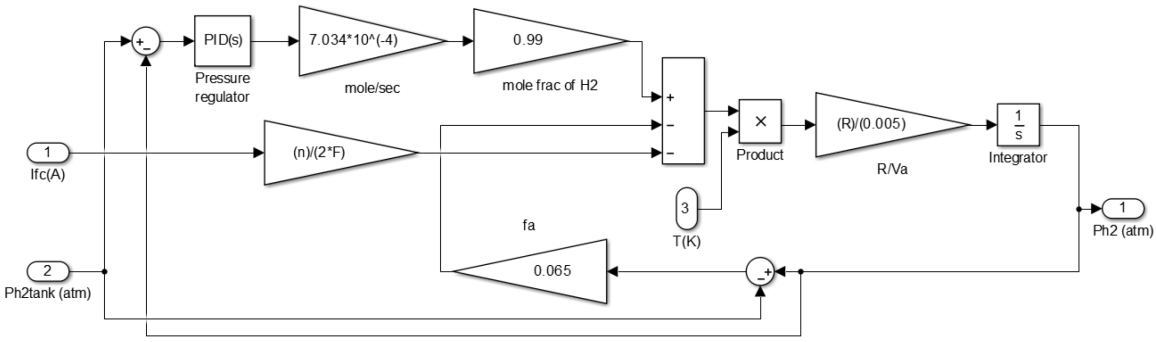

Fig. C.11. Anode flow model

The net output power (P_{out}) model and efficiency model of the PEMFC unit are shown in the following figures.

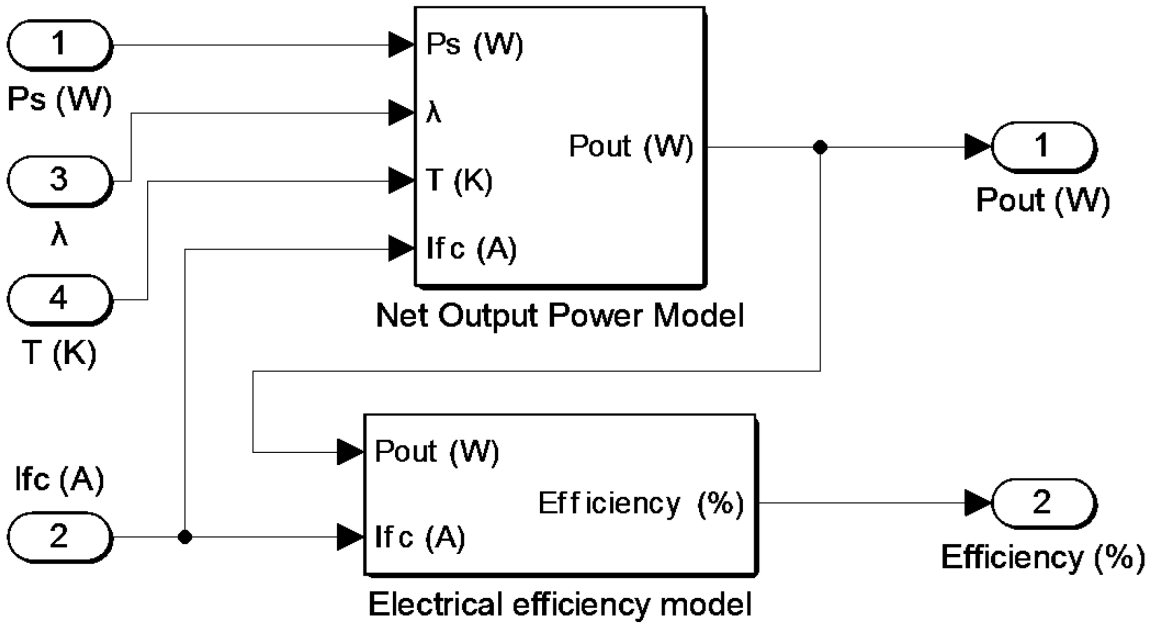

Fig. C.12. Net output power and efficiency model

The net output power model is shown in Fig. C.13.

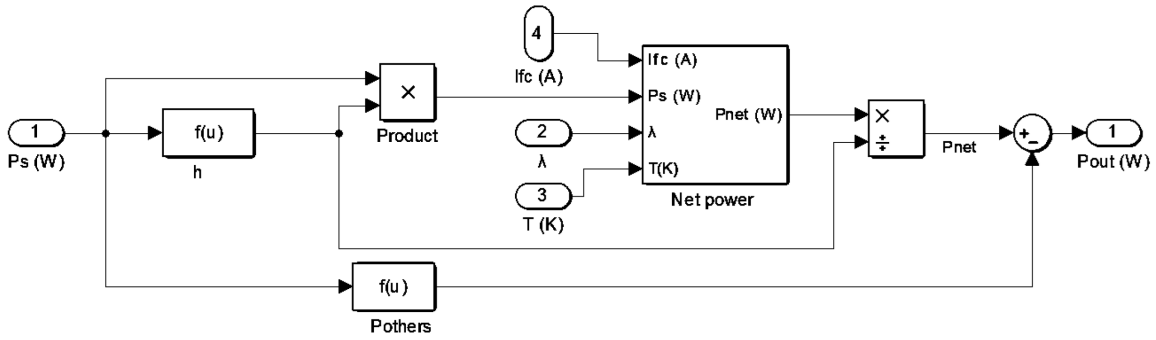

Fig. C.13. Net output power model

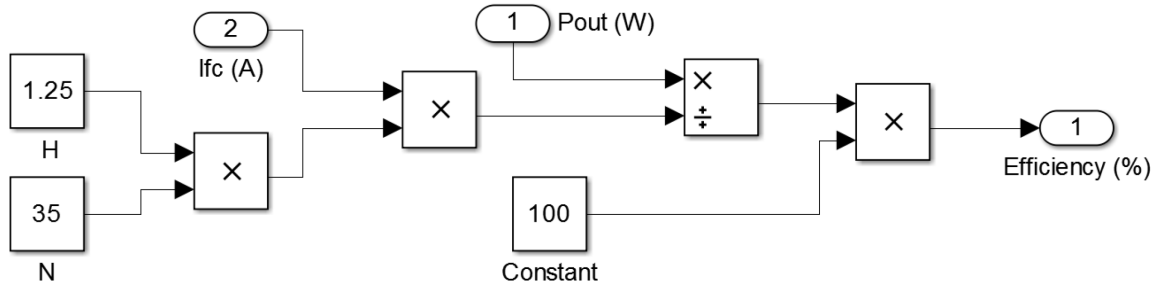

Fig. C.14. Efficiency model

C.3 DC-DC Boost Converter

The Simulink model of the DC-DC boost converter is shown in Fig. C.15.

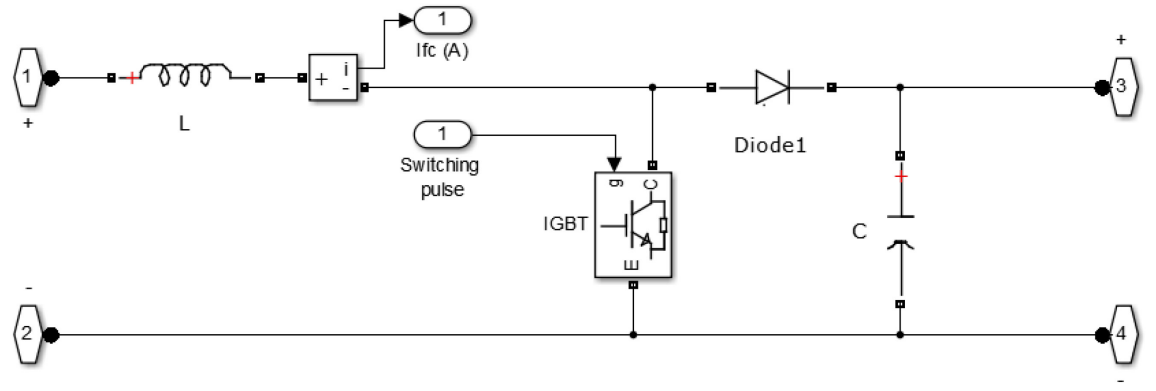

Fig. C.15. DC-DC boost converter

C.4 Hysteresis Current Controller

The Simulink diagram of the hysteresis current controller is shown in Fig. C.16.

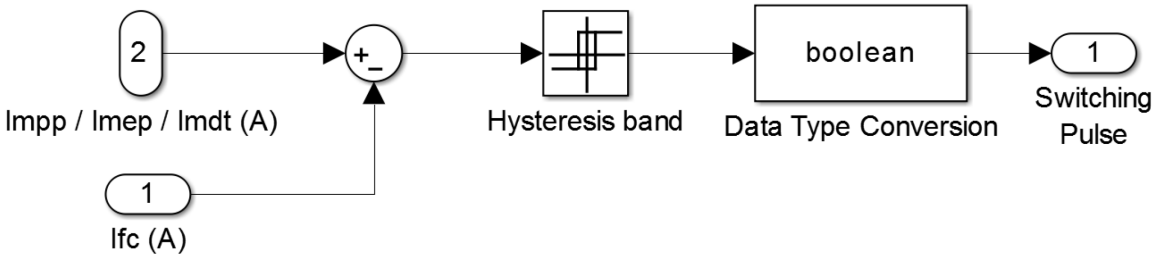

Fig. C.16. Hysteresis current controller

C.5 Tracking algorithms

The Simulink block diagrams of the extremum seeking control tracking algorithm and the perturb and observe tracking algorithm are presented in Fig. C.17 and Fig. C.18.

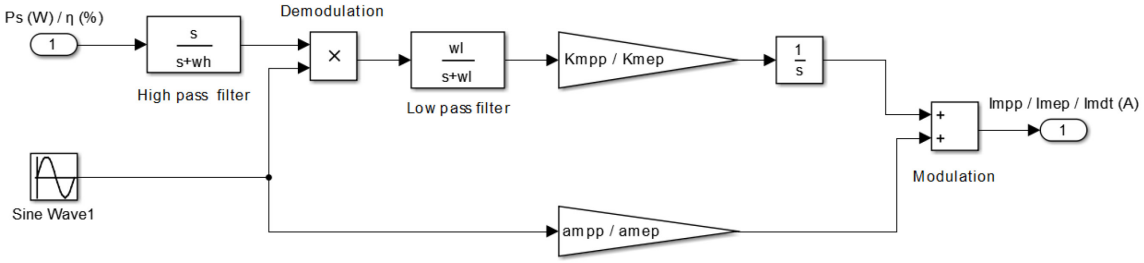

Fig. C.17. Extremum seeking control

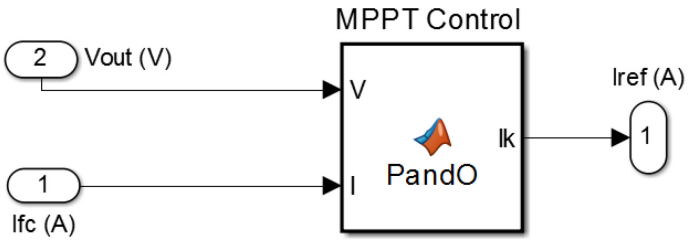

Fig. C.18. Perturb and observe model

The MATLAB code of the perturb and observe tracking algorithm is as follows:

```
function Ik  = PandO(V, I)
persistent Iold Pold;
dataType = 'double';
if isempty(Iold)
   Iold=1;
   Pold=0;
end
Ik=I;
P= V;
dI=0.0001;
Ik=Iold+0.1;
if (P>Pold)&&(I>Iold)
          Ik=I+dI;
else if (P<Pold)&&(I<Iold)
       Ik=I+dI;
   else if (P<Pold)&&(I>Iold)
          Ik=I-dI;
       else if (P>Pold)&&(I<Iold)
              Ik=I-dI;
          end
       end
   end
end
Iold=Ik;
Pold=P;
```

The Simulink block diagrams of the sliding mode control algorithm and midpoint tracking algorithm are shown in Fig. C.19 and Fig. C.20.

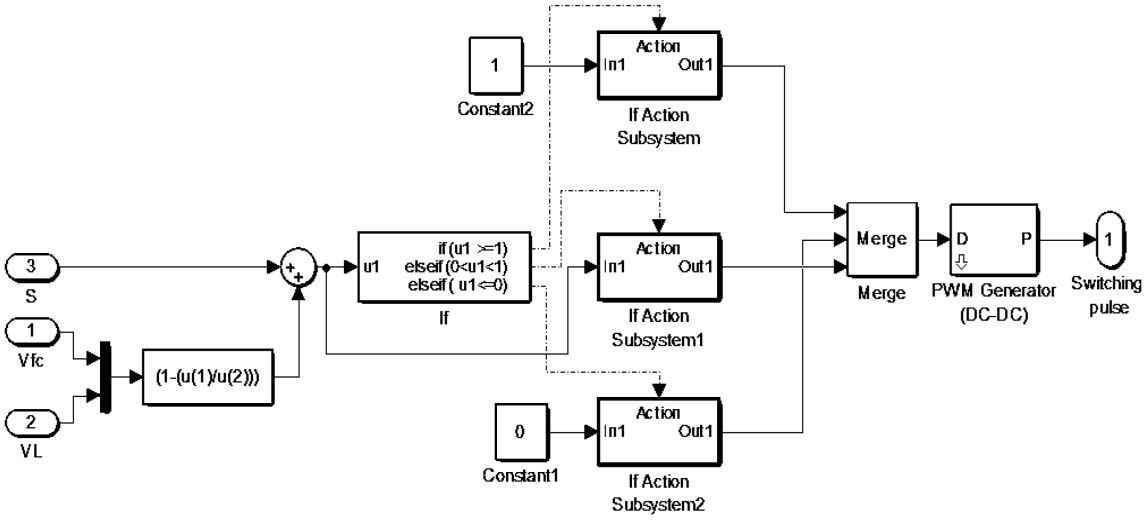

Fig. C.19. Sliding mode control

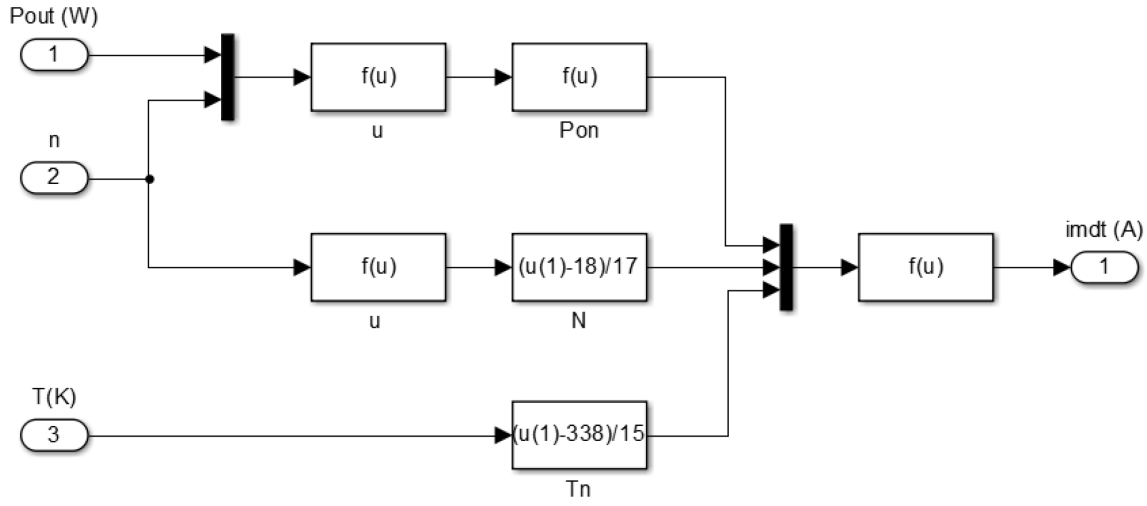

Fig. C.20. Midpoint tracking algorithm

C.6 Load

The Simulink diagram of the battery load connected to the DC-DC boost converter is shown in Fig. C.21.

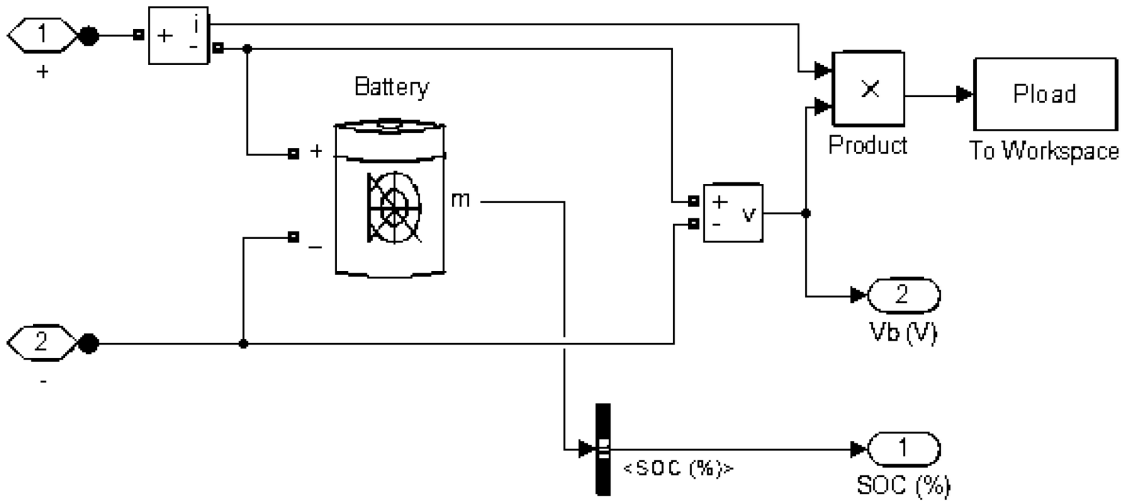

Fig. C.21. Load